

INFORMATION TO USERS

This manuscript has been reproduced from the microfilm master. UMI films the text directly from the original or copy submitted. Thus, some thesis and dissertation copies are in typewriter face, while others may be from any type of computer printer.

The quality of this reproduction is dependent upon the quality of the copy submitted. Broken or indistinct print, colored or poor quality illustrations and photographs, print bleedthrough, substandard margins, and improper alignment can adversely affect reproduction.

In the unlikely event that the author did not send UMI a complete manuscript and there are missing pages, these will be noted. Also, if unauthorized copyright material had to be removed, a note will indicate the deletion.

Oversize materials (e.g., maps, drawings, charts) are reproduced by sectioning the original, beginning at the upper left-hand corner and continuing from left to right in equal sections with small overlaps. Each original is also photographed in one exposure and is included in reduced form at the back of the book.

Photographs included in the original manuscript have been reproduced xerographically in this copy. Higher quality 6" x 9" black and white photographic prints are available for any photographs or illustrations appearing in this copy for an additional charge. Contact UMI directly to order.

UMI

A Bell & Howell Information Company
300 North Zeeb Road, Ann Arbor MI 48106-1346 USA
313/761-4700 800/521-0600

**SPECTRAL DEPENDENCE OF PHOTOSYNTHESIS
IN MARINE PHYTOPLANKTON**

by

Margareth Nnabuuma Kyewalyanga

**Submitted in partial fulfilment of the requirements
for the degree of Doctor of Philosophy**

at

Dalhousie University

Halifax, Nova Scotia

September, 1997

© Copyright by Margareth Nnabuuma Kyewalyanga, 1997



**National Library
of Canada**

**Acquisitions and
Bibliographic Services**

395 Wellington Street
Ottawa ON K1A 0N4
Canada

**Bibliothèque nationale
du Canada**

**Acquisitions et
services bibliographiques**

395, rue Wellington
Ottawa ON K1A 0N4
Canada

Your file Votre référence

Our file Notre référence

The author has granted a non-exclusive licence allowing the National Library of Canada to reproduce, loan, distribute or sell copies of this thesis in microform, paper or electronic formats.

The author retains ownership of the copyright in this thesis. Neither the thesis nor substantial extracts from it may be printed or otherwise reproduced without the author's permission.

L'auteur a accordé une licence non exclusive permettant à la Bibliothèque nationale du Canada de reproduire, prêter, distribuer ou vendre des copies de cette thèse sous la forme de microfiche/film, de reproduction sur papier ou sur format électronique.

L'auteur conserve la propriété du droit d'auteur qui protège cette thèse. Ni la thèse ni des extraits substantiels de celle-ci ne doivent être imprimés ou autrement reproduits sans son autorisation.

0-612-24750-3

Canada

DALHOUSIE UNIVERSITY

FACULTY OF GRADUATE STUDIES

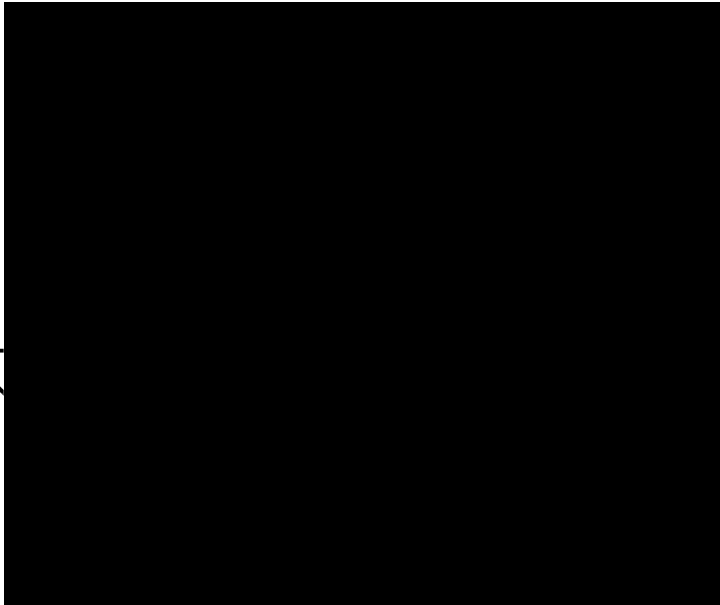
The undersigned hereby certify that they have read and recommend to the Faculty of Graduate Studies for acceptance a thesis entitled "Spectral Dependence of Photosynthesis in Marine Phytoplankton"

by Margareth Kyewalyanga

in partial fulfillment of the requirements for the degree of Doctor of Philosophy.

Dated: September 10, 1997

External Examiner
Research Supervisor
Examining Committee



DALHOUSIE UNIVERSITY

Date: September, 1997

Author: **Margareth Nnabuuma Kyewalyanga**

Title: **Spectral dependence of photosynthesis
in marine phytoplankton**

Department: **Oceanography**

Degree: **Ph.D.** Convocation: **October** Year: **1997**

Permission is herewith granted to Dalhousie University to circulate and to have copied for non-commercial purposes, at its discretion, the above title upon request of individuals or institutions.


Signature of the Author

THE AUTHOR RESERVES OTHER PUBLICATION RIGHTS, AND NEITHER THE THESIS NOR EXTENSIVE EXTRACTS FROM IT MAY BE PRINTED OR OTHERWISE REPRODUCED WITHOUT THE AUTHOR'S WRITTEN PERMISSION.

THE AUTHOR ATTESTS THAT PERMISSION HAS BEEN OBTAINED FOR THE USE OF ANY COPYRIGHTED MATERIAL APPEARING IN THIS THESIS (OTHER THAN BRIEF EXCERPTS REQUIRING ONLY PROPER ACKNOWLEDGEMENT IN SCHOLARLY WRITING) AND THAT ALL SUCH USE IS CLEARLY ACKNOWLEDGED.

To my dearest parents, and in memory of my brother Richard.

TABLE OF CONTENTS

| | |
|---|----------|
| Table of Contents | v |
| List of Figures | viii |
| List of Tables | xv |
| Abstract | xviii |
| List of Symbols | xix |
| Acknowledgements | xxii |
| | |
| Chapter 1: General Introduction | 1 |
| | |
| Chapter 2: Estimation of the Photosynthetic Action Spectrum: Implication for Primary Production Models | |
| 2.1 Introduction | 6 |
| 2.2 Data Collection and Analysis | 8 |
| 2.2.1 Study Area and Sampling | 8 |
| 2.2.2 Phytoplankton Absorption Spectrum | 12 |
| 2.2.3 Photosynthetic Action Spectrum | 13 |
| 2.2.4 Broad-band Photosynthesis-Light Parameters | 22 |
| 2.2.5 <i>In situ</i> Production | 26 |
| 2.2.6 Biomass Concentration and Profiles | 29 |
| 2.2.6 Construction of the Action Spectrum | 29 |
| 2.3 Results | 30 |
| 2.3.1 Comparison of Constructed and Measured Action Spectra | 30 |
| 2.3.2 The Effect of Non-photosynthetic Pigments on the Shape of the Constructed Action Spectrum | 36 |
| 2.3.3 The Effect of Random and Systematic Errors on the Constructed Action Spectrum | 43 |
| 2.3.4 Sensitivity Analysis of Random Errors | 43 |

| | | |
|-------|--|----|
| 2.3.5 | Sensitivity Analysis of Systematic Errors | 46 |
| 2.3.5 | Daily, Water-column, Primary Production: Comparison with Measured, <i>In situ</i> Production | 48 |
| 2.3.6 | Assignment of Action Spectra in Computing $P_{Z,T}$: Comparison of Results Achieved Using Different Approaches | 52 |
| 2.4 | Discussion | 53 |
| 2.5 | Concluding Remarks | 56 |

**Chapter 3: Variability in Physiological Parameters
of Phytoplankton across the North Atlantic**

| | | |
|-------|--|-----|
| 3.1 | Introduction | 58 |
| 3.2 | Materials and Methods | 59 |
| 3.2.1 | Sampling | 59 |
| 3.2.2 | Pigment Analyses and Nutrient Concentrations | 65 |
| 3.2.3 | Photosynthetic Action Spectra | 66 |
| 3.2.4 | Phytoplankton Absorption Spectra | 66 |
| 3.2.5 | Parameters of the Photosynthesis <i>vs.</i> Irradiance Curve | 68 |
| 3.2.6 | Constructed Action Spectra | 69 |
| 3.2.7 | Maximum Quantum Yield of Photosynthesis | 70 |
| 3.3 | Results | 71 |
| 3.3.1 | Parameters of the Photosynthesis–Irradiance Curve | 71 |
| 3.3.2 | Quantum Yield of Photosynthesis | 74 |
| 3.3.3 | Action and Absorption Spectra | 77 |
| 3.3.4 | Variations in α^B , P_m^B and ϕ_m with Independent Variables | 88 |
| 3.4 | Discussion | 96 |
| 3.4.1 | Predictability of the Physiological Parameters | 96 |
| 3.4.2 | Factors Affecting α^B | 97 |
| 3.4.3 | Factors Affecting P_m^B | 99 |
| 3.4.4 | Factors Affecting ϕ_m | 101 |

| | | |
|-------|---|-----|
| 3.4.5 | Effect of Silicate Concentration on Photosynthesis Parameters | 102 |
| 3.5 | Concluding Remarks | 106 |

**Chapter 4: Changes in Phytoplankton Population Structure:
Effects on the Action and Absorption Spectra**

| | | |
|-------|---|-----|
| 4.1 | Introduction | 108 |
| 4.2 | Materials and Methods | 109 |
| 4.3 | Results | 111 |
| 4.3.1 | Hydrography and Shapes of the Spectra | 111 |
| 4.3.2 | Phytoplankton Pigments | 125 |
| 4.3.3 | Physiological Parameters | 130 |
| 4.4 | Discussion | 135 |
| 4.5 | Concluding Remarks | 142 |

Chapter 5: Summary and Conclusions

| | | |
|-----|---|-----|
| 5.1 | Summary | 144 |
| 5.2 | Conclusions and Recommendations for Future Work | 145 |

| | | |
|-------------------|-----------|------------|
| Appendix I | | 151 |
|-------------------|-----------|------------|

| | | |
|--------------------|-----------|------------|
| Appendix II | | 154 |
|--------------------|-----------|------------|

| | | |
|-------------------|-----------|------------|
| References | | 156 |
|-------------------|-----------|------------|

LIST OF FIGURES

- Figure 2.1 Locations of 26 stations covered during the fall 1992 cruise from 19 September to 21 October. The track was sampled in the West–East and East–West directions. The final analysis included twenty stations (filled circles), out of the 26. The remaining six stations (filled diamonds) had very low phytoplankton biomass such that the action spectra could not be measured.
..... 10
- Figure 2.2 Shapes of absorption spectra of six phytoplankton species used in the sensitivity analysis. The spectra are normalized to 1 at 440 nm, to compare their shapes. The genus names are given in the figure.
..... 14
- Figure 2.3 An illustration of one incubation box, with its light source, used in the determination of the photosynthetic action spectrum. The box contains 16 light bottles and one dark bottle. The bottles are arranged one behind the other to provide a continuous attenuation of the available irradiance. The light source is a slide-projector lamp assembly (150 Watts), and the interference (colour) filter is fitted in a slide slot.
..... 16
- Figure 2.4 Shapes of measured spectra for all the 20 stations sampled during the cruise. The spectra are normalized to 1 at 440 nm to compare the shapes: (a) Action spectra (b) Absorption spectra. In both cases, the thick lines represent the average spectrum (of the 20 spectra).
..... 20
- Figure 2.5 Tungsten-halogen lamp spectra, normalized to their mean value to define the shape. The dashed line indicates the original shape of the spectrum,

the solid line shows the spectral shape of the irradiance reaching the last bottle in the incubator. The label “corrected” is used to indicate that absorption by the water sample and the bottle walls is accounted for. There is no significant change in the shape of the spectrum after passing through the bottles. The solid line was used in the computation of the correction factor X , as explained in the text.

. 23

Figure 2.6 Linear regression analyses of broad-band α^B on spectral average of $\alpha^B(\lambda)$ for twenty stations sampled during the 1992 cruise. (a) Originally measured α^B , not corrected for any bias, with regression equation $Y = (0.59 \pm 0.13)X$ ($n = 20$, $r^2 = 0.53$). In this case, the slope is significantly different from 1.0 at the 5% level. (b) Measured α^B , corrected for the bias introduced by the tungsten-halogen lamp spectrum: $Y = (0.91 \pm 0.21)X$ ($n = 20$, $r^2 = 0.52$), the slope is not significantly different from 1.0. The regression lines pass through the origin. The low r^2 , indicating high scatter along the regression line, is caused by pooling 20 different stations.

. 27

Figure 2.7 An example of the comparison of measured and constructed action spectra from Stn 4, (80 m); sampled on 21 September 1992: (a) The amplitudes and (b) the shapes; the spectra are normalized to their mean values. (c) Linear regression: the slope of 0.986 ($n = 12$, $r^2 = 0.98$) is not significantly different from 1.0 at the 1% level.

. 32

Figure 2.8 As in Figure (2.7) but for a station occupied on 4 October 1992. This is an example in which the slope of the regression line 0.61 ($n = 12$, $r^2 = 0.96$) was significantly lower than 1.0 at the 1% level.

. 34

Figure 2.9 Daily water-column primary production at each of the twenty stations, computed using different action spectra: solid line, $P_{Z,T}(1)$ (filled circles), the measured action spectra; dotted line, $P_{Z,T}(2)$, constructed action spectra, not corrected for non-photosynthetic pigments; short-dashed line, $P_{Z,T}(3)$, same as for the dotted line, but the spectra were corrected for the presence of non-photosynthetic pigments; and long-dashed line, $P_{Z,T}(4)$, a constant *shape* (an average of the 20 measured action spectra), scaled to broad-band α^B values.

. 41

Figure 2.10 Linear regression analysis of computed daily, water-column, primary production $P_{Z,T}$ on the *in situ* $P_{Z,T}$, for 14 stations. The filled circles show data sampled on the time-series location (this study); the empty circles represent data from Kyewalyanga et al. (1992), sampled from the Sargasso Sea in April 1990. The regression equation is $Y = (1.02 \pm 0.02)X$ ($n = 14$, $r^2 = 0.91$) with the slope not significantly different from 1.0 at the 5% significance level (the intercept was forced through the origin), indicating a good agreement between *in situ* and computed $P_{Z,T}$. The line is the 1:1 relation.

. 50

Figure 3.1 Locations of 26 stations sampled in the North Atlantic during the JGOFS 92 cruise (filled circles) and 36 stations occupied during the JGOFS 93 cruise (open circles).

. 61

Figure 3.2 Locations of five biogeochemical provinces in the North Atlantic, sampled during the two cruises across the track shown in Figure (3.1): NWCS, the Northwest Continental Shelf; GFST, the Gulf Stream; STGE, the Eastern Subtropical Gyre; STGW, the Western Subtropical Gyre; and

CNRY the Canary province. The insert box shows the four domains: Coastal, Trade-winds, Westerlies and Polar. Note that other provinces of the North Atlantic are also shown (from Sathyendranath et al. 1995, with permission).

. 63

Figure 3.3 Shapes of representative (a) action and (b) absorption spectra for the five biogeochemical provinces sampled during the JGOFS 92 cruise: GFST, the Gulf Stream; NWCS, the Northwest Continental Shelf; CNRY, the Canary; STGE, the Eastern Subtropical gyre; and STGW, the Western Subtropical gyre. Each spectrum is normalized to its mean value, averaged over the spectral range from 400 to 700 nm.

. 78

Figure 3.4 Comparison of shapes of measured and constructed action spectra in five biogeochemical provinces defined in Figure (3.2). The spectra are normalized to their mean values (averaged between 400 and 700 nm). The measured action spectra are shown by solid lines, and the constructed ones by the broken lines.

. 81

Figure 3.5 Regression analysis of constructed $\alpha_c^B(\lambda)$ on the measured $\alpha^B(\lambda)$, for pooled data, from each of the biogeochemical provinces referred to in Figure (3.3). The respective regression lines, the number of points, the r^2 values and the 1:1 lines are also shown.

. 84

Figure 3.6 As in Figure (3.3) but for the JGOFS 93 cruise and for the shapes of the representative absorption spectra only.

. 86

Figure 3.7 Semi-log plots showing the relation between the maximum quantum yield of photosynthesis, ϕ_m , and the concentration of nitrate plus nitrite for data collected during the JGOFS 92 cruise (open circles) and JGOFS 93 cruise (filled circles). (a) All data combined, (b) CNRY province, (c) GFST province, (d) NWCS province, (e) STGE province and (f) STGW province.

. 94

Figure 4.1 Profiles of temperature, salinity, photosynthetically available radiation (PAR) and chl-a concentration for two sampling dates in the Bedford Basin: (a & b) 17 August 1994 and (c & d) 19 October 1994. Nutrient concentrations for the whole sampling period are presented as a function of day of the year (1994): (e) nitrate plus nitrite, (f) silicate and (g) phosphate; in all cases, open circles indicate data collected at 1 m, filled circles joined by lines show data taken from 5 m and open squares indicate data sampled at 10 m. The meteorological data as a function of day of the year are given as daily averages (thin lines) and weekly averages, filled circles joined by thick lines: (h) air temperature, (i) rainfall, (j) hours of bright sunshine, (k) wind speed and (l) wind direction.

. 113

Figure 4.2 Shapes of action spectra for five months: (a) August, (b) September, (c) October, (d) November and (e) December, sampled in 1994, in the Bedford Basin. Each spectrum is normalized to its mean value, averaged over the spectral range from 400 to 700 nm.

. 118

Figure 4.3 As in Figure (4.2), but for the corresponding absorption spectra.

. 120

Figure 4.4 Time-series variation for data collected from the Bedford Basin between 10 August and 21 December 1994. (a) chlorophyll-a (chl-a) concentration, (b) concentration of dissolved oxygen, (c) water temperature, (d) the ratio of chlorophyll-b (chl-b) to chl-a, (e) ratio of chl-c₁+c₂ to chl-a and (f) the ratio of chl-c₃ to chl-a. The symbols are as defined in Figure (4.1)

. 126

Figure 4.5 Time-series variation in the ratios of carotenoids to chl-a for samples collected from 10 August to 21 December 1994 in the Bedford Basin. (a) fucoxanthin (fuco), (b) alloxanthin (allo), (c) peridinin (perid), (d) diadinoxanthin (diadi), (e) 19'-hexanoyloxy-fucoxanthin (19'hexa) and (f) zeaxanthin + lutein (ze+lut). The symbols are as defined in Figure (4.1)

. 128

Figure 4.6 Time-series variation in data collected at 5 m from the Bedford Basin between 10 August and 21 December 1994. (a) The quantum yield of carbon fixation, (b) the average value of the action spectrum, $\alpha^B(\lambda)$ [mg C (mg chl-a)⁻¹ h⁻¹ (μ mol m⁻² s⁻¹)⁻¹] and (c) the mean value of the biomass-specific absorption coefficients, $a_p^B(\lambda)$ [m² (mg chl-a)⁻¹].

. 131

Figure 4.7 Time-series variation in the amplitudes of the (a) action (b) absorption spectra for values at the blue peaks (filled circles) and at the red peaks (open circles), for data collected at 5 m in the Bedford Basin. (c) Ratios of blue-to-red values for the action spectra ($\alpha^B(440):\alpha^B(670)$; filled circles) and absorption spectra ($a_p(440):a_p(676)$; open circles).

. 133

Figure 4.8 Fourth-derivative spectrum (top panel) showing peaks of absorption maxima for different pigments present in the sample collected from 5 m on 19

October 1994 (bottom panel). The approximate positions of the peaks and shoulders corresponding to the peaks in the fourth-derivative spectrum are indicated by arrows. The contributing pigments are discussed in the text, but note the peak for phycoerythrin absorption at about 545 nm.

. 139

LIST OF TABLES

| | |
|--|----|
| <p>Table 2.1 Wavelengths of maximum transmission of the 12 interference filters used in the spectral incubator, and their relation with absorption bands of major phytoplankton pigments – chlorophyll-<i>a</i> (chl-<i>a</i>), chlorophyll-<i>b</i> (chl-<i>b</i>), chlorophyll-<i>c</i> (chl-<i>c</i>), carotenoids (carot.) and phycobilins (phycob), and the wavebands of the satellite sensor, the SeaWiFS. The SeaWiFS wavebands are taken from Hooker et al. (1992). The pigment absorption bands are taken from Neori et al. (1986); Lewis et al. (1986); Hoepffner and Sathyendranath (1991); and Johnsen et al. (1994a).</p> | 19 |
| <p>Table 2.2 Sensitivity analysis of errors in water-column primary production for a range of chlorophyll-<i>a</i> concentrations (mg m^{-3}); caused by random errors on the action spectrum of up to $\pm 20\%$. The averages were computed using absolute values of 50 relative errors. The computations were carried out for noon irradiance and $P_m^B = 12.0 \text{ mg C (mg chl-}a)^{-1} \text{ h}^{-1}$.</p> | 44 |
| <p>Table 2.3 Systematic errors on the action spectrum: Effect on water-column primary production ($\text{mg C m}^{-2} \text{ h}^{-1}$). The computations were carried out for noon irradiance, biomass of $1.0 \text{ mg chl-}a \text{ m}^{-3}$, and P_m^B of $12.0 \text{ mg C (mg chl-}a)^{-1} \text{ h}^{-1}$. Negative errors indicate underestimation and <i>vice versa</i>.</p> | 47 |
| <p>Table 2.4 <i>In situ</i> daily water-column primary production ($P_{Z,T}$ <i>in situ</i>) and daily water-column primary production $P_{Z,T}$ ($\text{g C m}^{-2} \text{ day}^{-1}$) computed using the measured and the constructed action spectra at each of the 20 stations sampled during the cruise. The percentage difference between the two computed $P_{Z,T}$ values is given in the last column.</p> | 49 |

Table 3.1a Data from two cruises showing average values (mean \pm SD) of the broad-band initial slope of the P^B vs. I curve, α^B [mg C (mg chl-*a*)⁻¹ h⁻¹ (μ mol m⁻² s⁻¹)⁻¹], in five provinces and for pooled results.

. 73

Table 3.1b As in Table (3.1a), but for the maximum photosynthetic rate, i.e., the plateau of the P^B vs. I curve, P_m^B [mg C (mg chl-*a*)⁻¹ h⁻¹].

. 73

Table 3.2a Range in the values of the maximum quantum yield of photosynthesis, ϕ_m [mol C (mol photons)⁻¹], for the two cruises, in each of the five biogeochemical provinces and for pooled data from all provinces. The dynamic range (Dynamic) is also given.

. 76

Table 3.2b Mean values (\pm SD) of the ϕ_m values [mol C (mol photons)⁻¹] for the provinces given in Table 3.2a.

. 76

Table 3.3 Analysis of variance (ANOVA) to test the variation in average *shapes* of action and absorption spectra in five biogeochemical provinces: NWCS, GFST, STGW, STGE and CNRY sampled during two cruises. The ANOVA was performed at the wavelengths shown, and the results are given as significantly different (sign.) or not significantly different (ns) at the 5% level.

. 80

Table 3.4a Independent variables that explain significant ($p < 0.05$) portion of the variation in the initial slope of the P^B vs. I curve, α^B [mg C (mg chl-*a*)⁻¹ h⁻¹ (μ mol m⁻² s⁻¹)⁻¹], for the two cruises, in each of the five biogeochemical provinces. The coefficient of determination (r^2) shows the

fraction of total variance (in percentage) explained by the independent variable(s). R_a is the blue-to-red absorption ratio, $a_p(435):a_p(676)$; R_c is the blue-to-red peak height ratio of chl-*a* absorption bands, $p(435):p(676)$; Z is the sampling depth; T is temperature; N , P and S_i are nitrate + nitrite, phosphate and silicate concentrations, respectively; C is chl-*a* concentration and Z_n is the distance between the sampling depth and the top of the nitracline. The number of data points (n) is given.

. 89

Table 3.4b As in Table (3.4a), but for the rate of photosynthesis at saturating irradiance, P_m^B [mg C (mg chl-*a*)⁻¹ h⁻¹].

. 90

Table 3.4c As in Table (3.4a) but for the realized, maximum quantum yield of photosynthesis, ϕ_m [mol C (mol quanta)⁻¹].

. 91

Table 3.5 Independent variables that explain significant ($p < 0.05$) portion of the variation in three physiological parameters: α^B , P_m^B and ϕ_m (units given in Tables 3.4a, 3.4b and 3.4c, respectively) in two domains: Coastal (COAST) and Westerlies (WESTL), across the North Atlantic. The r^2 (in percentage) gives the fraction of the total variance explained by the independent variable(s). The symbols of the variables are explained in Table (3.4a).

. 92

Table 4.1 Centers (nm) of peaks of the fourth-derivative spectra calculated for each absorption spectrum for samples collected from 5 m.

. 122

ABSTRACT

The main objectives of this work were to develop and apply a simple method of estimating the action spectrum and to explore, at different temporal and spatial scales, the variation in the action and absorption spectra, and the variation and predictability of the non-spectral photosynthesis parameters of phytoplankton in natural populations. These photosynthesis properties are central to the computation of primary production, given the underwater light field and biomass distribution.

In the first part of the study, a simple method of estimating the photosynthetic action spectrum, using the *shape* of the absorption spectrum and the *magnitude* of the broad-band initial slope of the photosynthesis-irradiance curve, was developed and tested by comparing the estimated spectra with actual measurements of the action spectrum. The constructed and measured spectra were then applied in the computation of primary production at different stations across the North Atlantic. There was a good agreement in the production computed using the measured and constructed action spectra, confirming that the newly-developed method worked well. Therefore, the method could be applied in the field or in the laboratory.

In the second part, the nature of variation in the spectrally-resolved and non-spectral photosynthesis parameters was explored. The data were collected in five large oceanic regions in the North Atlantic, known as biogeochemical provinces, during two different seasons, and at a single location in Bedford Basin (Nova Scotia) for twenty consecutive weeks. Some nine independent variables were tested for their ability to explain the variance in the photosynthesis parameters of phytoplankton.

It was found that seasonal variation in photosynthesis parameters and the shapes of action and absorption spectra was larger than that between the provinces in a given season. Several independent variables, individually or in combination, were shown to explain a significant fraction of the variance in the photosynthesis parameters. At the time-series station in Bedford Basin, changes in hydrographic conditions were found to induce changes in species composition, which in turn had a significant effect on both the shapes and amplitudes of the corresponding action and absorption spectra.

The results from this investigation should be useful for modelling primary production both at small and large scales.

LIST OF SYMBOLS

| Notation | Quantity [Units] |
|------------------|--|
| a_p | Absorption coefficient of phytoplankton [m^{-1}]. |
| $a_p(\lambda)$ | Absorption coefficient of phytoplankton at wavelength λ [m^{-1}]. |
| \bar{a}_p | Spectrally-averaged, unweighted mean of $a_p(\lambda)$ [m^{-1}]. |
| \bar{a}_T | Spectral mean absorption coefficient of phytoplankton weighted by the emission spectrum of the tungsten-halogen lamp [m^{-1}]. |
| $a_v(\lambda)$ | Average absorption spectrum in a given province [m^{-1}]. |
| \bar{a}_v | Spectrally-averaged mean value of $a_v(\lambda)$ [m^{-1}]. |
| $a'_p(\lambda)$ | Representative shape of the absorption spectrum in a given province calculated by normalizing $a_v(\lambda)$ to its mean value, \bar{a}_v [dimensionless]. |
| $a_p^B(\lambda)$ | Chlorophyll- <i>a</i> -specific absorption coefficient of phytoplankton at λ [$\text{m}^2 \text{mg}^{-1}$]. |
| \bar{a}_p^B | Spectrally-averaged mean value of $a_p^B(\lambda)$ [$\text{m}^2 \text{mg}^{-1}$]. |
| B | Phytoplankton biomass, as chl- <i>a</i> concentration [mg m^{-3}]. |
| B_0 | Background phytoplankton biomass as chl- <i>a</i> concentration [mg m^{-3}]. |
| $B(z)$ | Phytoplankton biomass at depth z [mg m^{-3}]. |
| C | Chlorophyll- <i>a</i> [mg m^{-3}]. |
| D_d | Optical density of detrital materials on the filter [dimensionless]. |
| D_f | Optical density of particulate matter on the filter [dimensionless]. |
| D_s | Optical density of particulate matter in suspension [dimensionless]. |
| F | Fractional absorption by photosynthetically-active pigments, relative to absorption by total phytoplankton pigments [dimensionless]. |
| F_{dv} | Ratio of divinyl chl- <i>a</i> to total chl- <i>a</i> [dimensionless]. |
| h | Total biomass concentration within the chlorophyll maximum peak [mg m^{-2}]. |
| I | Available irradiance [$\mu\text{mol m}^{-2} \text{s}^{-1}$]. |
| I_k | Irradiance at which the onset of saturation occurs, calculated as the ratio of P_m^B to α^B [$\mu\text{mol m}^{-2} \text{s}^{-1}$]. |

| | |
|-------------|--|
| I_d | Direct component of available irradiance [$\mu\text{mol m}^{-2} \text{s}^{-1}$]. |
| I_s | Diffuse component of available irradiance [$\mu\text{mol m}^{-2} \text{s}^{-1}$]. |
| I_T | Incident irradiance from the tungsten-halogen lamp [$\mu\text{mol m}^{-2} \text{s}^{-1}$]. |
| L | Pathlength of light through a filter [m]. |
| n | Number of data points. |
| N | Nitrate plus nitrite concentration [$\mu\text{g-at l}^{-1}$]. |
| P | Inorganic phosphate concentration [$\mu\text{g-at l}^{-1}$]. |
| P | Instantaneous rate of primary production [$\text{mg C m}^{-3} \text{h}^{-1}$]. |
| P^B | Production normalized to phytoplankton biomass [$\text{mg C (mg chl-}a\text{)}^{-1} \text{h}^{-1}$]. |
| P_m^B | Rate of photosynthesis at saturating irradiance, normalized to phytoplankton biomass [$\text{mg C (mg chl-}a\text{)}^{-1} \text{h}^{-1}$]. |
| P_{opt}^B | Maximum rate of photosynthesis in the water column [$\text{mg C (mg chl-}a\text{)}^{-1} \text{h}^{-1}$]. |
| $P(z)$ | Production at a given depth z [$\text{mg C m}^{-3} \text{h}^{-1}$]. |
| P_Z | Production integrated over depth [$\text{mg C m}^{-2} \text{h}^{-1}$]. |
| $P_{Z,T}$ | Production integrated over depth and time [$\text{mg C m}^{-2} \text{day}^{-1}$]. |
| PS I | Photosystem I reaction centre. |
| PS II | Photosystem II reaction centre. |
| $p(435)$ | Peak height of Gaussian absorption band for chl- a centered at 435 nm [m^{-1}]. |
| $p(676)$ | Peak height of Gaussian absorption band for chl- a centered at 676 nm [m^{-1}]. |
| R_a | Blue-to-red absorption ratio, $a_p(435):a_p(676)$ [dimensionless]. |
| R_c | Blue-to-red peak heights ratio of chl- a absorption bands, $p(435):p(676)$ [dimensionless]. |
| S_i | Silicate concentration [$\mu\text{g-at l}^{-1}$]. |
| T | Water temperature at a given sampling depth [$^{\circ}\text{C}$]. |
| X | Ratio of unweighed mean absorption coefficient of phytoplankton to the mean absorption coefficient weighted by the shape of the emission |

| | |
|-----------------------|--|
| | spectrum of the tungsten-halogen lamp [dimensionless]. |
| z | Depth [m]. |
| Z_n | Distance between the sampling depth and the top of the nitracline [m]. |
| Z_{I_k} | Light-saturation depth, defined as the depth at which the irradiance $I = I_k$ [m]. |
| α^B | Rate of photosynthesis at low irradiance, that is, the initial slope of the photosynthesis-irradiance curve, measured in broad-band light [mg C (mg chl- <i>a</i>) ⁻¹ h ⁻¹ (μ mol m ⁻² s ⁻¹) ⁻¹]. |
| $\alpha^B(\lambda)$ | Measured photosynthetic action spectrum, i.e., α^B determined in narrow-band light [mg C (mg chl- <i>a</i>) ⁻¹ h ⁻¹ (μ mol m ⁻² s ⁻¹) ⁻¹]. |
| $\alpha_c^B(\lambda)$ | Action spectrum constructed using the shape of the phytoplankton absorption spectrum and the magnitude of the broad-band α^B [mg C (mg chl- <i>a</i>) ⁻¹ h ⁻¹ (μ mol m ⁻² s ⁻¹) ⁻¹]. |
| $\alpha(\lambda_i)$ | Reference action spectrum constructed from the shape of the absorption spectrum of <i>Chaetoceros gracilis</i> , grown in cultures [mg C (mg chl- <i>a</i>) ⁻¹ h ⁻¹ (μ mol m ⁻² s ⁻¹) ⁻¹]. |
| $\alpha_v^B(\lambda)$ | Average action spectrum for a given biogeochemical province [mg C (mg chl- <i>a</i>) ⁻¹ h ⁻¹ (μ mol m ⁻² s ⁻¹) ⁻¹]. |
| $\bar{\alpha}_v^B$ | Mean value of $\alpha_v^B(\lambda)$, computed over the range from 400 to 700 nm [mg C (mg chl- <i>a</i>) ⁻¹ h ⁻¹ (μ mol m ⁻² s ⁻¹) ⁻¹]. |
| $\alpha'(\lambda)$ | Representative shape of the average action spectrum, in a given province, obtained by normalizing $\alpha_v^B(\lambda)$ to its mean value $\bar{\alpha}_v^B$ [dimensionless]. |
| β^B | Negative slope of the photosynthesis-irradiance curve, at photoinhibiting irradiances [mg C (mg chl- <i>a</i>) ⁻¹ h ⁻¹ (μ mol m ⁻² s ⁻¹) ⁻¹]. |
| β -factor | Pathlength amplification factor, defined as the ratio of optical to geometrical pathlength [dimensionless]. |
| λ | Wavelength [nm]. |
| ϕ_m | Maximum quantum yield of photosynthesis [mol C (mol photons) ⁻¹]. |
| σ | Thickness of the chlorophyll maximum peak [m]. |
| θ | Sun zenith angle in water [degrees]. |

ACKNOWLEDGEMENTS

First and foremost, I am very grateful to my supervisor Dr. Trevor Platt for his tremendous supervision, guidance and encouragement throughout my thesis work, and for his full financial support during the entire duration of my study. I deeply appreciate the help and guidance constantly provided by Dr. Shubha Sathyendranath at all stages of development of this thesis. I would like to thank the members of my supervisory committee: Drs. Eric Mills, Bruce Johnson, Glen Harrison and Carl Boyd for providing constructive ideas and comments on various drafts of this thesis. I am very honoured and I appreciate that Dr. Richard Barber, busy as he is, put aside all his important matters and came to Halifax to be my External Examiner. Thank you Dr. Barber for your very constructive comments, especially on the direction of my future research work.

I am grateful to my employer, the University of Dar-es-Salaam, for granting me a study leave, and for providing the necessary extensions that allowed me to complete my doctorate work. I also appreciate the support by my director, Dr. Julius Francis, at the Institute of Marine Science in Zanzibar (IMS), in different aspects. Thank you also all my colleagues at IMS in Zanzibar.

The field work, some data processing and technical work would have been difficult without the help I received from many colleagues and friends at one stage or another. It is not easy to mention all of you here, but you know who you are, and I want you to know that I really appreciate your help. In particular, I would like to thank the following for their significant contribution: Brian Irwin, Vivian Lutz, Jeff Anning, Heidi Maass, Gilberto Gaxiola, Hugo Benavides, Kathy Dower, Delphine Thibault, Germa Pizarro, Paul Dickie, Al MacDonald, Linda Payzant, George White, Ed Horne, Ravindran Pulysary, Carla Caverhill, Venetia Stuart, Erica Head, Heidi Bishop and Marilyn Landry.

A piece of mind is a necessity when one is writing her/his thesis. Therefore, I am indebted to my friends here in Canada and overseas, who gave the much needed encouragement and moral support. Again, it is impossible to mention all of you by names! However, some of you cannot go unmentioned. Thank you

Joan Duval for everything, for being there for me all the time, and for all you have done since we met eight years ago. Vivian Lutz: you are more than a sister to me, you have been on my side during all my ups and downs and much more. Sophie Carler, thank you for your special friendship! I thank the Lord for you Heidi Maass — you have done so much for me, and I will always treasure the beautiful song you wrote me. I am also very grateful for my good friends for their support and help: Angelica Peña, Osvaldo Ulloa, Philippe Fullsack, Heidi Maass, Delphine Thibault, Jean Marc Nicolas, Darlene Mossman, Amina Makame, Nolan and Shirley Harris, Kathy Dower, Edna Nyika, Amani and Veronica Ngusaru, Hilda Olomi, Mary and Alphonse Dubi, Jane Minja, Jacob Maiseli, Piotr Trela, Ajitha and Ravindran Pulysary, and many more.

Last, but not least, I would like to thank my family, from the depth of my heart, for their love, support, encouragement and for believing in me. My special gratitude goes to my dearest parents for everything! I would like to thank my sister Marygoreth for her continued moral support and encouragement all the time. I am also grateful to my other siblings: Severini, Rosemary, Tereza, Lydia and Akileo for making their presence felt, although they were thousands of kilometers away. My nieces Elizabeth and Bridget and nephews Ibrahim and John have been my inspiration in a special way!

CHAPTER 1

General Introduction

One of the current priorities in biological oceanography is to estimate accurately the daily water-column primary production at large scales, as a contribution to understanding the global carbon cycle. Satellite data on phytoplankton biomass and available light provide the most important information needed to attain this goal. However, maps of phytoplankton biomass cannot be directly interpreted as maps of primary production (Platt et al. 1991), and auxiliary information from field data is needed to supplement satellite-derived data for the calculation of water-column primary production (Platt and Sathyendranath 1988, Morel and Berthon 1989, Sathyendranath et al. 1991, Longhurst et al. 1995).

Considerable progress has been made in recent years in developing algorithms for chlorophyll retrieval and for computing primary production from remotely-sensed ocean colour (e.g., Gordon and Clark 1980, Gordon and Morel 1983, Platt and Sathyendranath 1988, 1991, Morel and Berthon 1989, Platt et al. 1990, Sathyendranath and Platt 1993a, b, Gordon and Wang 1994, Morel et al. 1996); and the future of remote sensing of primary production looks promising, given the advent of the new generation of satellite sensors for ocean colour such as the Ocean Color and Temperature Scanner (OCTS), the Moderate-Resolution Imaging Spectroradiometer (MODIS) and the Sea-viewing Wide Field-of-view Sensor (SeaWiFS) with increased radiometric sensitivity and more spectral bands than the first, satellite, ocean-colour sensor, the Coastal Zone Color Scanner (Hooker et al. 1992, Gordon and Wang 1994, Ishizaka et al. 1997).

Although the satellite-derived data are (and will be) readily accessible to the public, a limitation in estimating large-scale primary production could be the availability of complementary information from field data. The slow speed of the ships, the cost of equipment and chemicals, and the efficiency with which measurements

are made limit both the spatial and temporal coverage in the field. Therefore, there is a need to develop simple and efficient methods for estimating phytoplankton properties from field data (Chapter 2). The field-derived information needed includes the photosynthetic response P^B of phytoplankton to available light I (P^B vs. I curve) and the vertical structure of the photosynthetic biomass in the water column. In the absence of photoinhibition, the P^B vs. I curve is characterized by two independent parameters: α^B , the initial slope of the curve and P_m^B , the photosynthetic rate at saturating irradiance (Platt et al. 1980), where the superscripts indicate normalization to phytoplankton biomass B , usually measured as chlorophyll- a concentration. Note that in models based on absorbed rather than available light, α^B is represented as a product of the maximum quantum yield of photosynthesis ϕ_m and the spectral mean value of the biomass-specific absorption coefficients of phytoplankton, that is, the phytoplankton absorption spectrum $a_p^B(\lambda)$, where λ is the wavelength.

Vertical structure in phytoplankton biomass is not accessible directly to remote sensing, and this information is also usually supplied from *in situ* observations. The biomass profile has been parameterized using a Gaussian curve with four parameters, as follows (Platt et al. 1988, Sathyendranath and Platt 1989b): B_0 , the background biomass; z_m , the depth of chlorophyll maximum; σ , the thickness of the deep chlorophyll maximum layer, and h , the total biomass in the layer.

Several models are available for estimating primary production based on the photosynthetic response of phytoplankton to light. Sathyendranath and Platt (1993a) have pointed out that the choice of a primary production model depends, among other things, on computational demands; on availability of facilities to carry out the computations; and on acceptable magnitude of errors. For simplicity, or lack of relevant information, many production models assume uniform phytoplankton distribution, and also ignore the wavelength-dependency of the P^B vs. I parameters and the underwater light transmission. In most oceanic waters, however, a typical biomass profile has a deep chlorophyll maximum (Cullen 1982) which is usually invisible to satellites, given that about 90% of the signal received by the

satellite sensors comes from the first attenuation length, or reciprocal of the diffuse vertical attenuation coefficient (Gordon and McCluney 1975, Sathyendranath 1986, Platt and Sathyendranath 1988). Thus, the assumption of uniform biomass distribution can lead to significant errors if the water column is not homogeneous (Platt et al. 1988, Sathyendranath and Platt 1989b). Further, for accurate determination of water-column primary production, the wavelength-dependencies of the initial slope of the P^B vs. I curve, $\alpha^B(\lambda)$ the photosynthetic action spectrum (Lewis et al. 1985a, b, Schofield et al. 1990) and the underwater light transmission (Sathyendranath and Platt 1988) have to be considered (Sathyendranath and Platt 1989a, Sathyendranath et al. 1989, Kyewalyanga et al. 1992).

To estimate primary production at large horizontal scales, the main steps are as follows: first, a local algorithm is developed using local measurements, and validated by comparing the results with *in situ* measurements of primary production. Next, the parameters required to implement the algorithm are extrapolated to a large scale by using an appropriate scheme, as explained below. The models then combine the satellite-derived information, such as biomass distribution, with the parameters that are obtained from the field data, to compute primary production at each grid point. Once primary production is estimated at each grid point, the results are then summed over the region under consideration (e.g., Platt and Sathyendranath 1988, Platt et al. 1991, Longhurst et al. 1995). Unlike the satellite-derived data, the parameters from field measurements are not available at each grid point, consequently, some assumptions for extrapolation have to be made.

To extrapolate to a large scale, one of the possibilities is to predict the parameters from a variable that is measured by the satellite sensors, such as temperature, if a relation between the variable and the parameter has been found to exist from local measurements. Another alternative is to assume that the parameters of the photosynthesis-irradiance curve and those of the biomass profile are quasi-stable for large oceanic regions (Platt and Sathyendranath 1988, Mueller and Range 1989, Longhurst et al. 1995), in any one season. Indeed, this has been shown to be the

case in some areas (e.g., in the Sargasso Sea, Platt et al. 1992). On the other hand, if the parameters are highly variable in space and time, the primary production estimated at large scale, under the assumption of quasi-constant parameters, may contain unacceptable levels of error. For example, the maximum quantum yield of photosynthesis ϕ_m has been shown to exhibit considerable variability (Cleveland et al. 1989, Prézelin et al. 1991, Bidigare et al. 1992, Schofield et al. 1991, 1993, Babin et al. 1995, Sathyendranath et al. 1996, Sosik 1996). Therefore, there is a need to improve our understanding of the temporal and spatial variability of field-derived inputs in the models, with the aim of determining the consequence on the estimation of water-column primary production at large scales.

The following are the objectives of my thesis:

- 1) To develop a simple method for determining the photosynthetic action spectra using the *shape* of phytoplankton absorption spectra and the *magnitude* of the broad-band α^B measured on the same sample, and to compare the estimated spectra with their measured counterparts.
- 2) To test the performance of the method developed in Objective 1 by calculating daily water-column primary production using both the estimated (constructed) and measured action spectra, at different locations in the North Atlantic, and to assess the effect of the variation in the action spectra on the computed water-column primary production.
- 3) To examine the variation and predictability in the physiological parameters of phytoplankton: α^B , P_m^B and ϕ_m , and the *shapes* of action and absorption spectra in different large oceanic regions (biogeochemical provinces; Longhurst 1995) of the North Atlantic at a seasonal time-scale.
- 4) To conduct a study at a single location, to examine time-dependent variation in the physical, chemical and biological properties of coastal waters, and to evaluate the effect of changes in species composition on the *amplitudes* and *shapes* of the action and absorption spectra.

The results of this work are presented in three chapters. Objectives 1 and 2 are addressed in Chapter 2, in which I develop a simple method for estimating the photosynthetic action spectrum using the shape of the absorption spectrum and the broad-band α^B . Then, I test the method by comparing the estimated action spectra with those measured at different stations during a cruise conducted in the North Atlantic in fall of 1992. Finally, I compute daily water-column primary production at each station using the measured and estimated action spectra for comparison. Furthermore, I assess the magnitude of the error in the computed water-column primary production caused by random and systematic errors in the action spectrum.

Chapter 3 deals with the third objective. Here, I study the variability and predictability of the physiological parameters of phytoplankton at large spatial (biogeochemical provinces) and temporal (seasonal) scales. The method developed in Chapter 2 is used to construct action spectra using data collected during spring of 1993. With an extended data set from two cruises carried out in different seasons, I attempt to answer the question: How do the physiological parameters of phytoplankton and the shapes of action and absorption spectra vary between provinces and seasons? In this chapter, I also address the question: Can physiological parameters of phytoplankton, in a given biogeochemical province and season, be predicted by environmental variables that are routinely measured at sea?

In Chapter 4, I narrow down the study area to a single location in the Bedford Basin and consider only temporal variation. This chapter addresses Objective 4 in which I explore time-dependent variation in the amplitudes and shapes of the action and absorption spectra in relation to changes in structure of phytoplankton assemblage and associated environmental variables, i.e., physical, chemical and biological variables.

Finally, a general summary and some concluding remarks are given in Chapter 5.

CHAPTER 2

Estimation of the Photosynthetic Action Spectrum: Implication for Primary Production Models

2.1 Introduction

Spectral dependencies are often ignored in computations of primary production, even though it is well known that light transmission underwater, light absorption by phytoplankton, and the efficiency of utilization of the absorbed light in photosynthesis are all wavelength-dependent. That is to say, broad-band models are often used for simplicity and convenience, where spectral ones would be more realistic. This simplification, however, may lead to significant discrepancies when the estimates of primary production are compared with the results of *in situ* production measurements (Kiefer & Strickland 1970, Harrison et al. 1985, Sathyendranath et al. 1989, Kyewalyanga et al. 1992). Therefore, it is advisable, where possible, to use spectrally-resolved models for computation of primary production.

Among the essential information required for implementation of a spectrally-resolved model are α^B , the initial slope, and P_m^B , the assimilation number, which are both determined from the photosynthesis – irradiance (P^B vs. I) curve. The superscript B indicates normalization to phytoplankton biomass B . Of these two parameters, α^B is known to be dependent on wavelength λ , whereas P_m^B is usually taken to be wavelength-independent (Pickett & Myers 1966). The existing methods for directly determining the photosynthetic action spectrum, based on ^{14}C fixation (Lewis et al. 1985a, Warnock 1990, Schofield et al. 1990, 1991), are relatively complicated and time-consuming compared with the broad-band measurements of α^B . Because of this, very little data are available on the action spectra of natural phytoplankton populations. As a consequence, the use of the action spectrum in

computing water-column primary production is often limited to an average *shape* (scaled to the magnitude of the broad-band α^B) obtained from a few measurements (e.g., Platt & Sathyendranath 1988, Sathyendranath et al. 1989, Platt et al. 1991, Kyewalyanga et al. 1992, Sathyendranath et al. 1995). The implicit assumption in such computations is that errors in the computed production caused by ignoring possible variation in the shape of the action spectrum are negligible. However, this assumption has not been tested in the field due to lack of sufficient data on the photosynthetic action spectra of natural phytoplankton assemblages. The present data set, with twenty measured and twenty constructed action spectra, offered an opportunity for testing the assumption. In this chapter, I examine the validity of assuming a constant shape of the action spectrum in computing primary production.

It would also be advantageous to develop techniques for estimating the shape of the photosynthetic action spectrum, so that, if necessary, the restriction of a constant shape could be relaxed in computations of primary production. One possible approach is presented in this chapter, where the shape of the phytoplankton absorption spectrum and the magnitude of the broad-band α^B are used to construct the photosynthetic action spectrum. Here, it is assumed that the shape of the phytoplankton absorption spectrum is similar to that of the corresponding action spectrum, and that the broad-band α^B provides an appropriate estimate of the amplitude. Both the absorption spectrum and the broad-band α^B are easier to measure than the photosynthetic action spectrum.

However, there are some factors associated with the measurements that, if ignored, have the potential to cause errors in the constructed action spectrum. For example, if the measured phytoplankton absorption spectrum has a contribution from non-photosynthetic pigments such as the degradation products of chlorophyll (phaeopigments) and photoprotective carotenoids (Krinsky 1979, Siefermann-Harms 1987, Johnsen & Sakshaug 1993, Sosik & Mitchell 1995), the *shape* of the constructed action spectrum will be different from the actual one, in the spectral region where non-photosynthetic pigments absorb light. Similarly, if the estimated

broad-band α^B (the scaling factor) is subject to errors, the constructed spectrum will also be incorrect.

In this chapter, a method for constructing photosynthetic action spectra is presented, and applied to data from twenty stations across the North Atlantic. The constructed spectra are then compared with the directly-measured ones, and it is shown that the constructed action spectrum is a good estimator of the measured action spectrum. A theoretical study, using absorption spectra of six phytoplankton species, belonging to four phytoplankton groups (diatoms, prymnesiophytes, chlorophytes and cyanophytes), is also conducted to develop an approach for estimating potential errors due to non-photosynthetic pigments. The approach developed is then extended to the field samples, to quantify the effect of non-photosynthetic pigments on the constructed action spectra when the spectra are used to compute daily, water-column, primary production, $P_{Z,T}$. Next, the errors that could be introduced in the computed water-column primary production because of random or systematic errors on the action spectrum are assessed through a sensitivity analysis. The measured and the constructed action spectra at each station are compared. Both spectra are then used to compute daily, water-column, primary production, the results of which are discussed.

2.2 Data Collection and Analysis

2.2.1 Study Area and Sampling

Sampling was conducted twice (in the West–East and East–West directions) in the fall of 1992 (19 September to 21 October), along a track across the North Atlantic between Halifax, Canada, and Morocco (Figure 2.1). A variety of hydrographic regimes was encountered along the transect, including the cold continental

shelf waters off Nova Scotia, the warm Gulf Stream waters, the oligotrophic subtropical gyre waters, and the upwelling waters off the northwest coast of Africa. After the West–East transect, an 8-day time series station was occupied in the upwelling waters off the coast of Morocco.

At each station, a sample for the action spectrum was collected from one depth using a continuous pump sampler (Herman et al. 1984). The continuous pump was also used to collect samples for broad-band P^B vs. I parameters, absorption spectra and chlorophyll-*a* (chl-*a*) concentrations from three depths, including the one from which the water for measuring the action spectrum was collected. Samples for biomass profiles, depth-dependent *in situ* production measurements and nutrient profiles were collected from eleven or more depths in the upper 200 m, using a Niskin-bottle rosette attached to another CTD probe. In total, 26 stations were sampled during the cruise. In the present study, however, only 20 stations are considered; at the remaining six stations, the biomass was so low that the action spectra could not be measured (Figure 2.1).

Figure 2.1 Locations of 26 stations covered during the fall 1992 cruise from 19 September to 21 October. The track was sampled in the West-East and East-West directions. The final analysis included twenty stations (filled circles), out of the 26. The remaining six stations (filled diamonds) had very low phytoplankton biomass such that the action spectra could not be measured.

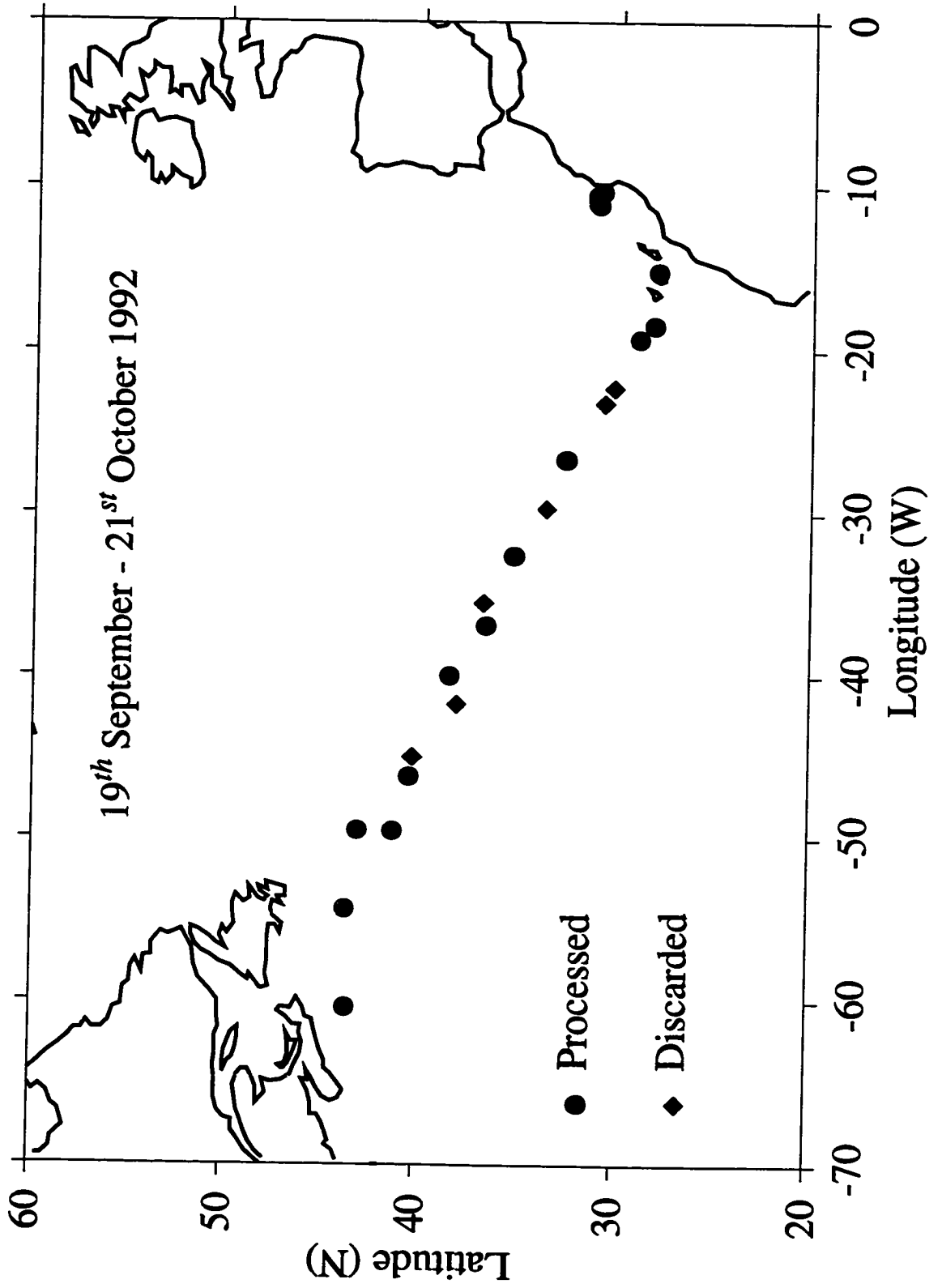


Figure 2.1

2.2.2 Phytoplankton Absorption Spectrum

A water sample (from 0.5 to 1.5 l, depending on the biomass concentration) was filtered onto 25-mm GF/F (Whatman) filters using a vacuum filtration pump, at low pressure. The optical density (absorbance) $D_t(\lambda)$ of total particulate materials at each wavelength λ , with the subscript t indicating total particles, was determined in a spectrophotometer (Beckman DU-64), using the filter technique (Yentsch 1962, Kiefer & SooHoo 1982, Mitchell & Kiefer 1984, Kishino et al. 1985, Hoepffner & Sathyendranath 1992, Cleveland & Weidemann 1993).

The pigments were extracted from the particles (Kishino et al. 1985) using a mixture of 90% acetone and dimethyl sulphoxide, as in Hoepffner & Sathyendranath (1992). The optical density of the residual particles $D_d(\lambda)$ was then measured. Both the $D_t(\lambda)$ and $D_d(\lambda)$ spectra were corrected for the pathlength-amplification factor, as in Hoepffner & Sathyendranath (1992), to get the optical density in suspension. The difference between $D_t(\lambda)$ and $D_d(\lambda)$ gave the phytoplankton optical density in suspension, $D_s(\lambda)$. The $D_s(\lambda)$ values were then converted to absorption coefficients of phytoplankton (m^{-1}), $a_p(\lambda)$, as follows:

$$a_p(\lambda) = \frac{2.3D_s(\lambda)}{L}, \quad (2.1)$$

where 2.3 is the conversion factor from decimal logarithms to natural logarithms and L (m) is the pathlength. The phytoplankton absorption spectra were then decomposed into Gaussian bands (Hoepffner & Sathyendranath 1991, 1993) representing absorption by major phytoplankton pigments, i.e., chlorophylls (a , b , and c) and carotenoids. The decomposed absorption spectra were used to study the potential effects on the proposed method, of partial absorption by photoprotective carotenoids and phaeopigments in certain spectral regions.

In addition to the field measurements, absorption spectra of six phytoplankton cultures – *Chaetoceros gracilis* (a diatom); *Thalassiosira weissflogii* (a diatom);

Phaeodactylum sp. (a diatom); *Dunaliella tertiolecta* (a chlorophyte); *Isochrysis galbana* (a prymnesiophyte); and *Synechococcus* sp. (a cyanophyte) – were determined using the method outlined above, except that no corrections for detrital materials were made. The cultures were grown at 20°C, in f/2 medium, under continuous light. With this range of cultures, a variety of shapes of absorption spectra could be obtained (see Figure 2.2), to study the contribution of non-photosynthetic pigments.

2.2.3 Photosynthetic Action Spectrum

The action spectrum was measured using a new spectral incubator developed at the Bedford Institute of Oceanography, Dartmouth, Nova Scotia, Canada. Incubation bottles (Corning, 70-ml polystyrene culture flasks) were filled with seawater samples, inoculated with $\text{NaH}^{14}\text{CO}_3$ (activity of 0.74 or 1.48 MBq in each bottle, depending on biomass concentrations) and placed in black incubation boxes. Each incubation box, containing 16 light bottles and one dark bottle, had a light-tight dark cover, a square glass window (36 cm^2) for illumination, and two openings for water circulation. The temperature in the box was maintained by circulating temperature-controlled water through it, at the temperature of the sampling depth.

The light source for each box was a slide-projector lamp assembly (150 Watts). The broad-band light produced by the lamp was screened using an interference filter (Corion), which was fitted in the position originally designed for the slide. The projector also had heat mirrors and a fan to dissipate the heat released by the bulb. Inside the box, the bottles were arranged one behind the other to provide a light gradient without the use of neutral density filters (Figure 2.3).

Figure 2.2. Shapes of absorption spectra of six phytoplankton species used in the sensitivity analysis. The spectra are normalized to 1 at 440 nm, to compare their shapes. The genus names are given in the figure.

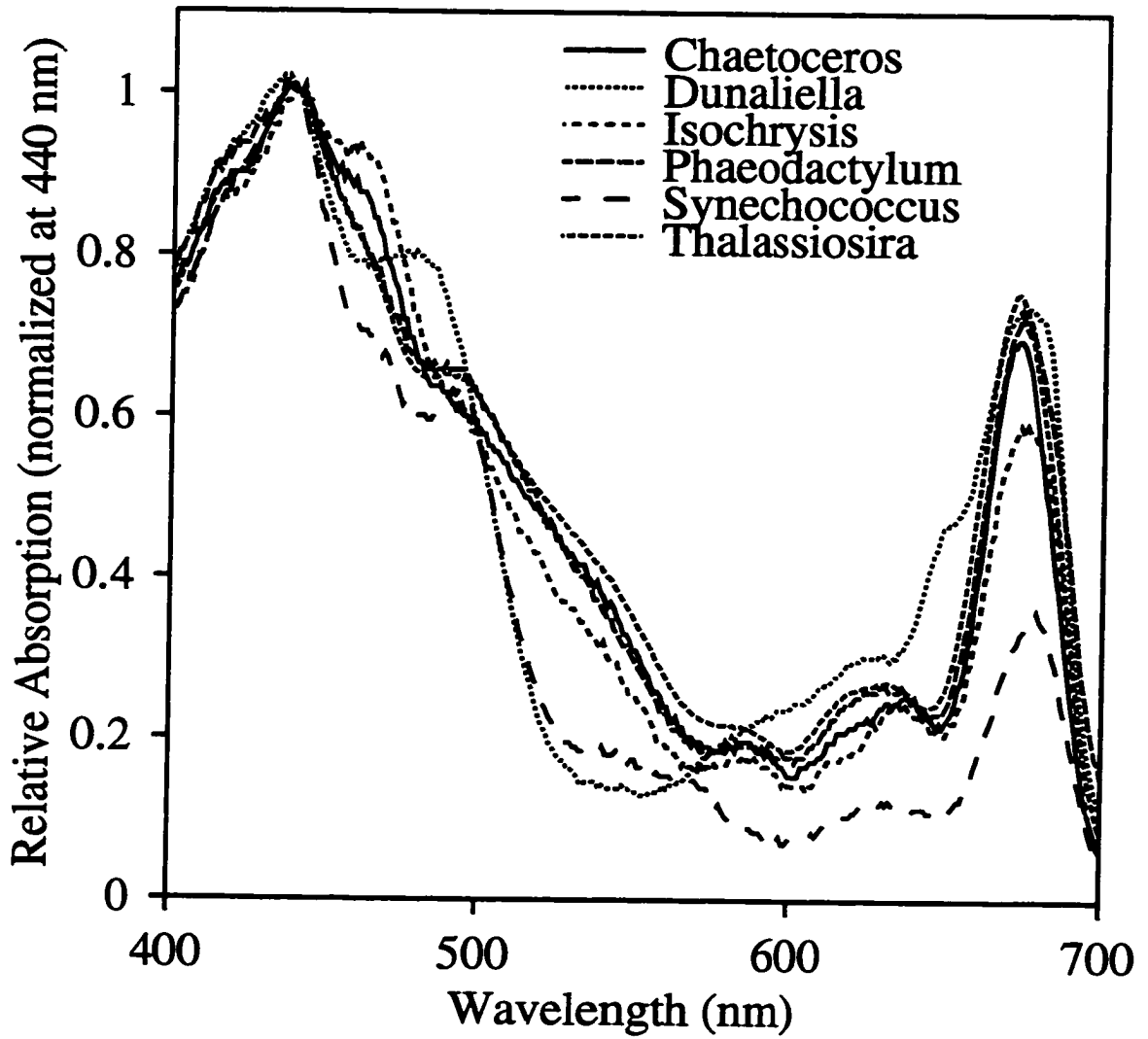


Figure 2.2

Figure 2.3. An illustration of one incubation box, with its light source, used in the determination of the photosynthetic action spectrum. The box contains 16 light bottles and one dark bottle. The bottles are arranged one behind the other to provide a continuous attenuation of the available irradiance. The light source is a slide-projector lamp assembly (150 Watts), and the interference (colour) filter is fitted in a slide slot.

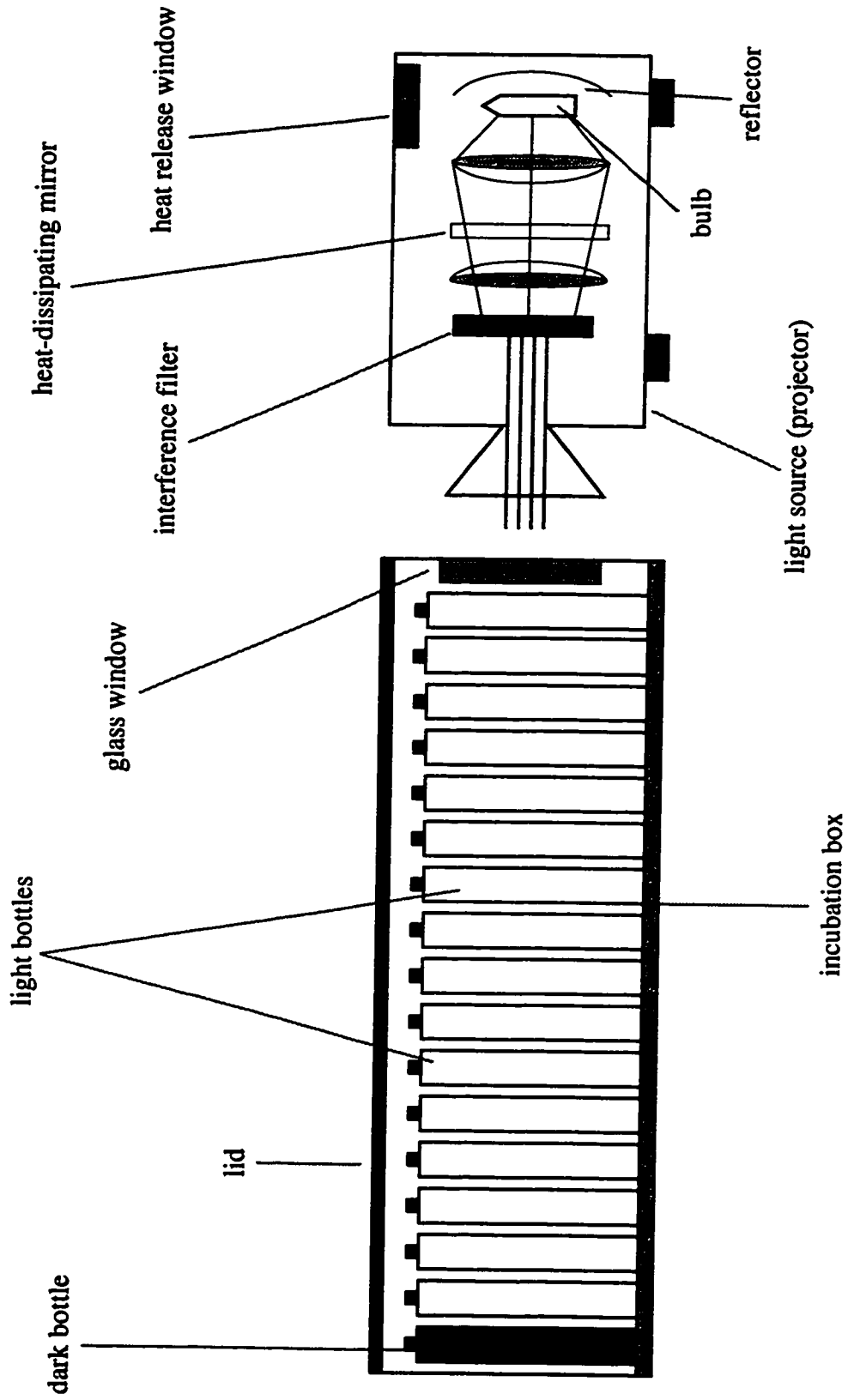


Figure 2.3

For each experiment, 12 identical boxes were used, each one illuminated by irradiance of a different waveband. The twelve bands were chosen to correspond to the maxima of absorption bands of major phytoplankton pigments (Hoepffner & Sathyendranath 1991) and the wavebands of the satellite sensor, Wide Field-of-view Sensor, SeaWiFS (Hooker et al. 1992). The selected interference filter wavelengths, the SeaWiFS wavebands and the absorption bands of phytoplankton pigments are shown in Table (2.1).

The samples were incubated for three hours and filtered immediately onto GF/F filters (Whatman); fumed with concentrated hydrochloric acid (for about five minutes) to purge unincorporated ^{14}C , and counted using a liquid scintillation counter (Beckman LS 5000 CE). The ^{14}C activity of the dark bottle was subtracted from that of the light bottles, and the carbon fixed was calculated according to Strickland & Parsons (1972). Production P ($\text{mg C m}^{-3} \text{ h}^{-1}$) was then normalized to biomass B ($\text{mg chl-}a \text{ m}^{-3}$) to yield biomass-specific production, P^B ($\text{mg C (mg chl-}a)^{-1} \text{ h}^{-1}$).

The irradiance I ($\mu\text{mol m}^{-2} \text{ s}^{-1}$) reaching the bottles was measured using a 4π -collector light meter (Biospherical Instruments), by inserting the sensor into each bottle. The initial slope of the P^B vs. I curve for a wavelength λ , $\alpha^B(\lambda)$ [$\text{mg C (mg chl-}a)^{-1} \text{ h}^{-1} (\mu\text{mol m}^{-2} \text{ s}^{-1})^{-1}$], was determined by linear regression of P^B on I (incident quanta) for each incubation waveband. Since I was interested in the linear part of the P^B vs. I curve, the data points tending to saturation, and any outliers, were detected and omitted at the 1% significance level (Snedecor & Cochran 1989). Linear regression results were excellent for all bands and stations, giving coefficients of determination $r^2 \geq 0.96$. A plot of $\alpha^B(\lambda)$ as a function of λ gave the photosynthetic action spectrum.

There was considerable variation in the shape of the measured action spectra from the different stations (see Figure 2.4a). The absorption spectra corresponding to the action spectra are also shown in Figure (2.4b), after normalization to 1 at 440 nm.

Table 2.1. Wavelengths of maximum transmission of the 12 interference filters used in the spectral incubator, and their relation to absorption bands of major phytoplankton pigments – chlorophyll-*a* (chl-*a*), chlorophyll-*b* (chl-*b*), chlorophyll-*c* (chl-*c*), carotenoids (carot.) and phycobilins (phycob), and the wavebands of the satellite sensor, the SeaWiFS. The SeaWiFS wavebands are taken from Hooker et al. (1992). The pigment absorption bands are taken from Neori et al. (1986); Lewis et al. (1986); Hoepffner and Sathyendranath (1991); and Johnsen et al. (1994a).

| Interference Filters | | | SeaWiFS Wavebands | | Pigment Absorption Bands | | |
|----------------------|----------|------------|-------------------|------------|--------------------------|-------------|----------------|
| Centre (nm) | Corion # | Width (nm) | Centre (nm) | Width (nm) | Pigment | Centre (nm) | Halfwidth (nm) |
| 415 | 204A | 10 | 412 | 20 | chl- <i>a</i> | 410-415 | 19-24 |
| 440 | P906 | 10 | 443 | 20 | chl- <i>a</i> | 433-436 | 29-37 |
| 460 | S264 | 10 | – | – | chl- <i>c</i> | 459-462 | 26-39 |
| 460 | | 10 | – | – | chl- <i>b</i> | 463-466 | 36-45 |
| 490 | P706 | 10 | 490 | 20 | carot. | 487-491 | 41-54 |
| 490 | | 10 | | | phycob | 490-500 | |
| 510 | U051 | 10 | 510 | 20 | phycob | 500-520 | |
| 532 | X721 | 10 | – | – | carot. | 529-536 | 45-54 |
| 550 | X489 | 25 | 555 | 20 | phycob | 540-565 | |
| 580 | V900 | 10 | – | – | chl- <i>c</i> | 579-586 | 43-54 |
| 600 | | 25 | – | – | – | – | – |
| 630 | U607 | 10 | – | – | chl- <i>c</i> | 625-645 | |
| 650 | 697A | 25 | – | – | chl- <i>b</i> | 640-654 | 21-37 |
| 670 | 409A | 10 | 670 | 20 | chl- <i>a</i> | 674-678 | 20-28 |

Figure 2.4. Shapes of measured spectra for all the 20 stations sampled during the cruise. The spectra are normalized to 1 at 440 nm to compare the shapes: (a) Action spectra (b) Absorption spectra. In both cases, the thick lines represent the average spectrum of the 20 spectra.

Measured Spectra for all Stations: 1992 Cruise

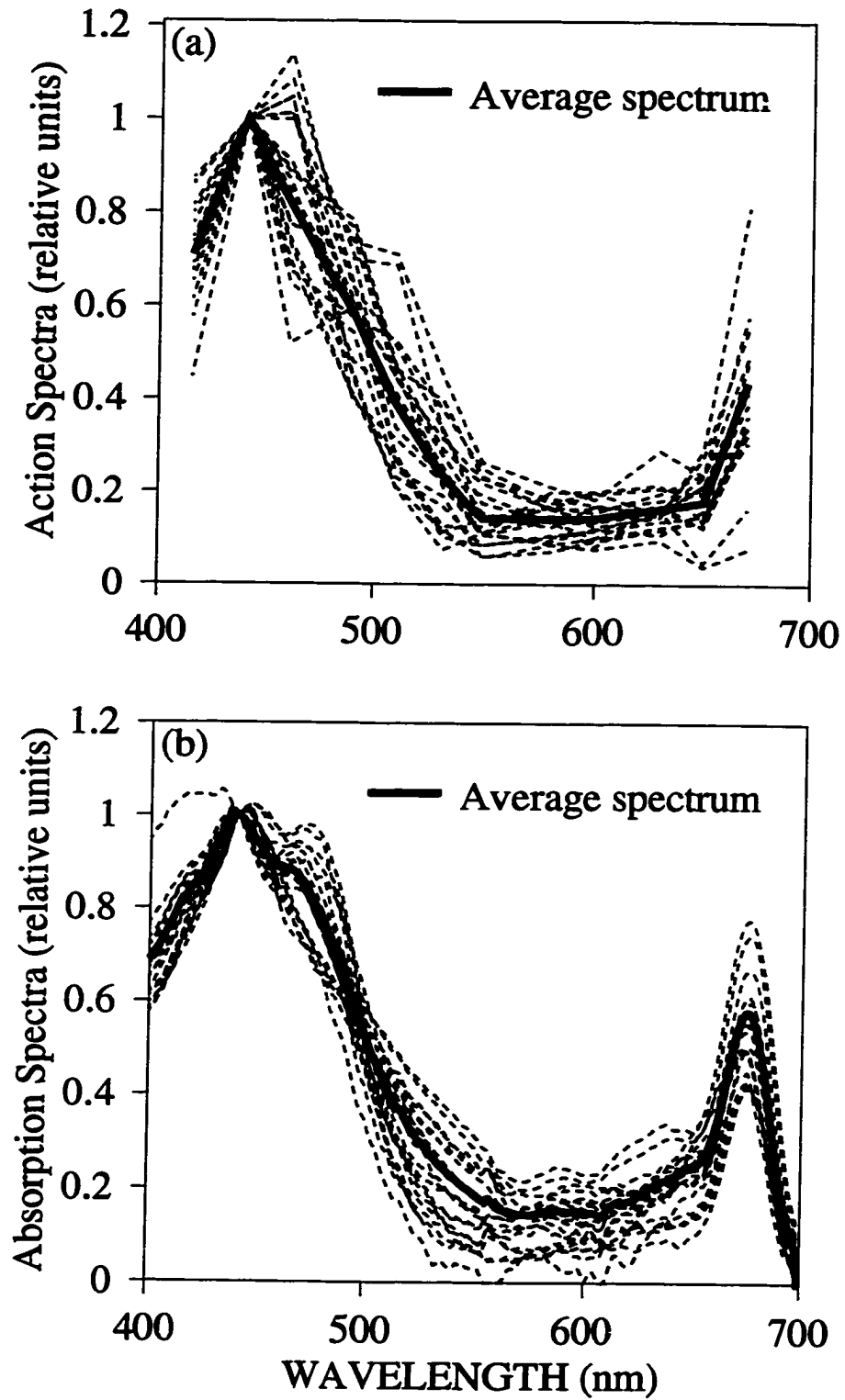


Figure 2.4

2.2.4 Broad-band Photosynthesis-Light Parameters

Broad-band P^B vs. I experiments were conducted by incubating phytoplankton samples for three hours onboard the ship, according to the procedure described in Irwin et al. (1990). The equation of Platt et al. (1980) was fitted to the P^B vs. I data, to give the photosynthetic parameters α^B and P_m^B ($\text{mg C (mg chl-}a)^{-1} \text{ h}^{-1}$), which is the value of P^B at saturating irradiance.

The broad-band α^B so-estimated was corrected for the bias due to the spectral quality of the incident irradiance. The emission spectrum of the tungsten-halogen lamp used in the incubator was not neutral; the spectral quality of the light could be further modified through absorption by water samples and by the walls of incubation bottles. To assess the change in spectral quality of the incident light from the first to the last bottle in the incubation box (pathlength of 0.27 m), the spectrum of the light incident on the last bottle was estimated using an exponential decay function, in which the exponent was set to the product of the measured absorption coefficient of a sample bottle filled with water (m^{-1}) and the pathlength (m).

The resulting spectrum was not significantly different from the spectrum of the light incident on the first bottle (Figure 2.5), suggesting that the deviation of the spectrum from its original shape, as it passed through the samples, was negligible and could be ignored. For a comparable pathlength (0.3 m), but with a different type of lamp, Babin et al. (1994) calculated the error in the computed light absorption, which might be incurred by assuming a constant irradiance spectrum, and also found it to be negligible. Therefore, the broad-band α^B was corrected only for the spectral quality of the light from the tungsten-halogen lamp.

Figure 2.5. Tungsten-halogen lamp spectra, normalized to their mean value to define the shape. The dashed line indicates the original shape of the spectrum; the solid line shows the spectral shape of the irradiance reaching the last bottle in the incubator. The label “corrected” is used to indicate that absorption by the water sample and the bottle walls is accounted for. There is no significant change in the shape of the spectrum after passing through the bottles. The solid line was used in the computation of the correction factor X , as explained in the text.

Tungsten Halogen Lamp Spectra

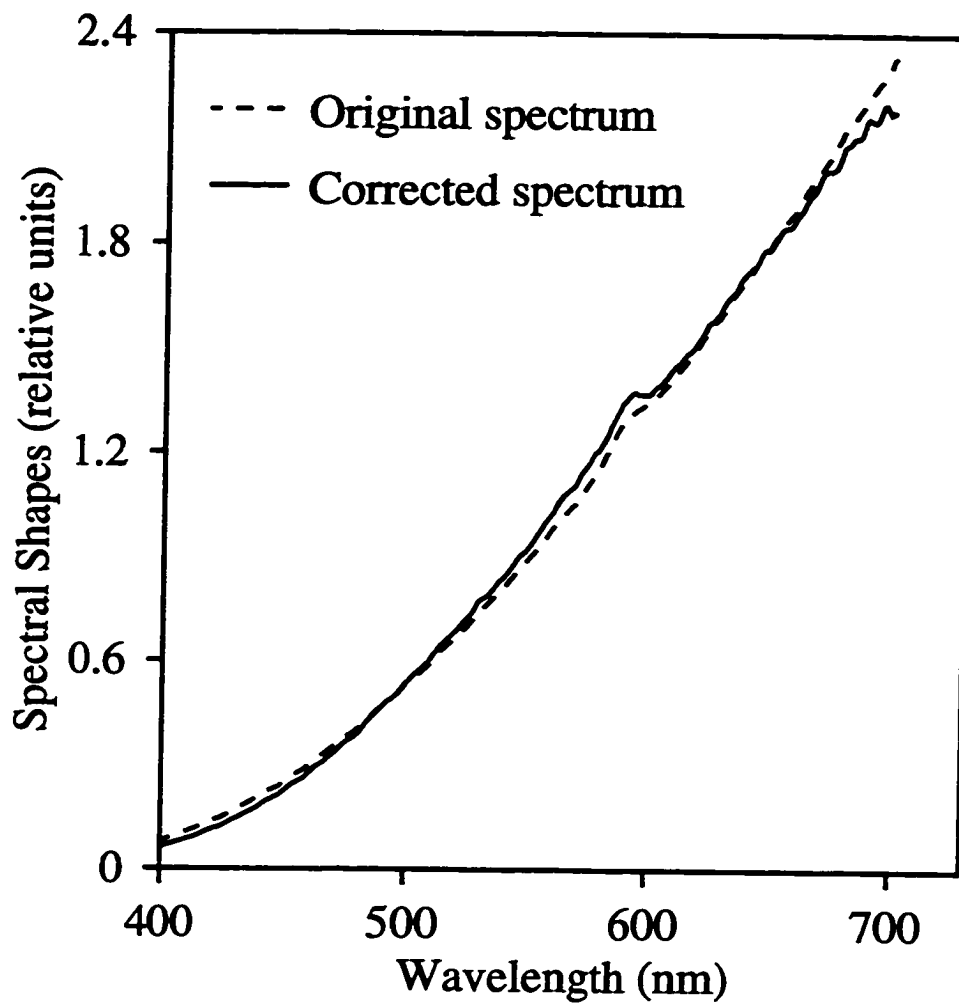


Figure 2.5

The tungsten-halogen lamp spectrum has a minimum in the blue and increases (quasi-linearly) to a maximum in the red part of the spectrum (Kingslake 1965, see also Figure 2.5). This implies that the light absorbed by the water sample will be different from what would be absorbed by the same sample if the incident light were spectrally neutral. To correct for this bias, the ratio (X , dimensionless) of the unweighted, spectral-mean absorption of phytoplankton to the mean absorption coefficient weighted by the shape of the emission spectrum of the tungsten-halogen lamp was used. The spectral, unweighted mean absorption of phytoplankton in the sample, \bar{a}_p , was given by:

$$\bar{a}_p = \frac{\int_{400}^{700} a_p(\lambda) d\lambda}{\int_{400}^{700} d\lambda}, \quad (2.2)$$

where $a_p(\lambda)$ is the phytoplankton absorption coefficient at λ . The weighted mean absorption that accounts for the spectral quality of the tungsten-halogen spectrum was computed as:

$$\bar{a}_T = \frac{\int_{400}^{700} a_p(\lambda) I_T(\lambda) d\lambda}{\int_{400}^{700} I_T(\lambda) d\lambda}, \quad (2.3)$$

where \bar{a}_T is the weighted mean absorption coefficient for the incubator and $I_T(\lambda)$ is the incident (tungsten-halogen lamp) irradiance in the incubator at λ .

The correction factor, the ratio X , is then given by:

$$X = \frac{\bar{a}_p}{\bar{a}_T}. \quad (2.4)$$

This kind of correction for the spectral quality of the incubation lamp has been applied by other workers (for example, Dubinsky et al. 1986, Cleveland et al. 1989, Schofield et al. 1991, Babin et al. 1995).

The calculated value of X ranged from 1.2 to 1.8, for the entire data set, showing that the mean absorption weighted by the tungsten-halogen spectrum was much lower than the unweighted mean. To test whether the use of this correction factor is justified, the linear regression of uncorrected broad-band α^B on the spectral

mean of $\alpha^B(\lambda)$ was examined, and it was found that the slope of $0.59 \pm 0.13(\text{SE})$ (Figure 2.6a) was significantly different from 1.0 at the 5% level (t -test, $n = 20$). When the same regression was repeated using the corrected α^B values (Figure 2.6b), the slope became 0.91 ± 0.21 , not significantly different from 1.0 ($n = 20$).

Therefore, each measured broad-band α^B was multiplied by its corresponding X , to correct for the bias introduced by the shape of the spectrum of the tungsten-halogen lamp. The corrected broad-band α^B , for all stations and depths sampled ($n = 60$), varied by a factor of about 11 (ranging from 0.013 to 0.142 mg C (mg chl-*a*)⁻¹ h⁻¹ ($\mu\text{mol m}^{-2} \text{s}^{-1}$)⁻¹); and the corresponding P_m^B , range from 1.22 to 11.22 mg C [mg chl-*a*]⁻¹ h⁻¹], varied by a factor of about 9.

2.2.5 *In situ* Production

In situ production was measured at seven stations, at the time-series location. Water samples were collected from 11 depths between the surface and 100 m. Incubations were made from dawn to dusk as explained in Irwin et al. (1990). Daily primary production at each depth (mg C m⁻³ day⁻¹) was calculated as in Strickland & Parsons (1972), and the integrated water-column primary production, $P_{Z,T}$ (mg C m⁻² day⁻¹), was computed using the trapezoid rule (Britton 1956). The *in situ* $P_{Z,T}$ ranged from 1.0 to 2.45 g C m⁻² day⁻¹.

Figure 2.6. Linear regression analyses of broad-band α^B on spectral average of $\alpha^B(\lambda)$ for twenty stations sampled during the 1992 cruise. (a) Originally measured α^B , not corrected for any bias, with regression equation $Y = (0.59 \pm 0.13)X$ ($n = 20$, $r^2 = 0.53$). In this case, the slope is significantly different from 1.0 at the 5% level. (b) Measured α^B , corrected for the bias introduced by the tungsten-halogen lamp spectrum: $Y = (0.91 \pm 0.21)X$ ($n = 20$, $r^2 = 0.52$), the slope is not significantly different from 1.0. The regression lines pass through the origin. The low r^2 , indicating high scatter along the regression line, is caused by pooling 20 different stations.

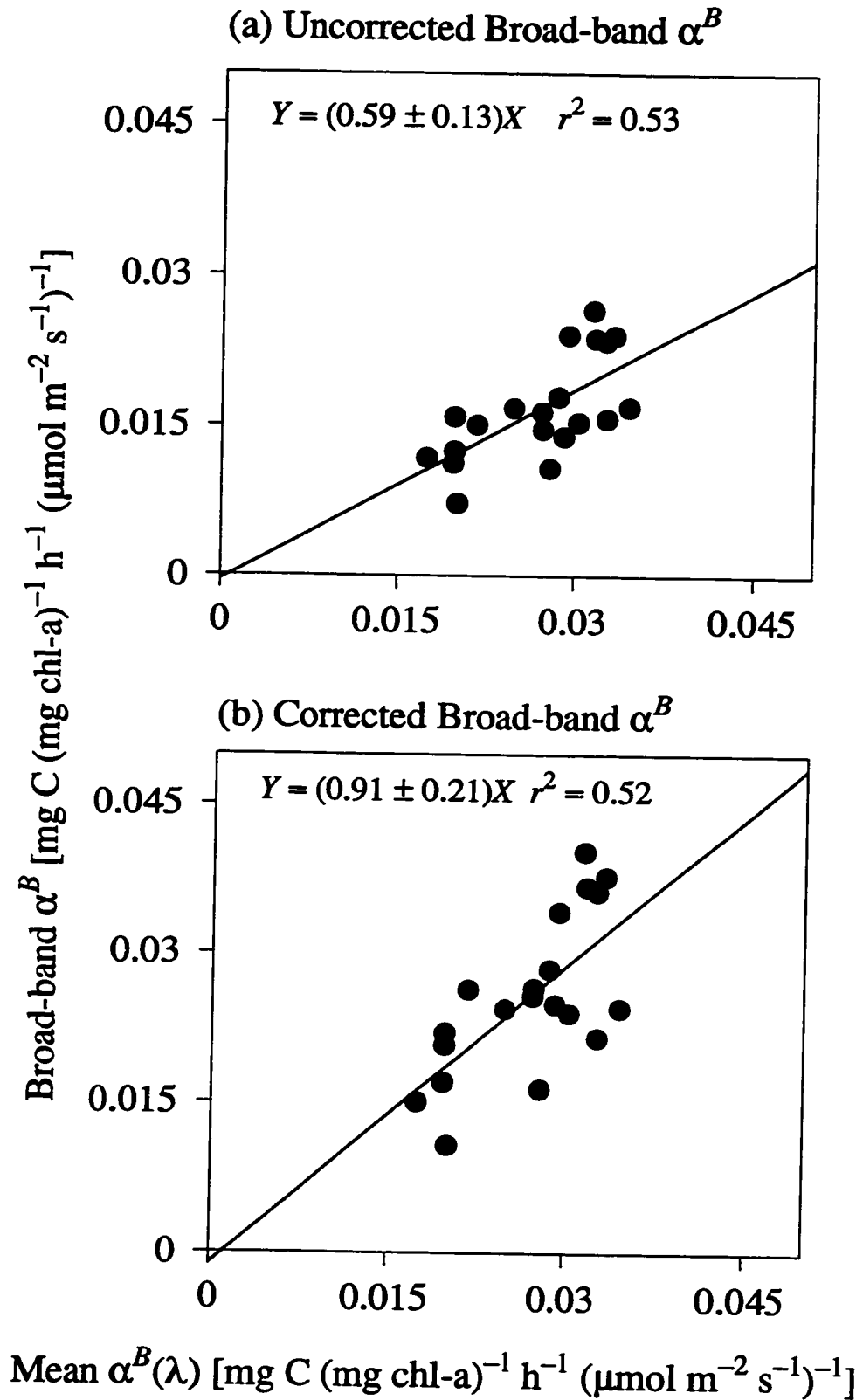


Figure 2.6

2.2.6 Biomass Concentration and Profiles

Water samples for chlorophyll-*a* measurements (three replicates 100-ml of samples) were filtered onto GF/F filters, then extracted in the dark using 90% acetone for 24 hours at 0°C. Chl-*a* concentration was determined fluorometrically by the method of Yentsch & Menzel (1963) as modified by Holm-Hansen et al. (1965). For determining the biomass profile, chl-*a* concentration was measured at 17 depths between the surface and 200 m. The biomass profile $B(z)$, where z is the depth, was then fitted to a shifted-Gaussian function (Platt et al. 1988):

$$B(z) = B_0 + h/(\sigma\sqrt{2\pi})\exp - ((z - z_m)^2/2\sigma^2), \quad (2.5)$$

where B_0 is the background pigment concentration (chl-*a* mg m⁻³); h is the total chlorophyll-*a* concentration within the peak (mg m⁻²); σ is the standard deviation around the peak value (m) and z_m is the depth of chlorophyll-*a* maximum (m). These four parameters were used to generate the chlorophyll-*a* concentration at each depth for the computation of water-column primary production.

2.2.7 Construction of the Action Spectrum

Spectrally-resolved primary production models that are based on available light require the action spectrum as one of the inputs. To measure the action spectrum using the ¹⁴C method, the samples have to be incubated at a range of irradiance levels for a series of wavelengths to get initial slopes of P^B vs. I curves as a function of wavelength. Methods for such direct determination of the action spectrum exist. Lewis et al. (1985a) developed a method for measuring the photosynthetic action spectrum by incubating 1-ml samples, in light of different wavelengths and magnitudes. Schofield et al. (1990) modified the method by including background light to account for the Emerson enhancement effect (Emerson 1957, see also Schofield et al. 1991, 1996).

Regardless of the method used, direct measurement of the photosynthetic action spectrum is expensive, complicated and labour-intensive, relative to broad-band α^B measurements. These limitations discourage routine determinations of the action spectrum at sea. As a consequence, only a few measurements have been made, mostly in the North Atlantic (e.g., Lewis et al. 1985a, b, 1988, Kyewalyanga et al. 1992) and some in the Southern California Bight (e.g., Schofield et al. 1991). Therefore, there is a need to develop simple and economical methods for determining the photosynthetic action spectrum.

In the present chapter, I explore the use of the shape of the phytoplankton absorption spectrum, and the magnitude of the broad-band α^B to construct the photosynthetic action spectrum. The main assumption underlying the method is that the shape of the action spectrum is similar to that of the phytoplankton absorption spectrum for a given water sample. For such an assumption to be valid, the effect of non-photosynthetic pigments on the shape of phytoplankton absorption and on the light energy transfer efficiency would have to be negligible. The validity of this assumption is discussed in the section (2.3.2) dealing with non-photosynthetic pigments.

The amplitude of the constructed action spectrum was determined from the magnitude of the broad-band α^B measured on the same sample, corrected for the spectral quality of the irradiance generated by the tungsten-halogen lamp. Thus, the action spectrum $\alpha_c^B(\lambda)$, with the subscript *c* indicating *constructed*, was estimated as:

$$\alpha_c^B(\lambda) = \frac{\alpha^B \times a_p(\lambda)}{\bar{a}_p}. \quad (2.6)$$

2.3 Results

2.3.1 Comparison of Constructed and Measured Action Spectra

The shape of the action spectrum (and that of the absorption spectrum) varies from one station to another (Figure 2.4). However, there is a good agreement between the shapes of the constructed and the measured action spectra at each station, for all the stations sampled (see Figure 2.7, for an example). When the constructed $\alpha^B(\lambda)$ are plotted against the measured values (Figure 2.7c), a slope of 1.0 would imply perfect agreement between amplitudes, and a high coefficient of determination (r^2) that the shapes of the spectra were well matched. A slope of less than 1.0 would show that the constructed spectrum had a lower amplitude compared with the measured one, and *vice versa*.

Out of the 20 stations, the slopes of 15 stations (75% of the data) were found to be not significantly different from 1.0, at the 1% significance level (*t*-test): the slopes of 4 stations were found to be significantly lower than 1.0, and only one station had a slope significantly higher than 1.0. The four stations that had slopes significantly less than 1.0 (see Figure 2.8 for an example) were located in coastal waters, two from the eastern and the other two from the western North Atlantic. These stations had low broad-band α^B , leading to low amplitudes of the constructed action spectra relative to the measured ones. None of the intercepts was significantly different from zero. On average, 93% of the variance in the shape of the measured action spectrum could be explained by the shape of the constructed action spectrum.

In the next section, I analyse various factors that could affect the constructed action spectrum, and assess the magnitude of errors caused by such factors, in the computed water-column primary production.

Figure 2.7. An example of the comparison of measured and constructed action spectra from Stn 4, (80 m); sampled on 21 September 1992: (a) The amplitudes and (b) the shapes; the spectra are normalized to their mean values. (c) Linear regression: the slope of 0.986 ($n = 12$, $r^2 = 0.98$) is not significantly different from 1.0 at the 1% level.

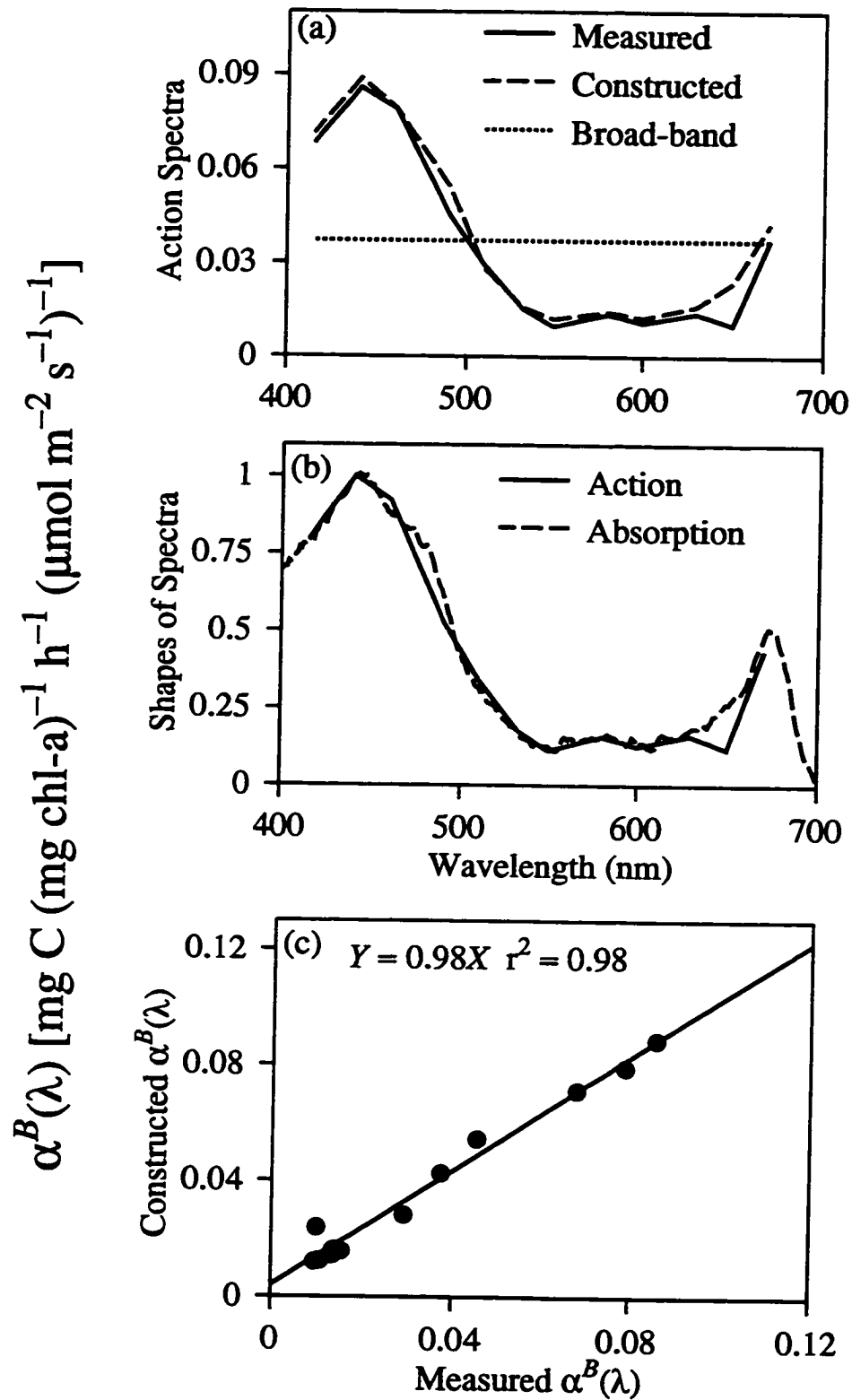
Station4: 21st September 1992

Figure 2.7

Figure 2.8 As in Figure (2.7), but for a station occupied on 4 October 1992. This is an example in which the slope of the regression line 0.61 ($n = 12$, $r^2 = 0.96$) being significantly lower than 1.0 at the 1% level.

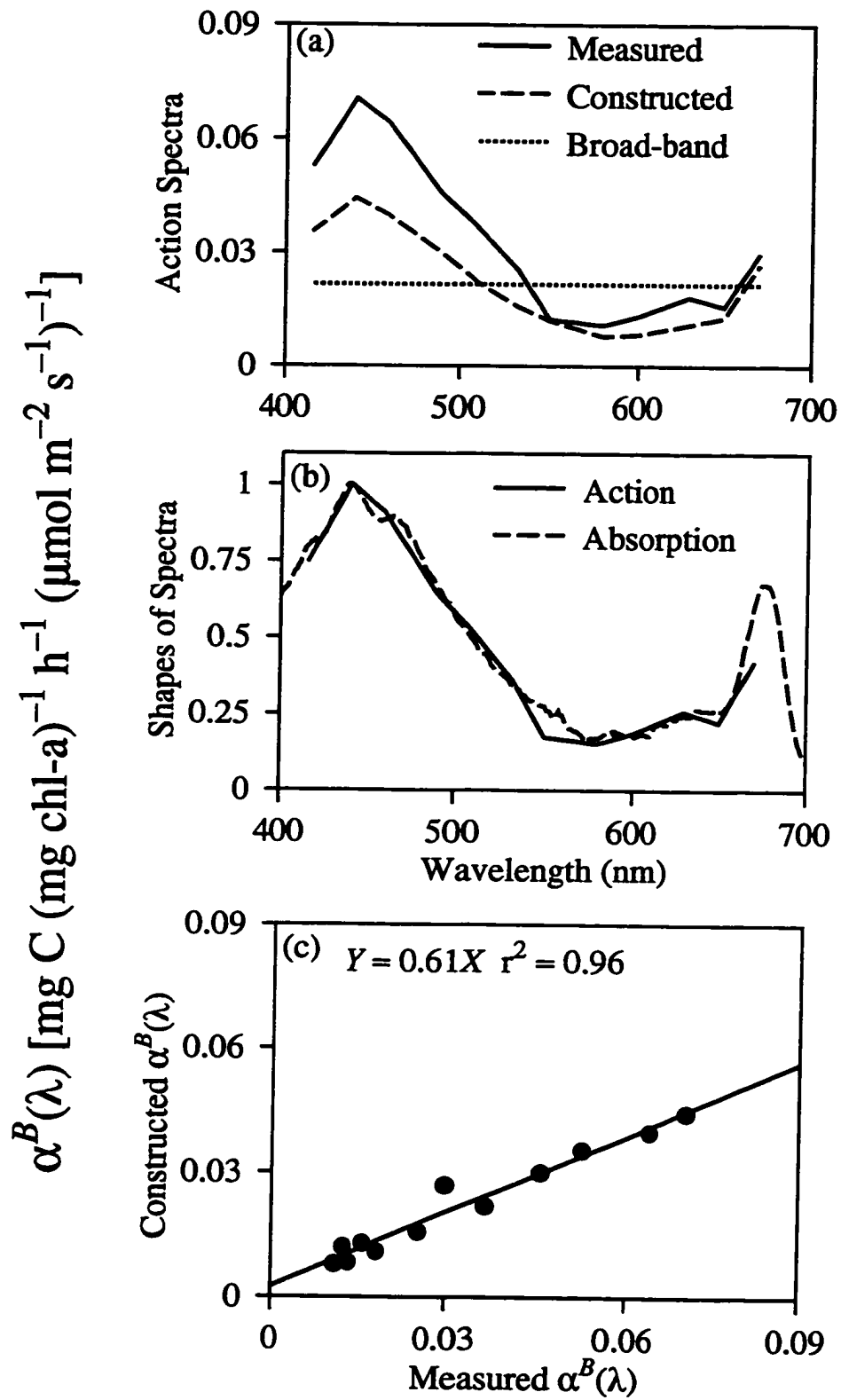
Station 17: 4th October, 1992

Figure 2.8

2.3.2 The Effect of Non-photosynthetic Pigments on the Shape of the Constructed Action Spectrum

The comparison of measured and constructed action spectra revealed some differences, though small, in the shapes of the spectra. In most cases, the mis-match in the shapes occurred near 415 and 490 nm. Assuming, for the moment, that the shape of the measured action spectrum is perfect, that is, with no measurement errors, then a possible source of the difference in shapes between the measured and constructed spectra could be the presence of photosynthetically-inactive pigments, which absorb light but do not transfer the energy to the reaction centers for use in photosynthesis. The commonly-known, non-photosynthetic pigments are photoprotective carotenoids. The degradation products of chlorophyll-*a* do not transfer excitation energy to reaction centers; therefore, they will also be regarded as non-photosynthetic pigments in this context.

It is known that phaeopigments have their blue absorption maximum near 409–415 nm (Zscheile & Comar 1941, Vernon 1960, Johnsen & Sakshaug 1993), whereas photoprotective pigments, such as zeaxanthin, diatoxanthin and diadinoxanthin (Siefermann-Harms 1987, Bidigare et al. 1989, Demers et al. 1991, Demmig-Adams & Adams 1992, Johnsen et al. 1994b) absorb in the same region as photosynthetic carotenoids, i.e., between 400 and 550 nm. Hoepffner & Sathyendranath (1991, 1993) decomposed the absorption spectrum of phytoplankton pigments into 13 Gaussian bands representing absorption by chlorophylls and carotenoids. Two of the bands had peaks centered nominally at 415 nm, and 490 nm. These two bands were adopted as the target bands to study the potential effects of absorption by phaeopigments (absorption peak at 415 nm) and photoprotective carotenoids (with absorption peak at 490 nm).

One of the approaches that could be used to assess the effect of non-photosynthetic pigments is the comparison of measured and constructed action spectra at the target wavelengths. The measured action spectrum is affected

only by photosynthetically-active pigments, whereas the constructed one, being derived from the absorption spectrum, is influenced by both photosynthetic and non-photosynthetic pigments. Therefore, the ratio of the measured $\alpha^B(\lambda)$ to the constructed $\alpha_c^B(\lambda)$, at a target Gaussian peak wavelength λ , would give the fractional absorption F (cf. Johnsen et al. 1994b) by photosynthetically-active pigments within that particular Gaussian band:

$$F = \frac{\alpha^B(\lambda)}{\alpha_c^B(\lambda)}. \quad (2.7)$$

Then, the fraction of absorption by non-photosynthetic pigments would be $[1 - F]$. This fraction $[1 - F]$ could be subtracted from the amplitude of the corresponding band and the process repeated for each of the target Gaussian bands. Next, the Gaussian bands so-corrected could be used to reconstruct an absorption spectrum free of the effects of non-photosynthetic pigments. Finally, the shape of the corrected absorption spectrum could be used to construct the action spectrum.

This proposed correction for non-photosynthetic pigments was tested under idealized conditions, using simulated action spectra of six phytoplankton species (cultures). To simulate the action spectra, first the absorption spectra of six cultures were decomposed into Gaussian absorption bands. Then, absorption spectra of photosynthetic pigments were generated, by assuming that 50% (an extreme case) of the absorption at the two target bands was due to non-photosynthetic pigments. This “photosynthetic absorption spectrum” was used to create the action spectrum, assuming a wavelength-independent quantum yield. The correction procedure outlined above was tested on these six pairs of absorption and action spectra, and it was seen that, at least under these ideal simulated conditions, the proposed procedure of retrieving the action spectrum from the shape of the absorption spectrum and the broad-band α^B , worked well for the absorption spectra of the six species chosen for the analysis (Figure 2.2).

Next, the F and $[1 - F]$ fractions at the two peak wavelengths for the field samples were calculated and used to correct the absorption spectra. Then, the

shapes of the corrected absorption spectra were used to construct the action spectra free of non-photosynthetic pigments. The calculated fractions of non-photosynthetic pigments at the two target wavelengths (415 and 490 nm) ranged from 0 to 28% and 0 to 39%, respectively. However, at most of the stations, the contribution of non-photosynthetic pigments at the target bands was low (below 10%), suggesting that these pigments did not have a big influence on the shapes of the measured absorption spectra. To evaluate the impact of this correction on water-column production, the constructed (corrected) action spectra were used to compute primary production at each station with a spectrally-resolved model (Sathyendranath & Platt 1989), according to which, production $P(z)$ at depth is given by,

$$P(z) = \frac{B(z)\Pi(z)}{\sqrt{1 + (\Pi(z)/P_m^B(z))^2}}, \quad (2.8)$$

where, $B(z)$ is the biomass at depth z , and $\Pi(z)$ is given by:

$$\Pi(z) = \sec \theta \int_{400}^{700} \alpha^B(\lambda) I_d(z, \lambda, \theta) d\lambda + 1.20 \int_{400}^{700} \alpha^B(\lambda) I_s(z, \lambda) d\lambda, \quad (2.9)$$

where I_d and I_s are the direct and diffuse components of the available light, as computed in Sathyendranath & Platt (1988), θ is the sun zenith angle in water and 1.20 is the inverse of the mean cosine for perfectly diffuse skylight after refraction at a flat sea surface.

First, the depth at which the irradiance reached 0.01% of the surface irradiance was determined for each station. This depth was assumed to be, or to exceed, the photic depth (it ranged from 52 to 130 m for the 20 stations processed). Next, the water-column from the surface to the photic depth was partitioned into 250 layers. Therefore, the depth interval varied from station to station, depending on the photic depth. The shape and amplitude of the action spectrum were assumed to be the same throughout the water-column. However, the magnitude of P_m^B and the total particulate absorption spectrum (for computation of underwater light transmission)

were allowed to vary between the mixed layer and the deep layer. The mixed-layer depth was defined as the depth at which the temperature change between the surface and that depth was ≥ 0.1 °C.

Values of P_m^B and particulate absorption (required for computation of spectral light transmission underwater) in the two layers were assigned based on the broad-band incubations of samples and the measured total particulate absorption spectra from three depths at each station. If one depth was sampled for P^B vs. I parameters and particulate absorption in the mixed-layer or the deep-layer, its value was used throughout that layer. If two depths were sampled in either of the layers, the parameters or spectra were averaged and the averages were used in the layer. If all three depths sampled were situated in the mixed-layer, then the average of the three measurements was used for the entire water-column. Other inputs, such as the biomass distribution and the available irradiance were computed for each of the 250 layers of the photic zone.

Using the trapezoid rule, the computed $P(z)$ values were integrated from the surface to the photic depth to give water-column production, which was then integrated over the day-length (at time intervals of 30 minutes) to give daily, water-column, primary production at each station $P_{Z,T}$ ($\text{g C m}^{-2} \text{ day}^{-1}$).

The calculation was then repeated using the constructed (uncorrected) action spectrum. The two $P_{Z,T}$ values (at each station) were compared, and the maximum relative difference was only 2.3% (see Figure 2.9). This indicates that, at least for the data discussed here, the effects of the degradation products of chl-*a* and that of the photoprotective carotenoids on the constructed shapes of the action spectra had negligible consequences for computed water-column production.

The procedure applied here of comparing the shapes of measured and constructed action spectra, is one of the ways to quantify the effect of non-photosynthetic pigments. It was possible to apply the procedure to the field samples because the measured action spectra were available. Otherwise, an independent estimate of the pigments would have to be made (Jeffrey 1981, Mantoura & Llewellyn

1983, Bidigare et al. 1989, Sakshaug et al. 1991, Head & Horne 1993, Johnsen et al. 1994b), and information on the *in vivo*, specific absorption coefficients for these pigments would be needed.

Other approaches to determine action or absorption spectra free of non-photosynthetic pigments have been proposed (Neori et al. 1986, Bidigare et al. 1987, Sakshaug et al. 1991, Johnsen et al. 1994b, Sosik & Mitchell 1995). Bidigare et al. (1987, 1989) used a spectral reconstruction method, in which the absorption spectrum is reconstructed from *in vivo* absorption coefficients of the individual pigments and their respective concentrations. This method requires prior knowledge of major phytoplankton pigments present in the sample and their *in vitro* absorption spectra, which have to be wavelength-shifted to match their *in vivo* counterparts before the reconstruction process. Note that, to be able to incorporate the flattening effect of particles in suspension (Duysens 1956), additional information on the size distribution of particles would also be required.

Another approach is to use the *in vivo* fluorescence excitation spectrum, because it is influenced only by photosynthetically-active pigments. Neori et al. (1986, 1988) showed that the shape of the chlorophyll-*a* excitation spectrum is a good proxy for the photosystem (PS) II O₂-evolution action spectrum. The *in vivo* fluorescence excitation spectrum was also used by Sakshaug et al. (1991) (see also Johnsen et al. 1992, Johnsen & Sakshaug 1993), and by Sosik and Mitchell (1995), who showed a significant difference between the absorption spectrum of total phytoplankton pigments and that of photosynthetically-active pigments. The results from this study do not necessarily contradict the findings of Sosik & Mitchell (1995), since they apply only to a particular region and time of year. Regional and seasonal effects depend on the phytoplankton populations present, their light history, and physiological state, which could influence the amount and type of non-photosynthetic pigments present.

Figure 2.9. Daily water-column primary production at each of the twenty stations, computed using different action spectra: solid line, $P_{Z,T}(1)$ (filled circles), the measured action spectra; dotted line, $P_{Z,T}(2)$, constructed action spectra, not corrected for non-photosynthetic pigments; short-dashed line, $P_{Z,T}(3)$, same as for the dotted line, but the spectra were corrected for the presence of non-photosynthetic pigments; and long-dashed line, $P_{Z,T}(4)$, a constant *shape* (an average of the 20 measured action spectra), scaled to broad-band α^B values. For more details, see Table (2.4).

Daily Water-Column Primary Production

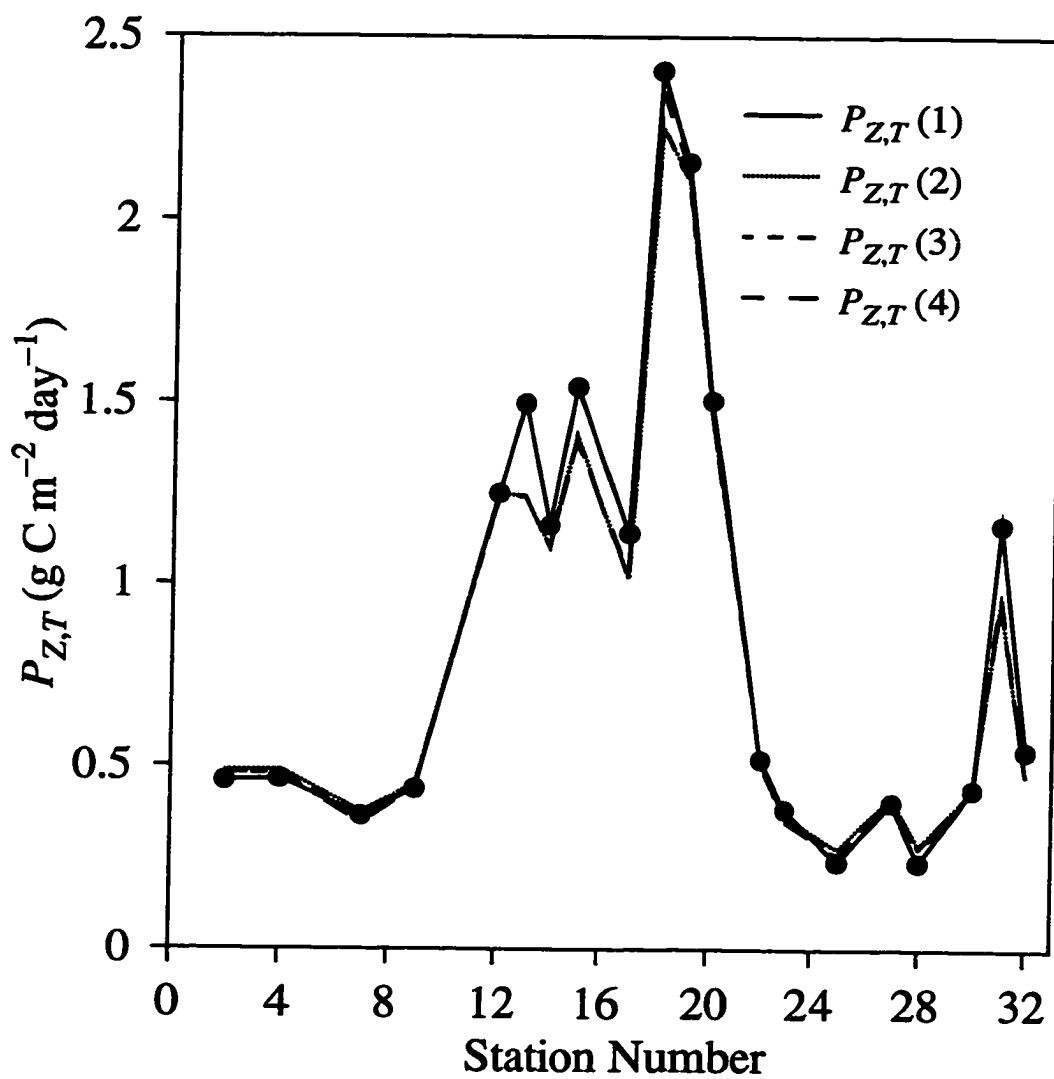


Figure 2.9

2.3.3 The Effect of Random and Systematic Errors on the Constructed Action Spectrum

Having assessed the effect of non-photosynthetic pigments on the shape of the constructed action spectrum, I next examined the effects of random and systematic errors in estimating the action spectrum, on the computed water-column primary production. A simulated 12-point action spectrum (simulated from the absorption spectrum of *Chaetoceros gracilis* grown in cultures) was chosen as the reference (error-free) for this analysis.

2.3.4 Sensitivity Analysis of Random Errors

Given the *Chaetoceros gracilis* action spectrum as a reference, a random-number generator was used to create errors that were less than or equal to $\pm 20\%$ of the reference values. Each of these numbers was then used to modify the $\alpha(\lambda_i)$ of the reference action spectrum, to simulate spectra with random measurement errors. The figure of 20% was assigned arbitrarily, but it was based on the results of Platt et al. (1977), who showed the standard error of the mean for estimation of α^B , in both algal cultures and natural phytoplankton populations, to be about 18%.

Some 50 action spectra were produced in this manner, and used to calculate primary production as a function of depth, $P(z)$ (Equation 2.8), computed for sun at the zenith using the atmospheric transmission model of Bird (1984) as implemented by Sathyendranath & Platt (1988). For simplicity, the action spectrum, P_m^B , and chlorophyll-*a* concentration were kept constant with depth. The calculation was repeated using a range of chl-*a* concentrations (between 0.01 and 10.0 mg m⁻³) to assess the sensitivity of errors in the computed production to changing biomass. Furthermore, calculations were repeated using the minimum and the maximum P_m^B values encountered during the cruise, of about 1.0 and 12.0 mg C (mg chl-*a*)⁻¹ h⁻¹,

respectively. The $P(z)$ values were integrated (trapezoid rule) over depth to give water-column primary production, P_Z , for comparison with P_Z computed using the reference action spectrum.

The errors in the realized P_Z values relative to the reference could be positive or negative. An average of the 50 relative errors for each chl-*a* concentration was computed from *absolute* values of the errors, to avoid cancellation of signs. Table (2.2) shows the average and the range of relative errors for each chl-*a* concentration for the maximum P_m^B value. The errors increased with decreasing biomass. The average errors were lower for the minimum P_m^B (the highest average error was less than 0.8%) than for the maximum P_m^B . This may be explained as follows. Assume a euphotic zone divided into two layers separated by a saturation depth, Z_{I_k} , defined as the depth at which the irradiance $I = I_k = P_m^B/\alpha^B$, the nominal irradiance at which light saturation sets in. Above Z_{I_k} , production is light-saturated and, thus, P_m^B has a significant influence on $P(z)$ compared with α^B . Below the saturation depth, however, production is light-limited. Therefore, α^B has a significant influence on $P(z)$ below the saturation depth. Thus, when P_m^B is high, the light-saturation layer will be less deep (shallow Z_{I_k}) than when P_m^B is low. In such cases, the light-limited area of the euphotic zone would be a significant part of the total euphotic layer, and consequently errors in α^B would have a large effect on the integrated, water-column, primary production. The reverse would be true for a low P_m^B value. Overall, the average errors did not exceed 1.8% for the entire range of biomass and the two P_m^B values tested.

Table 2.2. Sensitivity analysis of errors in water-column primary production for a range of chlorophyll-*a* concentrations (mg m^{-3}) caused by random errors on the action spectrum of up to $\pm 20\%$. The averages were computed using absolute values of 50 relative errors. The computations were carried out for noon irradiance and $P_m^B = 12.0 \text{ mg C (mg chl-}a)^{-1} \text{ h}^{-1}$.

| Biomass Chlorophyll- <i>a</i> | Relative Errors in Primary Production | | |
|----------------------------------|---------------------------------------|-----------|-----------|
| | % Average | % Maximum | % Minimum |
| 0.01 | 1.82 | 4.69 | 0.11 |
| 0.05 | 1.79 | 4.66 | 0.04 |
| 0.10 | 1.76 | 4.62 | 0.03 |
| 0.20 | 1.70 | 4.51 | 0.07 |
| 0.30 | 1.65 | 4.42 | 0.02 |
| 0.40 | 1.61 | 4.32 | 0.00 |
| 0.50 | 1.58 | 4.25 | 0.01 |
| 0.60 | 1.55 | 4.19 | 0.01 |
| 0.70 | 1.52 | 4.11 | 0.02 |
| 0.80 | 1.51 | 4.04 | 0.02 |
| 0.90 | 1.49 | 3.99 | 0.01 |
| 1.00 | 1.48 | 3.94 | 0.03 |
| 2.00 | 1.38 | 3.58 | 0.21 |
| 3.00 | 1.33 | 3.37 | 0.10 |
| 4.00 | 1.29 | 3.23 | 0.06 |
| 5.00 | 1.27 | 3.12 | 0.03 |
| 6.00 | 1.25 | 3.04 | 0.02 |
| 7.00 | 1.24 | 2.98 | 0.00 |
| 8.00 | 1.23 | 2.93 | 0.01 |
| 9.00 | 1.22 | 2.89 | 0.01 |
| 10.00 | 1.22 | 2.86 | 0.00 |

2.3.5 Sensitivity Analysis of Systematic Errors

To assess how water-column primary production is affected by systematic errors in the action spectrum, the reference, simulated, action spectrum of *C. gracilis* was again used. The reference action spectrum was subjected to systematic errors of up to $\pm 20\%$ in steps of $\pm 5\%$. In other words, all twelve $\alpha(\lambda_i)$ of the spectrum were either increased or decreased by 5, 10, 15 or 20%, to generate a total of eight action spectra, which differed systematically from the reference spectrum. Water-column primary production was computed using the different action spectra (one reference and eight subjected to systematic errors). The computation was done using noon irradiance, for biomass of $1.0 \text{ mg chl-}a \text{ m}^{-3}$, and the maximum P_m^B of $12.0 \text{ mg C (mg chl-}a)^{-1} \text{ h}^{-1}$.

The results of this computation are shown in Table (2.3). As expected, when $\alpha(\lambda_i)$ values were systematically underestimated, the water-column primary production was also underestimated (negative relative errors), and *vice versa*. The errors in water-column primary production ranged from -10.95 to 9.13% (Table 2.3), with an average of (absolute values) 6.3%. For comparison, *random* errors at the same biomass ($1.0 \text{ mg chl-}a \text{ m}^{-3}$) and P_m^B value ($12.0 \text{ mg C (mg chl-}a)^{-1} \text{ h}^{-1}$) ranged from 0 to 3.9%, with an average of about 1.5% (Table 2.2). Therefore, the errors in water-column primary production caused by systematic errors in the action spectrum are higher than those caused by random errors in the spectrum.

Table 2.3. Systematic errors on the action spectrum: Effect on water-column primary production ($\text{mg C m}^{-2} \text{ h}^{-1}$). The computations were carried out for noon irradiance, biomass of $1.0 \text{ mg chl-}a \text{ m}^{-3}$, and P_m^B of $12.0 \text{ mg C (mg chl-}a)^{-1} \text{ h}^{-1}$. Negative errors indicate underestimation and *vice versa*.

| Incremental Errors (%) | Primary Production | Relative Errors in Primary Production (%) |
|------------------------|--------------------|---|
| -20 | 194 | -10.95 |
| -15 | 201 | -8.22 |
| -10 | 207 | -5.48 |
| -5 | 213 | -2.74 |
| 0 | 219 | 0.00 |
| +5 | 224 | +2.28 |
| +10 | 229 | +4.57 |
| +15 | 234 | +6.85 |
| +20 | 239 | +9.13 |

2.3.6 Daily, Water-column, Primary Production: Comparison with Measured, *In Situ* Production

As in the last two sections, equation (2.8) was used to compute primary production $P(z)$, using the measured action spectrum (Sathyendranath & Platt 1989). Then, $P(z)$ was integrated over both depth and time, to get daily, water-column, primary production $P_{Z,T}$. These $P_{Z,T}$ values were then compared with the seven *in situ* $P_{Z,T}$ values measured at the time-series location. The *in situ* $P_{Z,T}$ (at Stns 12 to 20) ranged from 1 to 2.45 g C m⁻² day⁻¹, with a peak at Stn 18 (Table 2.4). The corresponding $P_{Z,T}$ computed using the measured action spectrum at the same stations (Stns 12 to 20) showed a similar range (from 1.25 to 2.41 g C m⁻² day⁻¹).

In addition, similar data of Kyewalyanga et al. (1992, spectrally-computed and *in situ* $P_{Z,T}$) from the Sargasso Sea, collected in April 1990, were included in the comparison. The *in situ* $P_{Z,T}$ values were used as benchmarks to test the performance of the spectrally-resolved model. A linear regression analysis of the computed $P_{Z,T}$ values on the *in situ* ones was performed ($r^2 = 0.91$). Because the intercept was not significantly different from zero (at the 5% level, *t*-test), the analysis was repeated with the regression line forced through the origin. The slope of the line, 1.02 ± 0.02 (slope \pm standard error), not significantly different from 1.0 (at $p = 0.05$, $n = 14$), showed a good agreement between *in situ* and spectrally-computed $P_{Z,T}$ (Figure 2.10).

Further, the r^2 value showed that 91% of the variation in the *in situ* $P_{Z,T}$ could be explained by the results of the spectrally-resolved model. Although Figure (2.10) shows only values greater than 0.8 g C m⁻² day⁻¹, the agreement between *in situ* and spectrally-computed $P_{Z,T}$ is known to hold for lower production values as well. Platt & Sathyendranath (1988) have shown a nearly one-to-one relation for data collected from diverse environments (five different regions sampled between 1983 and 1987), with $P_{Z,T}$ ranging from less than 0.1 to 2.5 g C m⁻² day⁻¹.

Table 2.4. *In situ* daily water-column primary production ($P_{Z,T}$ *in situ*) and daily water-column primary production $P_{Z,T}$ ($\text{g C m}^{-2} \text{ day}^{-1}$) computed using the measured and the constructed action spectra at each of the 20 stations sampled during the cruise. The percentage difference between the two computed $P_{Z,T}$ values is given in the last column.

| Station | $P_{Z,T}$ <i>in situ</i> | $P_{Z,T}^\dagger$ | $P_{Z,T}^\S$ | %¶ |
|---------|--------------------------|-------------------|--------------|-------|
| 2 | — | 0.460 | 0.488 | -6.2 |
| 4 | — | 0.465 | 0.490 | -5.5 |
| 7 | — | 0.364 | 0.375 | -3.0 |
| 9 | — | 0.438 | 0.450 | -2.7 |
| 12 | 1.067 | 1.250 | 1.250 | 0.0 |
| 13 | 1.403 | 1.497 | 1.243 | 17.0 |
| 14 | 1.397 | 1.163 | 1.103 | 5.2 |
| 15 | 1.304 | 1.542 | 1.409 | 8.6 |
| 17 | — | 1.140 | 1.107 | 10.8 |
| 18 | 2.450 | 2.407 | 2.254 | 6.3 |
| 19 | 1.939 | 2.158 | 2.117 | 1.9 |
| 20 | 1.003 | 1.505 | 1.476 | 1.9 |
| 22 | — | 0.519 | 0.519 | 0.0 |
| 23 | — | 0.383 | 0.366 | 4.5 |
| 25 | — | 0.240 | 0.275 | -14.4 |
| 27 | — | 0.402 | 0.419 | -4.2 |
| 28 | — | 0.238 | 0.283 | -18.6 |
| 30 | — | 0.439 | 0.438 | 0.3 |
| 31 | — | 1.165 | 0.952 | 18.3 |
| 32 | — | 0.545 | 0.473 | 13.3 |

† $P_{Z,T}$ computed using the measured action spectrum.

§ $P_{Z,T}$ computed using the constructed action spectrum.

¶ Percentage difference in the two computed $P_{Z,T}$ values.

Figure 2.10. Linear regression analysis of computed daily, water-column, primary production $P_{Z,T}$ on the *in situ* $P_{Z,T}$, for 14 stations. The filled circles show data sampled on the time-series location (this study); the empty circles represent data from Kyewalyanga et al. (1992), sampled from the Sargasso Sea in April 1990. The regression equation is $Y = (1.02 \pm 0.02)X$ ($n = 14$, $r^2 = 0.91$) with the slope not significantly different from 1.0 at the 5% significance level (the intercept was forced through the origin), indicating a good agreement between *in situ* and computed $P_{Z,T}$. The line is the 1:1 relation.

Daily Water-Column Primary Production
For Different Locations and Seasons

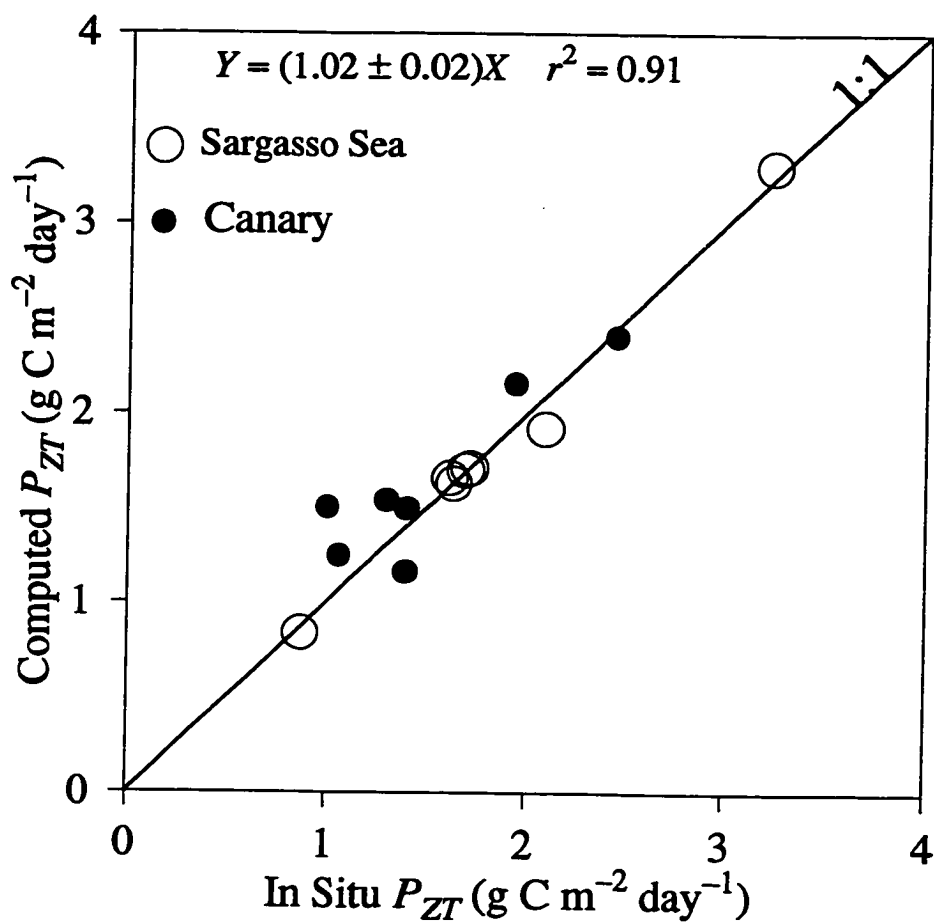


Figure 2.10

2.3.7 Assignment of Action Spectra in Computing $P_{Z,T}$: Comparison of Results Achieved Using Different Approaches

Since the computations of water-column primary production using the measured action spectrum were seen to perform well, they were used as the standard against which other computations were evaluated. The other computations were the same as the standard calculations in all respects, except in the assignment of action spectra. I have examined three alternative assignments: (a) constructed action spectra corrected for the effects of non-photosynthetic pigments; (b) constructed action spectra uncorrected for non-photosynthetic pigments; and (c) an invariant shape of the action spectrum throughout all the stations.

To compute $P_{Z,T}$ using a constant shape of the action spectrum for all the stations, an average spectrum of the twenty measured action spectra was determined (Figure 2.4a), and this average shape was scaled to the magnitude of the broad-band α^B measured at each station. For comparison, $P_{Z,T}$ was also computed using the shape of the action spectrum presented in Sathyendranath et al. (1989, their Figure 1), which is the commonly-applied spectral shape (see also Platt & Sathyendranath 1988, Platt et al. 1991, Sathyendranath et al. 1995). This shape was also scaled to the magnitude of the broad-band α^B measured at each station. Daily, water-column, primary production at each of the twenty stations computed using each of the assignments of action spectra is plotted in Figure (2.9) against station number.

The computed primary production using the measured action spectra (Figure 2.9, $P_{Z,T}(1)$) ranged from 0.24 to 2.41 g C m⁻² day⁻¹ during the entire cruise (see also Table 2.4). The highest values were observed at the time-series location, which was situated in the biomass-rich, upwelling, waters off the coast of Morocco (Stns 12 to 20). Also, Stn 31, located in the Labrador high-biomass waters, had higher $P_{Z,T}$ compared with the oligotrophic stations (Stns 2 to 9 and 22 to 30; Table 2.4 & Figure 2.9). The $P_{Z,T}$ computed using the four different assignments of action spectra showed similar variation among the stations, with notable difference only at

five stations (the productive ones, Figure 2.9). Overall, the difference between $P_{Z,T}$ calculated using the measured spectra and that calculated using the constructed action spectra (uncorrected) ranged from 0 to 18%. A similar comparison, but with $P_{Z,T}$ calculated using the invariant spectral shape of $\alpha^B(\lambda)$ (the average of the spectra measured in this study) ranged from 0 to 17%. The maximum error was only slightly higher (19%) when the spectral shape reported in Sathyendranath et al. (1989) was used for all the stations.

To evaluate the effect of variation in just the *shape* of the action spectrum on the computed primary production, the $P_{Z,T}$ computed using the average shapes (the average computed here, and the one from the literature) can be compared with the $P_{Z,T}$ computed using the constructed action spectra (uncorrected), in which the spectral shapes were allowed to vary from station to station. The difference in $P_{Z,T}$ between the computations based on the average shape of the action spectrum presented here (Figure 2.4a) and those based on the individual constructed action spectra ranged from -4.4 to 8.5% . A similar comparison, but for $P_{Z,T}$ computed using the shape of the action spectrum from the literature (Sathyendranath et al. 1989), showed differences ranging from -1.4 to 18.2% .

2.4 Discussion

The procedure used to construct the action spectrum has the following advantage: one needs only to measure the broad-band α^B and the phytoplankton absorption spectrum. Such measurements are much easier than the direct determination of the action spectrum. In narrow-band light determinations of the action spectrum (e.g., Lewis et al. 1985, Warnock 1990, and this study), the measurement, for some species, would be biased towards the absorption spectrum of PS II reaction center, because PS II is capable of transferring its excess excitation energy to PS I, whereas the reverse is not possible. That is to say, if a phytoplankton sample were illuminated by light of a wavelength absorbed by PS II pigments alone, some of the absorbed energy could be transferred to PS I, for use in photosynthesis.

On the other hand, if the supplied light were of a wavelength absorbed by only PS I pigments, no energy could be transferred to PS II, leading to an imbalance in the operation of the photosystems, thereby affecting the overall photosynthetic efficiency. To avoid this bias, which might occur in narrow-band light measurements, Emerson (1957) suggested that enhancement background light, of wavelengths absorbed by PS II pigments, ought to be supplied (see Schofield et al. 1990, 1991, 1996). In the method developed here, these issues associated with narrow-wavelength determinations (without enhancement background light) are avoided by use of the broad-band α^B determined from polychromatic light (covering the range from 400 to 700 nm) incubations in which the two photosystems (I and II) operate together. Furthermore, the shape of the absorption spectrum which is used in this method is influenced by all the photosynthetic pigments, regardless of whether they are associated with photosystem I or II.

We have seen from the sensitivity analysis how the constructed action spectrum could be affected by both random and systematic errors. The amplitude of the constructed action spectrum depends on the scaling factor, the broad-band α^B . That is to say, a bias in α^B will be translated directly into errors in the magnitude of the constructed action spectrum. For example, the spectral quality of the tungsten-lamp irradiance (Figure 2.5) in the broad-band incubator was shown to introduce a large bias, which, if ignored, could introduce a significant bias in the computed production.

Random and systematic errors on the action spectrum could also affect the computed water-column primary production. If the maximum possible error in $\alpha^B(\lambda)$ were set at $\pm 20\%$, I found that the random errors would have relatively little effect (with the maximum error of about 4%) on the computed production, whereas systematic ones would cause errors in the computed production of up to 11%. This error might appear small, but it should be noted that the computation to assess systematic errors was carried out for noon irradiance; the errors could

be higher for water-column primary production computed for early morning, late afternoon, or integrated over the day.

For noon irradiance, production in a large part of the euphotic zone is light-saturated, with the consequence that P_m^B exerts greater influence than α^B in the computed water-column production. At low irradiance levels, however, production in the water-column is mostly light-limited, that is, α^B has a greater influence than P_m^B . In this case (of low irradiance), an error in α^B will result in large errors in the water-column production. For example, when the computations were repeated for a low irradiance (10% of the noon irradiance), given a 20% error in the action spectrum, there was nearly a 2-fold increase in relative errors (from 11% to 19%) in the computed water-column production.

One would like to know how comparable these errors are to the precision attained in measuring *in situ* primary production. Therriault & Platt (1978) studied spatial and temporal variability of *in situ* production (and other biological, chemical and physical variables) throughout one year in St. Margaret's Bay. The authors showed a coefficient of variation in *in situ* production replicates of about 10%, on average. In comparison, the sensitivity analysis predicts that for a maximum of 20% error in the action spectrum, random errors would cause, on average, 1.5% error in the water-column production and systematic errors would cause about 6% error.

In cases where information on the measured action spectrum is scarce or lacking, a single *shape* of the action spectrum is commonly applied (for example, Platt & Sathyendranath 1988, Sathyendranath et al. 1989, 1995, Platt et al. 1991, Kye-walyanga et al. 1992). In such applications, it is assumed that ignoring the variation in the shape of $\alpha^B(\lambda)$ would cause negligible errors in the computed water-column primary production. How valid is this assumption? Does the use of a constant (invariant) shape for the action spectrum introduce significant errors in the computed water-column production? These questions have been addressed in this work.

It is interesting to find that the use of an average *shape* of the action spectrum gave results comparable to those in which the shape was allowed to vary from station to station (the relative error was, on average about 2%, ranging from -4 to 8%), confirming that the assumption is valid, at least for the North Atlantic. However, the spectral shape to be used should be representative of the region in question, that is derived from measurements made in that region, otherwise higher errors could be introduced. For example, when another *shape* (Sathyendranath et al. 1989) was used for the action spectrum, the relative errors increased (range -1 to 18%).

In the California Current System region, Sosik (1996) made a sensitivity analysis on the use of constant parameters for computing large (spatial) scale primary production, and reached a similar conclusion.

2.5 Concluding Remarks

A method was developed and applied to construct the photosynthetic action spectrum of natural phytoplankton populations from the shape of the phytoplankton absorption spectrum and the measured broad-band α^B . The method is simple, fast and accurate; therefore, photosynthetic action spectra may easily be determined at sea.

Comparison of the measured and the constructed action spectra showed good agreement, indicating that the constructed spectrum is a good proxy for the measured action spectrum. Through a sensitivity analysis, I have analysed the effect on water-column primary production, of random and systematic errors on $\alpha^B(\lambda)$, and also of the presence of non-photosynthetic pigments in the phytoplankton absorption spectrum. The results from the analysis suggest that, in computing water-column primary production, systematic errors in the action spectrum would cause larger errors than random errors or the presence of non-photosynthetic pigments. Thus, in computing water-column primary production, it is important to have good estimates of the *magnitude* of α^B .

On the other hand, realistic variations in the *shape* of the action spectra are likely to have only a small effect on the computed primary production. However, even these errors can be decreased if one has reasonable estimates of the shape of the spectrum for a given locality. This conclusion is supported by the results from the sensitivity analysis, and by the computations of primary production using an invariant shape for the action spectrum.

CHAPTER 3

Variability in Physiological Parameters of Phytoplankton across the North Atlantic

3.1 Introduction

In a previous study carried out at different stations across the North Atlantic in the fall of 1992 (Chapter 2), I developed and applied a method to estimate the photosynthetic action spectrum, which uses the *shape* of the phytoplankton absorption spectrum and the *magnitude* of α^B , the initial slope of the photosynthesis-irradiance (P^B vs. I) curve for broad-band illumination (the superscripts B indicate normalization to phytoplankton biomass B). Further, it was demonstrated that water-column primary production computed using a spectrally-resolved P^B vs. I model and measured parameters gave good results when compared with *in situ* measurements.

Extending the results to large scales using satellite-derived data requires some rules (or assumptions) for extrapolation of the locally-measured parameters to large scales. This is an important problem: a possible solution is to partition the ocean into subregions or biogeochemical provinces (Platt and Sathyendranath 1988, Mueller and Lange 1989, Longhurst et al. 1995) in which the parameter values could be treated as quasi-stable or predictable, at least in a given season.

In this chapter, therefore, I examine the applicability of this approach in the North Atlantic. Here, a method developed earlier (Chapter 2) is used to construct the action spectra at different stations in the North Atlantic, during the spring. These spectra are then combined with data from the same region collected in the fall. I then use the extended data set (collected from five biogeochemical provinces in two seasons) to examine the variability and predictability of phytoplankton physiological parameters, and the consequences for modelling primary production at large scales.

3.2 Materials and Methods

3.2.1 Sampling

Samples were collected during two cruises conducted along four transects across the North Atlantic, from the east coast of Canada to the coast of Morocco. The two cruises (Figure 3.1) were the Canadian Joint Global Ocean Flux Study (JGOFS) 1992 cruise, carried out in early fall, from 19 September to 21 October, and the Canadian JGOFS 1993 cruise, carried out during spring, from 7 April to 6 June. In both cruises, sampling was undertaken in both the West–East and East–West directions.

The sampled track covered five biogeochemical provinces (Longhurst 1995): the NW Atlantic continental shelf (NWCS), the Gulf Stream (GFST), the Western North Atlantic Subtropical Gyre (STGW), the Eastern North Atlantic Subtropical Gyre (STGE), and the Eastern Atlantic or Canary (CNRV) province (Figure 3.2). I have used the demarcation of the provinces as given in Sathyendranath et al. (1995), although, in principle, it is known that these boundaries are dynamic (Platt and Sathyendranath 1988, Sathyendranath et al. 1995, Longhurst et al. 1995). The number of stations in each province varied depending on the size of the province and on the number of sampling days spent therein. A total of 26 stations was sampled during the JGOFS 92 cruise, whereas 38 stations were occupied during the JGOFS 93 cruise.

The physical characteristics of the provinces could be summarized as follows: The coastally-located Northeastern Atlantic or Canary (CNRV) province is characterized by seasonal upwelling, which is a function of the orientation of the coast, bottom topography, wind speed and wind direction (Van Camp et al. 1991). The North Atlantic Subtropical Gyre is separated into the western (STGW) and eastern (STGE) provinces by the Mid-Atlantic Ridge (Longhurst et al. 1995, Sathyendranath et al. 1995). Because of this bottom topography, the two provinces have

different circulation patterns, which in turn could affect their biology (Olaizola et al. 1996). The GFST province is under the influence of the Gulf Stream current, with its associated eddies. The eddies may enclose the cold nutrient-rich slope waters or the warm nutrient-poor Sargasso Sea waters (Longhurst 1995). The Northwest Atlantic Continental Shelf province (NWCS) is a coastally-located province, like the CNRY. It is influenced by upwelling (though not as intense as in the CNRY province) and by having anomalously deep continental shelf in some parts (see Longhurst 1995).

The track could also be partitioned into domains (as defined by Longhurst 1995): the CNRY and NWCS provinces are situated in the Coastal (i.e., coastal-boundary) domain and the remaining three provinces (GFST, STGE and STGW) are located in the Westerlies (west-wind) domain. The characteristic features of these domains are given in Longhurst et al. (1995) and Sathyendranath et al. (1995).

Figure 3.1 Locations of 26 stations sampled in the North Atlantic during the JGOFS 92 cruise (filled circles) and 36 stations occupied during the JGOFS 93 cruise (open circles).

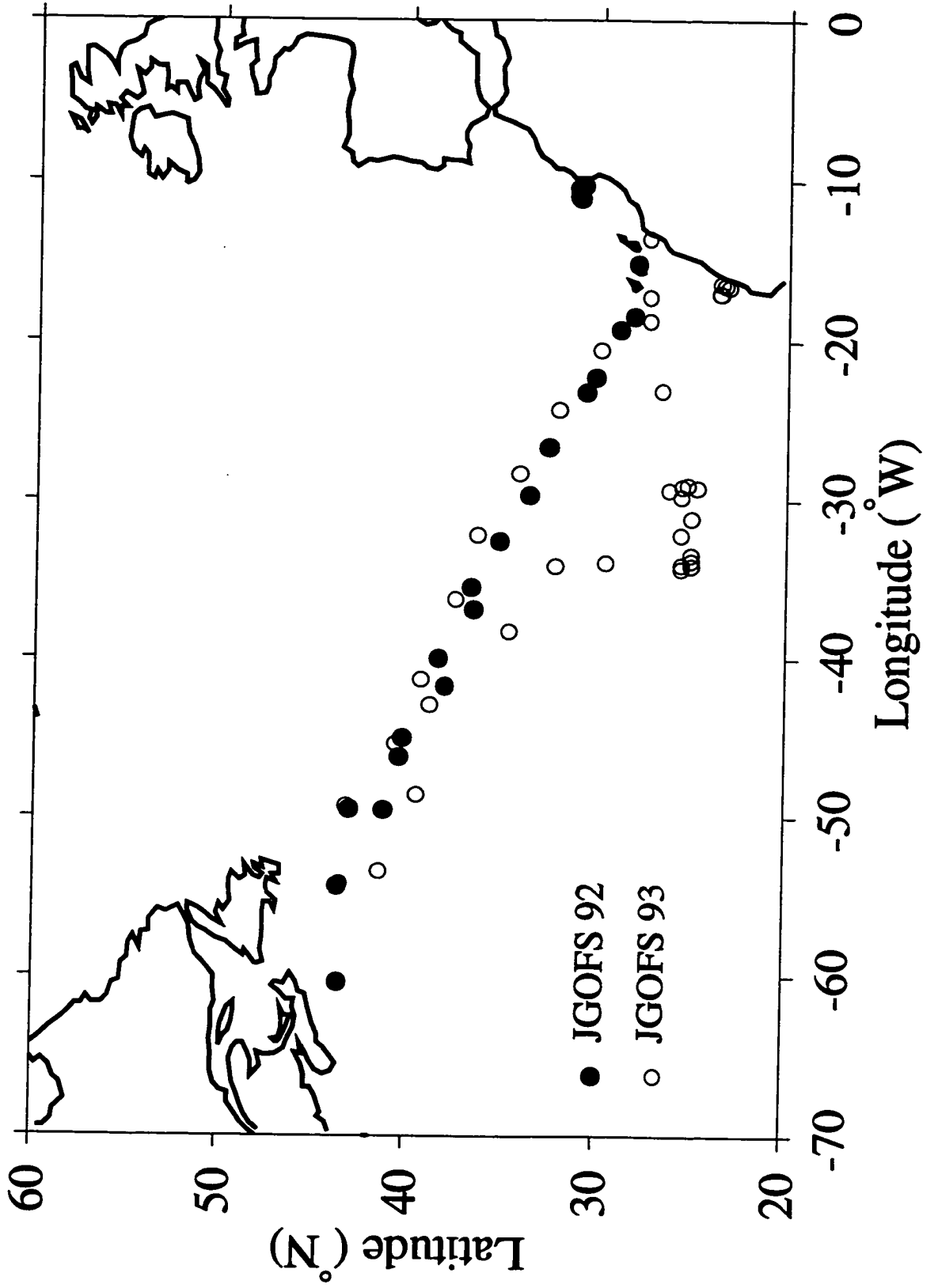


Figure 3.1

Figure 3.2 Locations of the five biogeochemical provinces during the North Atlantic, sampled during the two cruises across the track shown in Figure (3.1): NWCS, the Northwest Continental Shelf; GFST, the Gulf Stream; STGE, the Eastern Subtropical Gyre; STGW, the Western Subtropical Gyre; and CNRY the Canary province. The insert box shows the four domains: Coastal, Trade-winds, Westerlies and Polar. Note that other provinces of the North Atlantic are also shown (from Sathyendranath et al. 1995, with permission).

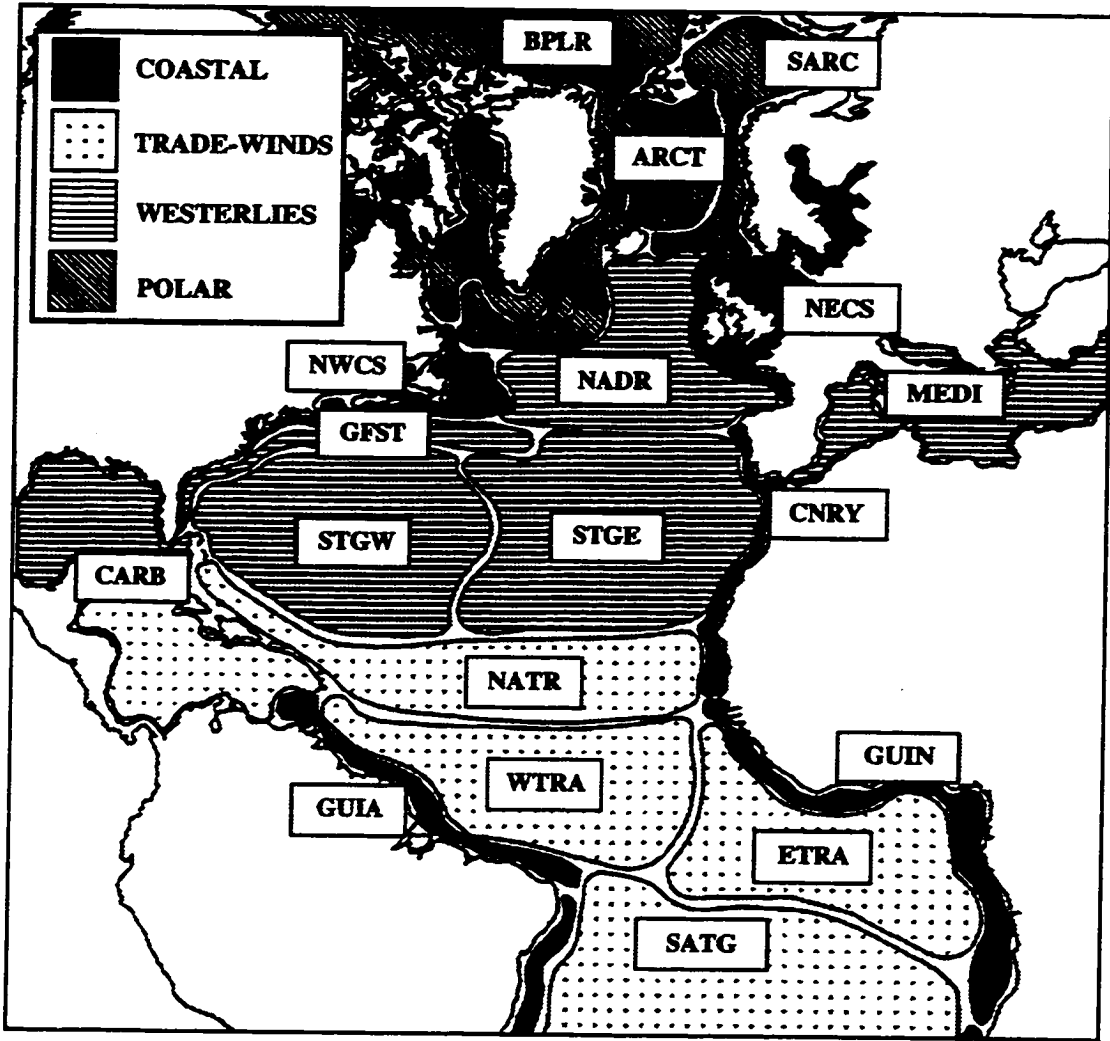


Figure 3.2

At each station, water samples for the determination of absorption spectra, parameters of the broad-band P^B vs. I curve, chlorophyll-*a* (chl-*a*) concentration, and pigment analysis by High Performance Liquid Chromatography (HPLC) were collected at three depths in the photic zone (depth range from the surface to 80 m), using a continuous pump sampler (Herman et al. 1984). The sample for measuring the action spectrum was taken at one depth among the three (arbitrarily chosen). In addition, water samples for determining the biomass and nutrient (nitrate plus nitrite, silicate, phosphate) profiles were collected using a Niskin-bottle rosette, attached to a conductivity-temperature-depth (CTD) probe. The rosette samples were collected at 14 depths in the top 200 m of the water column.

3.2.2 Pigment Analyses and Nutrient Concentrations

Filters containing samples for pigment analysis were ground in 90% acetone and centrifuged: the supernatant was analysed using a High Performance Liquid Chromatography system (Beckman System-Gold HPLC) following the method of Head and Horne (1993). Pigment analysis by HPLC was done for the JGOFS 93 cruise only; the pigments determined were chlorophylls *a*, *b* and *c* (including divinyl chl-*a* and chl-*b*), phaeopigments and carotenoids (those found in significant concentration were: fucoxanthin, peridinin, 19'hexanoyloxy-fucoxanthin, 19'butanoyloxy-fucoxanthin, lutein + zeaxanthin, diatoxanthin, diadinoxanthin and β -carotene). Chlorophyll-*a* concentration (B) was also determined fluorometrically by the method of Holm-Hansen et al. (1965). Samples for the determination of nitrate plus nitrite, silicate and inorganic phosphate concentrations were analysed by a standard automated method using an Alpkem autoanalyser, as explained in Irwin et al. (1989).

3.2.3 Photosynthetic Action Spectra

To determine the action spectra, 70-ml polystyrene incubation bottles were filled with water samples, inoculated with $\text{NaH}^{14}\text{CO}_3$ and incubated for three hours, at irradiance of different wavelengths, in a spectral incubator. Twelve different wavelengths, covering a range between 400 and 700 nm, were used in the incubations. These wavelengths were produced by screening the broad-band light using interference filters (Corion, Holliston, MA). A detailed account of the experimental procedure is given in Chapter 2.

The measured action spectra were partitioned into their respective provinces. In each province, a mean action spectrum $\alpha_v^B(\lambda)$ was computed by averaging all the measured action spectra from that province. To define the *shapes* of the action spectra, for comparison between provinces, each average spectrum was normalized to its mean value $\bar{\alpha}_v^B$, taken over the spectral range from 400 to 700 nm. Then, the spectral shape $\alpha'(\lambda)$ was determined by:

$$\alpha'(\lambda) = \frac{\alpha_v^B(\lambda)}{\bar{\alpha}_v^B}. \quad (3.1)$$

One-way analysis of variance (ANOVA) was used to test the difference in the spectral shapes between provinces. In the analysis, the mean $\alpha'(\lambda)$ values at each of the twelve wavelengths from all the provinces were compared at the probability level of 5%. This comparison was made for only the JGOFS 92 data. The measured action spectra for JGOFS 93 cruise were noisy due to low phytoplankton abundance ($\text{chl-}a \leq 0.05 \text{ mg m}^{-3}$, in most cases); therefore, only constructed action spectra were considered for this cruise.

3.2.4 Phytoplankton Absorption Spectra

Total particle absorption for both cruises was determined using the filter technique (e.g., Yentsch et al. 1962, Kishino et al. 1985). The data for JGOFS 92 were

then processed as outlined in Chapter 2, that is, correction for detrital absorption and for the pathlength amplification (the β factor) was undertaken following the procedure of Hoepffner and Sathyendranath (1992). In the JGOFS 93 cruise, these corrections were made using a different procedure, because: 1) phytoplankton biomass was low and therefore the absorption spectra were noisy, and 2) pigment analysis by HPLC was made for this cruise, which gave us an idea of the dominant phytoplankton groups.

In this cruise (JGOFS 93), prochlorophytes were found to be more abundant (in terms of numbers), than other groups, especially in the subtropical gyre region (Li 1995). A ratio of divinyl chl-*a*, a marker for prochlorophytes, to total chl-*a* ranged from 0 to 63%. Therefore, a β factor that took into consideration the contribution by prochlorophytes was used. First, the ratio of divinyl chlorophyll-*a* (DV-chl-*a*, determined by HPLC) to total chl-*a*, denoted here as F_{dv} , was computed for each sample. The F_{dv} fraction was assigned the β -factor coefficients for prochlorophytes published by Moore et al. (1995). The remaining fraction ($1 - F_{dv}$) was assigned the coefficients from Hoepffner and Sathyendranath (1992):

$$D_s(\lambda) = F_{dv}[A_1 D_f(\lambda) + B_1 (D_f(\lambda))^2] + (1 - F_{dv})[A_2 D_f(\lambda) + B_2 (D_f(\lambda))^2] \quad (3.2)$$

where $D_s(\lambda)$ is the optical density in suspension, $D_f(\lambda)$ is the optical density on the filter, A_1 and B_1 are coefficients for prochlorophytes (= 0.291 and 0.051, respectively; Moore et al. 1995), and A_2 and B_2 are coefficients for other phytoplankton groups (= 0.31 and 0.57, respectively; Hoepffner and Sathyendranath 1992). After correcting for the β factor, the optical density (in suspension) was converted to an absorption coefficient for total particles. Because the spectra were noisy, absorption by detrital materials was approximated using an exponential function (theoretical approach) proposed by Hoepffner and Sathyendranath (1993).

Phytoplankton absorption coefficients, $a_p(\lambda)$, were determined as a difference between total particle and detrital absorption. The $a_p(\lambda)$ values were normalized

to the biomass B (mg chl- a m^{-3}) to yield biomass-specific absorption coefficients, $a_p^B(\lambda)$ [m^2 (mg chl- a) $^{-1}$]. The average of $a_p^B(\lambda)$ coefficients (over the spectral range from 400 to 700 nm) was used in the computation of the maximum quantum yield of photosynthesis, ϕ_m .

The ratio of absorption by phytoplankton at the blue and red maxima, $a_p(435):a_p(676)$, was computed for each sample, for use in the regression analyses. Next, the phytoplankton absorption spectra $a_p(\lambda)$ were decomposed into Gaussian bands representative of absorption by major phytoplankton pigments (Hoepffner and Sathyendranath 1991, 1993). The ratio of Gaussian peak height for chl- a absorption band at 435 nm, $p(435)$, to that at 676 nm, $p(676)$, was also determined (Sathyendranath et al. 1996) and used in the regression analyses.

In the same way as for the measured action spectra, an average absorption spectrum was calculated (in each province) from all the absorption spectra measured in the province. The *shape* $a'_p(\lambda)$ of the absorption spectrum was subsequently defined by normalizing each average spectrum to its corresponding mean value:

$$a'_p(\lambda) = \frac{a_v(\lambda)}{\bar{a}_v}. \quad (3.3)$$

The shapes of the absorption spectra from the five provinces were compared, as in the case of the action spectra, using the Kruskal-Wallis ANOVA test, for data from both cruises. A total of 12 wavelengths between 400 and 700 nm, matching those used in the comparison of the measured action spectra, was selected for the comparison of absorption spectra.

3.2.5 Parameters of the Photosynthesis *vs.* Irradiance Curve

To determine the parameters of the P^B *vs.* I curve for broad-band illumination (α^B [mg C (mg chl- a) $^{-1}$ h $^{-1}$ (μ mol m^{-2} s $^{-1}$) $^{-1}$] and P_m^B [mg C (mg chl- a) $^{-1}$ h $^{-1}$]), samples were incubated and processed according to Irwin et al. (1990). The equation of Platt et al. (1980) was fitted to the P^B *vs.* I data to retrieve the parameters. The

initial slope α^B was then corrected for the bias introduced by the spectral shape of the irradiance generated by the tungsten-halogen lamp in the incubator, as in Chapter 2.

The mean values of α^B and P_m^B were computed in each province, for each cruise. To test whether there was a significant difference in the parameters between provinces and seasons, the Kruskal-Wallis one-way analysis of variance was used. Linear regression analyses were performed to examine the predictability of α^B and P_m^B , for each province and season, from different independent variables: temperature, sampling depth, nutrient concentrations, a proxy for nitrogen supply (distance between the sampling depth and the top of the nitricline) and the ratio of phytoplankton absorption or chl-*a* absorption in the blue (435 nm) to that in the red (676 nm). The magnitude of the blue-to-red absorption ratio, $a_p(435):a_p(676)$, and that of the peak height ratio of chl-*a* absorption, $p(435):p(676)$, could reflect the physiological state of phytoplankton and changes in phytoplankton populations (Margalef 1963, Cleveland et al. 1989, Sathyendranath et al. 1996).

Before performing the analyses, the data were tested to check if they satisfied all the required assumptions (linearity, normality and homoscedasticity); if any of the assumptions failed, no further analysis was performed. For each independent variable, a minimum of five observations was required; that is to say, in provinces with less than ten observations, only simple linear regressions were done. First, the best-subset regression analysis was performed to select a combination of environmental variables which best explained the variance in α^B or P_m^B (at $p \leq 0.05$), then multiple regression was performed on the selected variables.

3.2.6 Constructed Action Spectra

The action spectra were constructed for the JGOFS 93 cruise, and for some depths for the JGOFS 92 cruise (the depths used were those for which α^B and $a_p(\lambda)$ were determined, but not action spectra), using the *magnitude* of the broad-band

α^B and the *shape* of the corresponding phytoplankton absorption spectra, as in Chapter 2:

$$\alpha_c^B(\lambda) = \frac{a_p(\lambda) \times \alpha^B}{\bar{a}_p}, \quad (3.4)$$

where $\alpha_c^B(\lambda)$ is the constructed action spectrum (with the subscript *c* indicating *constructed*), α^B is the broad-band, initial slope of the P^B vs. I curve, corrected for the shape of the irradiance spectrum of the lamp in the incubator, $a_p(\lambda)$ is the phytoplankton absorption spectrum and \bar{a}_p is the spectrally-averaged mean phytoplankton absorption coefficient.

The constructed action spectra, $\alpha_c^B(\lambda)$, were also partitioned into the five biogeochemical provinces, and the average spectral shapes determined (as explained previously, Equation 3.3). In addition, for the JGOFS 92 data set, the constructed $\alpha_c^B(\lambda)$ in each province (pooled data) were regressed against their measured counterparts to investigate the agreement in amplitudes. The slopes of the regression lines were tested against 1.0, at the 5% significance level (Student's *t*-test).

3.2.7 Maximum Quantum Yield of Photosynthesis

The realized maximum quantum yield of photosynthesis, ϕ_m [mol C (mol photons)⁻¹], was determined as the ratio of the broad-band α^B to the spectrally-averaged, biomass-specific, absorption coefficient of phytoplankton, \bar{a}_p^B :

$$\phi_m = 0.0231 \times \frac{\alpha^B}{\bar{a}_p^B}, \quad (3.5)$$

where the constant 0.0231 converts mg C to moles, hours to seconds and μmol to moles of photons. The weighting of \bar{a}_p^B by the irradiance of the incubator lamp (e.g., Dubinsky et al. 1986, Cleveland et al. 1989, Babin et al. 1995, 1996) is implicit in Equation (3.5) via the correction factor applied to α^B (Chapter 2).

The values of ϕ_m were then partitioned into the five biogeochemical provinces. The mean value in each province and for each cruise was calculated. Differences

between provinces (within a given cruise) were tested using the Kruskal-Wallis one-way analysis of variance on ranks. The differences in the mean ϕ_m values between cruises (in each province) were tested for statistical significance using the Student's *t*-test. In both tests, the deciding probability level was set at 5%.

The ϕ_m was also tested for correlation with environmental variables, which included temperature, sampling depth, chl-*a* concentration, nutrient (nitrate plus nitrite, phosphate and silicate) concentrations, distance between the sampling depth and the top of the nitricline, the ratio of blue-to-red absorption at two chosen wavelengths [$a_p(435):a_p(676)$], and the ratio of Gaussian peak heights for chl-*a* absorption bands, $p(435):p(676)$. The regression analyses were performed based on the same criteria i.e., regarding the number of observations, the required assumptions (linearity, normality and homoscedasticity), and the *p* value (< 0.05), applied to the P^B vs. *I* parameters.

3.3 Results

3.3.1 Parameters of the Photosynthesis–Irradiance Curve

The broad-band α^B for the JGOFS 92 cruise, pooled from all the five biogeochemical provinces, varied by a factor of 11. The values ranged from 0.013 to 0.142, with a mean (\pm SD) of 0.034 (\pm 0.024, $n = 70$) [$\text{mg C (mg chl-}a)^{-1} \text{ h}^{-1} (\mu\text{mol m}^{-2} \text{ s}^{-1})^{-1}$]. The corresponding P_m^B values had a mean of 4.4 (\pm 2.12) $\text{mg C (mg chl-}a)^{-1} \text{ h}^{-1}$ and varied from 1.2 to 11 (a factor of about 9). In the JGOFS 93 cruise, the α^B values showed a dynamic range of about 10, varying from 0.018 to 0.177, with an average of 0.078 (\pm 0.033, $n = 114$) [$\text{mg C (mg chl-}a)^{-1} \text{ h}^{-1} (\mu\text{mol m}^{-2} \text{ s}^{-1})^{-1}$]. The P_m^B for this cruise varied by a factor of 18. The values ranged from 0.8 to 14, and had an average of 7.1 (\pm 3.2) $\text{mg C (mg chl-}a)^{-1} \text{ h}^{-1}$.

The mean values (\pm SD) of α^B and P_m^B in each of the five provinces, and for the *pooled* data, are given in Table (3.1). The average parameter values from pooled data (both α^B and P_m^B) were significantly different between cruises (Student's *t*-test, $p < 0.05$), suggesting seasonal differences. In the individual provinces, the mean α^B and P_m^B values for the JGOFS 93 cruise were consistently higher than those for the JGOFS 92 cruise (Tables 3.1a & 3.1b).

To test if the seasonal differences were significant, the average parameters from the two cruises, within each province, were compared (Student's *t*-test). The results showed that mean α^B values were significantly different between seasons in all provinces and P_m^B values were significantly different for the CNRY, STGE and STGW, but not significant for the GFST and NWCS provinces.

Within seasons (cruises), the differences between provinces were tested by ANOVA, followed by a pairwise multiple comparison test (Dunn's method). For the JGOFS 92 data, P_m^B values were not significantly different, whereas the mean α^B values were significantly different in six pairs (out of ten) of provinces. A similar comparison for the JGOFS 93 cruise showed no significant difference between any of the ten pairs for α^B values, although a significant difference in P_m^B was found in four of the ten pairs.

Table 3.1a. Data from two cruises showing average values (mean \pm SD) of the broad-band initial slope of the P^B vs I curve, α^B [$\text{mg C (mg chl-}a)^{-1} \text{ h}^{-1} (\mu\text{mol m}^{-2} \text{ s}^{-1})^{-1}$], in five provinces and for pooled results.

| Province | JGOFS 92 | | JGOFS 93 | |
|---------------|-------------------|-----|-------------------|-----|
| | Mean α^B | n | Mean α^B | n |
| CNRY | 0.023 \pm 0.008 | 24 | 0.069 \pm 0.032 | 27 |
| STGE | 0.049 \pm 0.037 | 19 | 0.078 \pm 0.025 | 51 |
| STGW | 0.037 \pm 0.006 | 8 | 0.075 \pm 0.028 | 15 |
| GFST | 0.040 \pm 0.020 | 13 | 0.100 \pm 0.045 | 12 |
| NWCS | 0.019 \pm 0.007 | 6 | 0.073 \pm 0.048 | 9 |
| All Provinces | 0.034 \pm 0.024 | 70 | 0.078 \pm 0.033 | 114 |

Table 3.1b. As in Table (3.1a), but for the maximum photosynthetic rate, i.e., the plateau of the P^B vs I curve, P_m^B [$\text{mg C (mg chl-}a)^{-1} \text{ h}^{-1}$].

| Province | JGOFS92 | | JGOFS93 | |
|---------------|-----------------|-----|-----------------|-----|
| | Mean P_m^B | n | Mean P_m^B | n |
| CNRY | 4.88 \pm 1.28 | 24 | 6.64 \pm 3.37 | 27 |
| STGE | 4.34 \pm 2.68 | 21 | 8.23 \pm 2.62 | 51 |
| STGW | 4.58 \pm 2.32 | 9 | 6.88 \pm 3.30 | 15 |
| GFST | 4.51 \pm 2.09 | 13 | 6.01 \pm 2.35 | 12 |
| NWCS | 2.24 \pm 1.56 | 6 | 3.30 \pm 2.63 | 9 |
| All Provinces | 4.40 \pm 2.12 | 73 | 7.05 \pm 3.15 | 114 |

3.3.2 Quantum Yield of Photosynthesis

In the JGOFS 92 cruise, the realized maximum quantum yield of photosynthesis, ϕ_m , showed a dynamic range of 8.9, and varied from 0.011 to 0.094 throughout the cruise, with a mean value of 0.032 ± 0.015 mol C (mol photons)⁻¹ (Tables 3.2a & b). The maximum value was almost as high as that reported by Cleveland et al. (1989) for data collected in the Sargasso Sea (which ranged from 0.033 to 0.0102 mol C (mol photons)⁻¹). The highest values were found in the eastern part of the sampled track (the CNRY and STGE provinces) and were similar to the values found by Babin et al. (1995) in the estuary and Gulf of St. Lawrence (ϕ_m of up to about 0.08 mol C (mol photons)⁻¹), and those observed by Babin et al. (1996) for oligotrophic northeast tropical Atlantic. The western part of the track (NWCS, GFST and STGW provinces) had the maximum values ranging from 0.041 to 0.056 mol C (mol photons)⁻¹ (Table 3.2a). These values were in the same range as the ϕ_m observed by Babin et al. (1996) for the eutrophic and mesotrophic sites in the tropical northeast Atlantic (highest values between 0.035 and 0.05 mol C (mol photons)⁻¹).

In the JGOFS 93 cruise (all provinces), the ϕ_m values were consistently lower than those for the JGOFS 92 data set; they ranged from 0.004 to 0.047, with a mean of 0.017 mol C (mol photons)⁻¹ (Tables 3.2a & b). The correction for the β factor using coefficients for prochlorophytes (from Moore et al. 1995) would have an effect of reducing absorption compared to the use of coefficients given in Hoepffner and Sathyendranath (1992). Thus, the computed ϕ_m would be high. The fact that ϕ_m values for the JGOFS 93 were consistently lower than those for the JGOFS 92 cruise shows that the difference is real, that it is not caused by methodological differences in β -factor correction.

Unlike the JGOFS 92 values, there was no clear distinction between the eastern and the western parts of the cruise track. Sampling on the East-West direction, during the JGOFS 93 cruise, Olaizola et al. (1996) found that quantum yield (based

on fluorescence measurements) was higher in the eastern basin than in the western part; consistent with the pattern in ϕ_m values determined for the JGOFS 92 cruise.

Regardless of differences in locations, the range in ϕ_m in the provinces for the JGOFS 93 data set (Table 3.2a) were similar to those reported by Tilzer et al. (1985), for the Antarctic Ocean, ranging from 0.0015 to 0.035 mol C (mol photons)⁻¹; Lizotte and Priscu (1994), for perennially ice-covered lakes in Antarctica, ranging from 0.0015 to 0.051 mol C (mol photons)⁻¹; Sathyendranath et al. (1996), for the NW Indian Ocean (values from the mixed layer), ranging from 0.004 to 0.028 mol C (mol photons)⁻¹; and by Kishino et al. (1986), for values found off Shikoku Island in surface waters, ranging from 0.005 to 0.033 mol C (mol photons)⁻¹.

The mean values of ϕ_m in each of the biogeochemical provinces, for each of the cruises, are given in Table (3.2b). Between cruises (seasons) in a given province, the mean values were significantly different (*t*-test, $p < 0.05$, all cases). The values from the fall cruise were consistently higher than those in the spring, by up to 2 fold. Statistically, the mean ϕ_m values were not significantly different between provinces in each cruise (ANOVA, $p > 0.05$).

Table 3.2a. Range in the values of the maximum quantum yield of photosynthesis, ϕ_m [mol C (mol photons)⁻¹], for the two cruises, in each of the five biogeochemical provinces and for pooled data from all provinces. The dynamic range (Dynamic) is also given.

| Province | JGOFS92 | | JGOFS93 | |
|---------------|-------------------|---------|-------------------|---------|
| | Range in ϕ_m | Dynamic | Range in ϕ_m | Dynamic |
| CNRY | 0.018 – 0.094 | 5.1 | 0.004 – 0.035 | 8.8 |
| STGE | 0.011 – 0.083 | 7.8 | 0.006 – 0.047 | 7.8 |
| STGW | 0.015 – 0.051 | 3.5 | 0.008 – 0.035 | 4.4 |
| GFST | 0.017 – 0.056 | 3.3 | 0.012 – 0.042 | 3.5 |
| NWCS | 0.017 – 0.041 | 2.5 | 0.007 – 0.030 | 4.3 |
| All Provinces | 0.011 – 0.094 | 8.9 | 0.004 – 0.047 | 11.8 |

Table 3.2b. Mean values (\pm SD) of the ϕ_m values [mol C (mol photons)⁻¹] for the provinces given in Table (3.4a).

| Province | JGOFS92 | | JGOFS93 | |
|---------------|-------------------|-----|-------------------|-----|
| | Mean ϕ_m | n | Mean ϕ_m | n |
| CNRY | 0.031 \pm 0.014 | 24 | 0.015 \pm 0.007 | 27 |
| STGE | 0.035 \pm 0.021 | 19 | 0.016 \pm 0.006 | 51 |
| STGW | 0.029 \pm 0.011 | 8 | 0.017 \pm 0.008 | 15 |
| GFST | 0.033 \pm 0.011 | 13 | 0.023 \pm 0.009 | 12 |
| NWCS | 0.031 \pm 0.008 | 6 | 0.019 \pm 0.009 | 9 |
| All Provinces | 0.032 \pm 0.015 | 70 | 0.017 \pm 0.007 | 114 |

3.3.3 Action and Absorption Spectra

The five, province-representative *shapes* of the measured action spectra determined during the JGOFS 92 cruise are shown in Figure (3.3a). The variation in the five representative shapes of action spectra was determined using the ANOVA test. Table (3.3; column 2) shows the results of the analysis (significant or not, at the 5% level) of the mean values at each of the twelve wavelengths used in the spectral incubator. The differences in the shapes of the representative action spectra were found to be significant in the spectral region between 440 and 580 nm, the region in which accessory chlorophylls and carotenoids have their maximum absorption. The differences at 415 nm and at $\lambda \geq 600$ nm were not significant. The shapes of the corresponding absorption spectra closely resembled those of the representative action spectra (Figure 3.3b), with significant differences in the region from 440 to 630 nm (Table 3.3; column 3). For example, if we compare the spectral shapes of the STGE and the NWCS provinces, we see that both the action and the absorption spectra from the STGE province were narrower and overshot the other spectra in the blue part of the spectrum, whereas those from the NWCS province were broader, with their blue peaks relatively lower than the others (Figures 3.3a & b).

The pairwise comparison test (Dunn's method) was performed on both the shapes of the action and absorption spectra. It was revealed that not all ten pairs of provinces were significantly different, at those wavelengths, all the time; the provinces that frequently caused the difference were the STGE, the CNRY and the NWCS.

The shapes of the absorption spectra are proxies for those of the constructed action spectra (Chapter 2). The results of analysis of variance (Table 3.3) for the JGOFS 92 cruise confirm that the representative *shapes* of the measured and constructed action spectra, in each of the provinces, were well matched, as illustrated in Figure (3.4).

Figure 3.3 Shapes of representative (a) action and (b) absorption spectra for five biogeochemical provinces sampled in the JGOFS 92 cruise: GFST, the Gulf Stream; NWCS, the Northwest Continental Shelf; CNRY, the Canary; STGE, the Eastern Subtropical gyre; and STGW, the Western Subtropical gyre. Each spectrum is normalized to its mean value, averaged over the spectral range from 400 to 700 nm.

Shapes of Action and Absorption Spectra: JGOFS 92

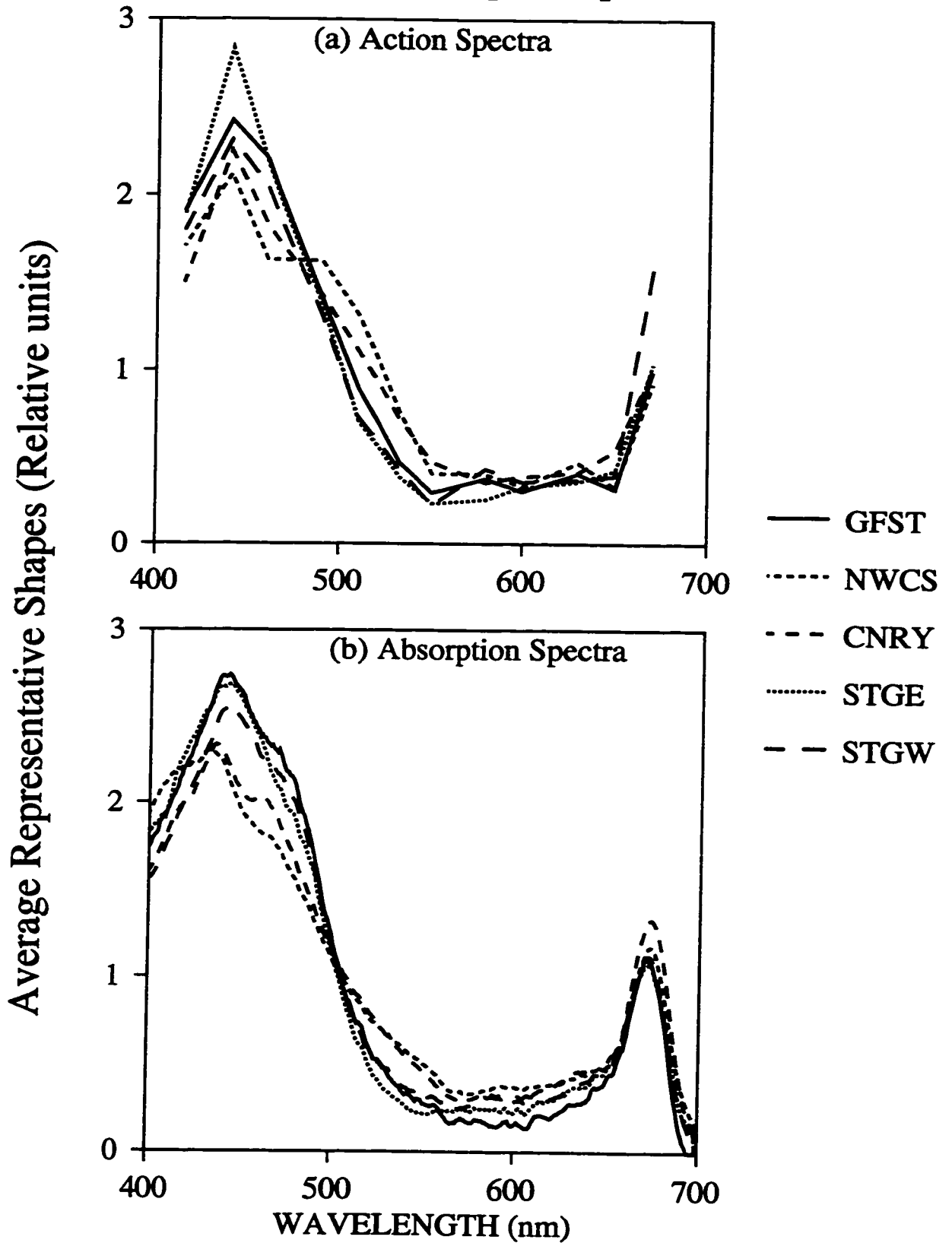


Figure 3.3

Table 3.3. Analysis of variance (ANOVA) to test the variation in average *shapes* of action and absorption in five biogeochemical provinces: NWCS, GFST, STGW, STGE and CNRY sampled during two cruises. The ANOVA was performed at the wavelengths shown, and the results are given as significantly different (sign.) or not significantly different (ns) at the 5% level.

| Wavelength | Action Spectra | | Absorption Spectra | |
|----------------|----------------|--|--------------------|-------|
| λ (nm) | JGOFS 92 | | JGOFS 92 | |
| | | | JGOFS 93 | |
| 415 | ns | | ns | sign. |
| 440 | sign. | | sign. | sign. |
| 460 | sign. | | sign. | sign. |
| 490 | ns | | sign. | sign. |
| 510 | sign. | | sign. | sign. |
| 532 | sign. | | sign. | sign. |
| 550 | sign. | | sign. | sign. |
| 580 | sign. | | sign. | sign. |
| 600 | ns | | sign. | sign. |
| 630 | ns | | sign. | sign. |
| 650 | ns | | ns | sign. |
| 670 | ns | | ns | sign. |

Figure 3.4 Comparison of shapes of measured and constructed action spectra in five biogeochemical provinces defined in Figure (3.3). The spectra are normalized to their mean values (averaged between 400 and 700 nm). The measured action spectra are shown by solid lines, and the constructed ones by the broken lines.

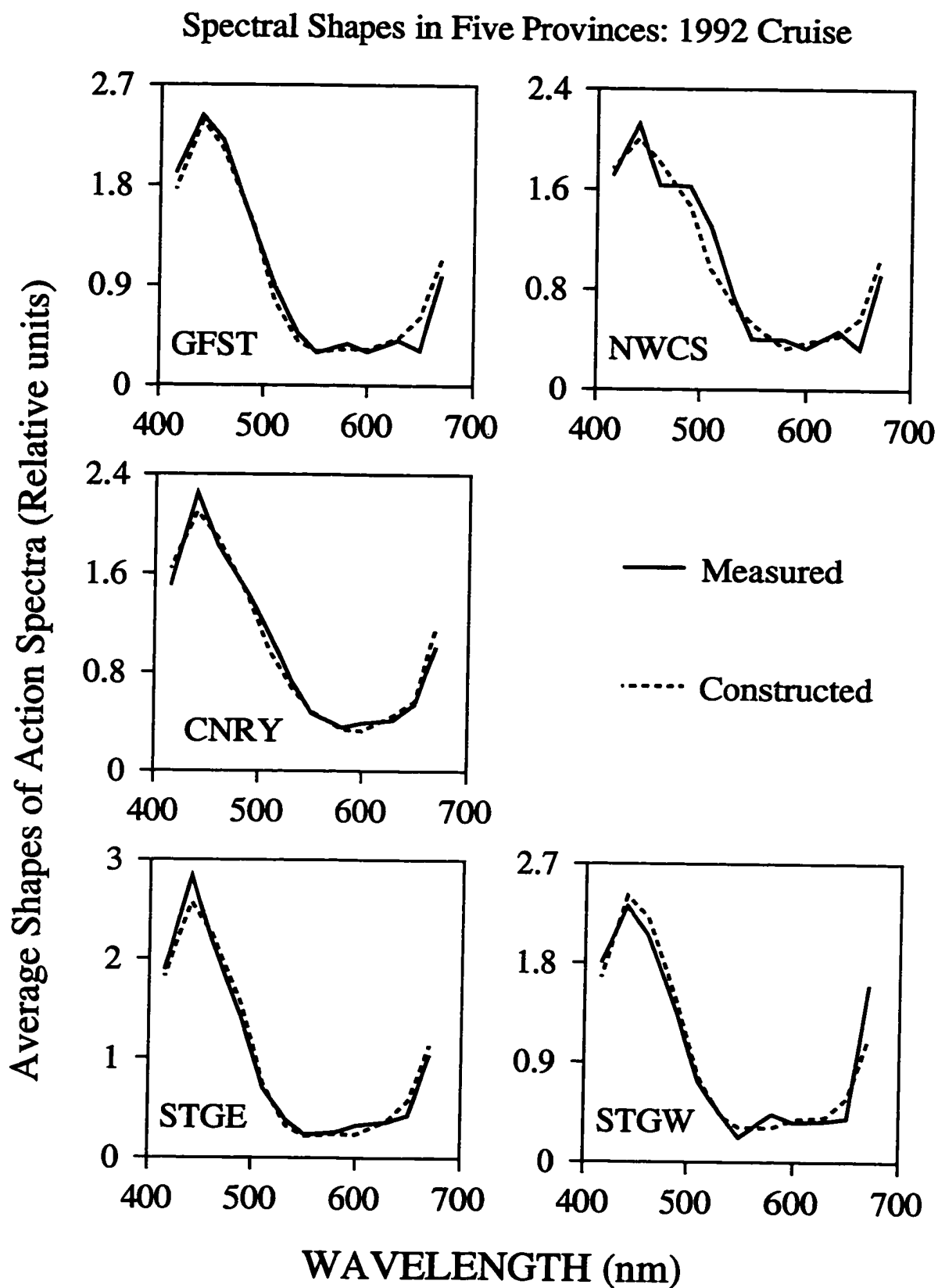


Figure 3.4

Agreement in the *amplitudes* of the constructed and measured action spectra was tested by linear regression of $\alpha_c^B(\lambda)$ against $\alpha^B(\lambda)$, for combined (all wavelengths) data in each province (Figure 3.5). A slope of 1.0 and an intercept of zero would imply perfect agreement in amplitudes: the slopes of the lines for the GFST, the STGE and the STGW provinces were not significantly different from 1.0 (at a probability level of 5%); the slopes of the remaining two provinces (NWCS and CNRY) were significantly less than 1.0, implying that the constructed $\alpha_c^B(\lambda)$ had lower amplitudes than the measured $\alpha^B(\lambda)$. Nevertheless, the data showed low scatter in all provinces and the intercepts were not significantly different from zero, confirming that the shapes of the constructed spectra were good representatives of the measured ones.

In the JGOFS 93 cruise, the differences in the representative *shapes* of the absorption spectra between provinces (Figure 3.6) were statistically different at all the 12 wavelengths tested (Table 3.3; column 4). The pairwise comparison test (Dunn's method) showed that at each wavelength, the difference was caused by four pairs (out of 10; which were NWCS *vs.* STGE, GFST *vs.* STGE, CNRY *vs.* STGE and STGW *vs.* STGE) primarily due to the shape from the STGE province. The ratio of divinyl chl-*a* to total chl-*a* was highest in this province (ranging from 20 to 63%), indicating that prochlorophytes were the dominant phytoplankton group.

Figure 3.5 Regression analysis of constructed $\alpha_c^B(\lambda)$ on the measured $\alpha^B(\lambda)$, for pooled data, from each of the biogeochemical provinces referred to in Figure (3.3). The respective regression lines, the number of points, the r^2 values and the 1:1 lines are also shown.

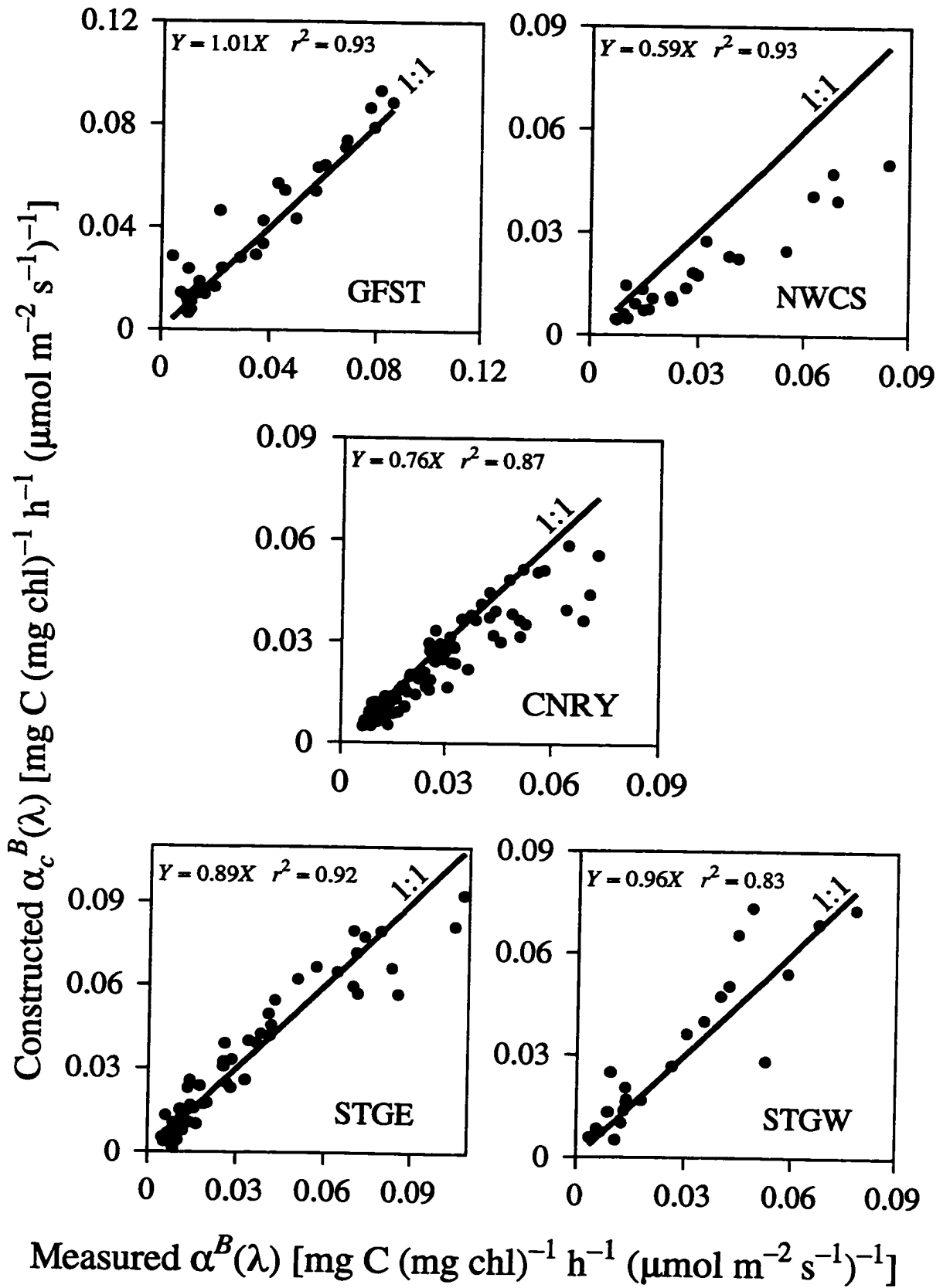


Figure 3.5

Figure 3.6 As in Figure (3.3) but for the JGOFS 93 cruise and for the shapes of the representative absorption spectra only.

Shapes of Absorption Spectra: 1993 Cruise

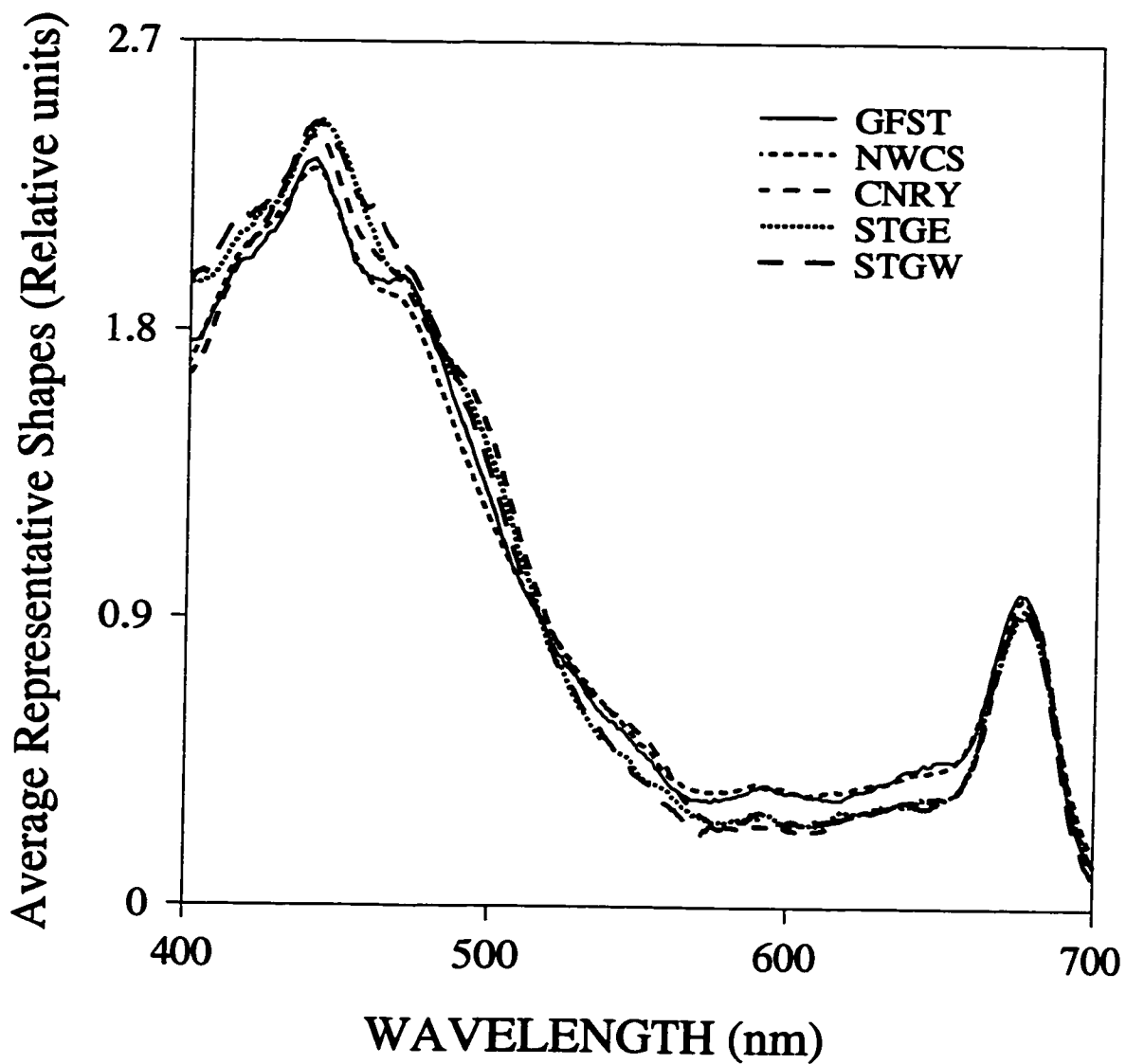


Figure 3.6

3.3.4 Variations in α^B , P_m^B and ϕ_m with Independent Variables

Using linear regression analysis, some nine independent variables were assessed for their ability to explain the variance in α^B , P_m^B and ϕ_m (only eight variables were tested for the parameters of the P^B vs. I curve; chlorophyll-*a* concentration was excluded because these parameters were normalized to the biomass) in each province and season. The results of analyses for α^B , P_m^B and ϕ_m are summarized in Tables (3.4a), (3.4b) & (3.4c), respectively. The fraction of total variance explained by the independent variables (r^2 , in %) and the number of data points are also given in the Tables. The regression equations describing the dependence of the parameters on independent variables are given in Appendix I. Several sets of variables (sometimes a single variable) could explain a significant fraction of the variance in the parameters in the different provinces (Tables 3.4a, b & c). However, in some cases, none of the independent variables could explain the variation in α^B (for the NWCS and STGE, JGOFS 92) or ϕ_m (for the CNRY and STGW in the JGOFS 92 and STGE and GFST in the JGOFS 93 cruise).

The provinces were then grouped into two domains: the Coastal domain (NWCS & CNRY) and the Westerlies domain (GFST, STGE & STGW), to examine if a better correlation between the parameters and the independent variables could be obtained, especially for the provinces in which no significant correlation was observed. The results for JGOFS 92 showed that there was a significant difference in the mean α^B values between the domains, but not in P_m^B or ϕ_m . In the JGOFS 93 data, P_m^B was significantly different between the domains, although α^B and ϕ_m were not. However, the seasonal difference was significant in both domains, for the three parameters. As in the case of the provinces, the independent variables were tested for their ability to predict the parameters in the two domains, for both cruises. The results are summarized in Table (3.5), and the regression equations are given in Appendix II.

Table 3.4a. Independent variables that explain significant ($p < 0.05$) portion of the variation in the initial slope of the P^B vs I curve, α^B [$\text{mg C (mg chl-}a)^{-1} \text{ h}^{-1} (\mu\text{mol m}^{-2} \text{ s}^{-1})^{-1}$], for the two cruises, in each of the five biogeochemical provinces. The coefficient of determination (r^2) shows the fraction of total variance (in percentage) explained by the independent variable(s). R_a is the blue-to-red absorption ratio, $a_p(435):a_p(676)$; R_c is the blue-to-red peak height ratio of chl- a absorption bands, $p(435):p(676)$; Z is the sampling depth; T is temperature; N , P and S_i are nitrate + nitrite, phosphate and silicate concentrations, respectively; C is chl- a concentration and Z_n is the distance between the sampling depth and the top of the nitracline. The number of data points (n) is given.

| Province | JGOFS 92 | | | JGOFS 93 | | |
|----------|-------------|----------|-----------|---------------------|----------|-----------|
| | Name | Variable | $r^2(\%)$ | n | Variable | $r^2(\%)$ |
| CNRV | R_a | 31 | 24 | S_i | 21 | 27 |
| | | | | S_i & R_a | 44 | 27 |
| | | | | S_i & R_c | 36 | 27 |
| STGE | - | - | - | T | 31 | 51 |
| | | | | S_i | 23 | 51 |
| | | | | Z & T | 41 | 51 |
| | | | | S_i & P | 32 | 51 |
| | | | | S_i & R_a | 29 | 51 |
| | | | | Z , S_i & Z_n | 48 | 51 |
| STGW | Z & R_a | 66 | 10 | S_i | 58 | 15 |
| | | | | P | 48 | 15 |
| GFST | Z & S_i | 54 | 12 | S_i | 72 | 12 |
| | | | | P | 79 | 12 |
| | | | | R_c | 46 | 12 |
| NWCS | - | - | - | N | 67 | 9 |

Table 3.4b. As in Table (3.4a), but for the rate of photosynthesis at saturating irradiance, P_m^B [mg C (mg chl-*a*)⁻¹ h⁻¹].

| Province | JGOFS 92 | | | JGOFS 93 | | |
|----------|----------------|-----------|-----|---------------------------------|-----------|-----|
| Name | Variable | $r^2(\%)$ | n | Variable | $r^2(\%)$ | n |
| CNRV | T & Z | 66 | 24 | Z | 21 | 27 |
| | | | | T | 57 | 27 |
| | | | | Z & S _i | 33 | 27 |
| STGE | Z _n | 76 | 18 | Z | 25 | 51 |
| | | | | T | 32 | 51 |
| | | | | Z & T | 41 | 51 |
| STGW | S _i | 56 | 8 | S _i | 34 | 15 |
| | | | | T & S _i | 84 | 15 |
| | | | | N & S _i | 74 | 15 |
| | | | | N & P | 65 | 15 |
| | | | | S _i & Z _n | 15 | 15 |
| GFST | Z _n | 74 | 13 | Z & N | 61 | 12 |
| | | | | Z & S _i | 57 | 12 |
| | | | | T & N | 69 | 12 |
| | | | | T & S _i | 60 | 12 |
| | | | | N & Z _n | 56 | 12 |
| | | | | S _i & Z _n | 55 | 12 |
| NWCS | S _i | 95 | 5 | T | 60 | 9 |

Table 3.4c. As in Table (3.4a) but for the realized, maximum quantum yield of photosynthesis, ϕ_m [mol C (mol quanta)⁻¹].

| Province | JGOFS 92 | | | JGOFS 93 | | |
|----------|----------|-----------|-----|-----------|-----------|-----|
| Name | Variable | $r^2(\%)$ | n | Variable | $r^2(\%)$ | n |
| CNRY | – | – | – | C | 28 | 27 |
| STGE | S_i | 49 | 17 | – | – | – |
| STGW | – | – | – | S_i | 43 | 15 |
| | | | | P | 29 | 15 |
| | | | | P & R_a | 49 | 15 |
| | | | | P & R_c | 50 | 15 |
| GFST | Z | 55 | 11 | – | – | – |
| NWCS | S_i | 65 | 5 | S_i | 64 | 9 |
| | | | | P | 45 | 9 |

Table 3.5. Independent variables that explain significant ($p < 0.05$) portion of the variation in three physiological parameters: α^B , P_m^B and ϕ_m (units given in Tables 3.4a, 3.4b and 3.4c, respectively) in two domains: Coastal (COAST) and Westerlies (WESTL), across the North Atlantic. The r^2 (in percentage) gives the fraction of the total variance explained by the independent variable(s). The symbols of the variables are explained in Table (3.4a).

| Domain | Parameter | JGOFS 92 | | | JGOFS 93 | | |
|--------|------------|--------------|-----------|-----|--------------|-----------|-----|
| Name | Name | Variable | $r^2(\%)$ | n | Variable | $r^2(\%)$ | n |
| COAST | α^B | T & R_a | 69 | 30 | – | – | – |
| COAST | α^B | T & R_c | 60 | 30 | – | – | – |
| WESTL | α^B | – | – | – | N | 28 | 78 |
| WESTL | α^B | – | – | – | T & N | 45 | 78 |
| COAST | P_m^B | T & Z | 75 | 30 | T | 40 | 36 |
| WESTL | P_m^B | T | 39 | 39 | Z | 22 | 78 |
| WESTL | P_m^B | Z_n | 53 | 39 | T | 36 | 78 |
| WESTL | P_m^B | Z & S_i | 85 | 39 | Z & T | 47 | 78 |
| WESTL | P_m^B | – | – | – | Z, T & S_i | 52 | 78 |
| WESTL | P_m^B | – | – | – | T & N | 41 | 78 |
| COAST | ϕ_m | R_a | 43 | 30 | C & N | 37 | 36 |
| COAST | ϕ_m | R_c | 26 | 30 | C & R_a | 27 | 36 |
| COAST | ϕ_m | T, C & R_a | 60 | 30 | C & Z_n | 29 | 36 |
| COAST | ϕ_m | T, C & R_c | 44 | 30 | – | – | – |
| WESTL | ϕ_m | R_a | 22 | 40 | – | – | – |
| WESTL | ϕ_m | R_c | 23 | 40 | – | – | – |

Because ϕ_m was not significantly different between domains in either cruise, the values were combined. The relationship with nitrate plus nitrite was examined, as in Babin et al. (1996). The pooled data did not show any clear pattern (Figure 3.7a). Therefore, the data were regrouped into respective provinces and the relationship was re-examined. A slight increase in ϕ_m with increasing nitrate plus nitrite concentration (as in Babin et al. 1996) could be seen in the CNRY province (Figure 3.7b) and in the GFST province (Figure 3.7c), especially for the JGOFS 93 data. For the remaining three provinces (Figures 3.7d-f), the pattern was masked by high scatter in the data points (especially those from the JGOFS 92 cruise). It should also be noted that the data points with nitrate plus nitrite concentration below the detection limit of the autoanalyser ($0.05 \mu\text{M}$) have to be interpreted with caution. For the purpose of this analysis, all samples with undetectable nitrate + nitrite concentration were assigned a value of $0.01 \mu\text{M}$. These were the values that confounded, to a great extent, the relation between ϕ_m and nitrate plus nitrite concentration in the GFST, NWCS and STGW provinces (Figures 3.7c, d and f).

Figure 3.7 Semi-log plots showing the relation between the maximum quantum yield of photosynthesis, ϕ_m , and the concentration of nitrate plus nitrite for data collected during the JGOFS 92 cruise (open circles) and JGOFS 93 cruise (filled circles). (a) All data combined, (b) CNRY province, (c) GFST province, (d) NWCS province, (e) STGE province and (f) STGW province.

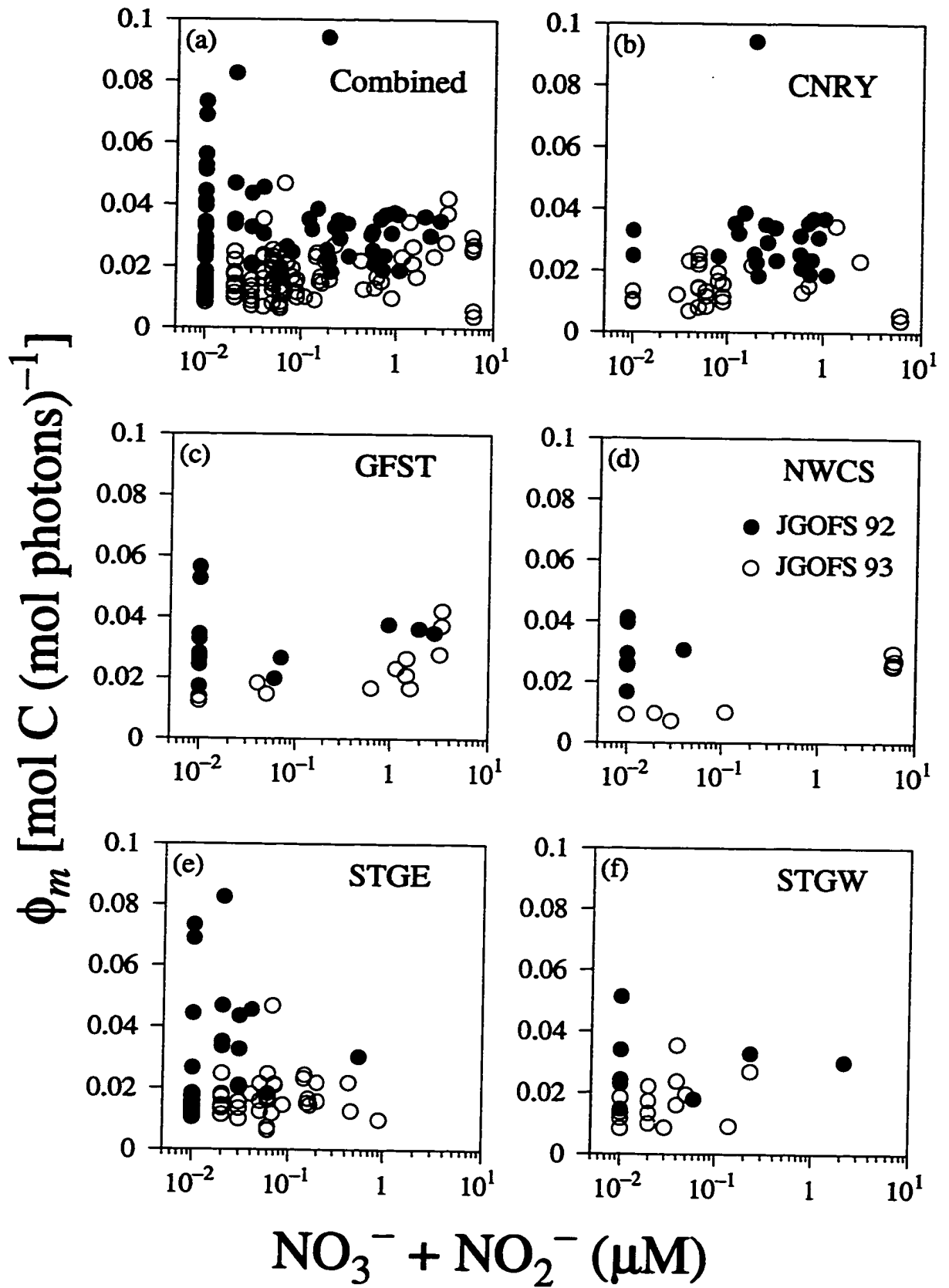


Figure 3.7

3.4 Discussion

3.4.1 Predictability of the Physiological Parameters

Several studies have examined the relationship between the parameters of the P^B vs. I curve and its biological or environmental covariables (e.g., Platt and Jassby 1976, Williams 1978, Lastein and Gargas 1978, Harrison and Platt 1980, Côté and Platt 1983, 1984). Research effort has also been channeled towards identifying key biological and environmental variables (such as temperature, light, nutrients, and absorption by phytoplankton pigments) that could be used as predictors of ϕ_m and other physiological parameters (Cleveland et al. 1989, Kolber et al. 1990, Platt et al. 1992, Schofield et al. 1993, Sosik and Mitchell 1995, Sathyendranath et al. 1996, Olaizola et al. 1996, Sosik 1996, Babin et al. 1996).

In this study, conducted in two different seasons (spring and fall) on transects across the North Atlantic that covered five biogeochemical provinces, I have attempted to describe the dependency of the photosynthesis parameters (α^B , P_m^B and ϕ_m) on various independent variables. The results showed that different independent variables were able to explain a significant fraction of the total variance in the efficiency of photosynthesis at low irradiance α^B (Table 3.4a), in the rate of photosynthesis at saturating irradiance P_m^B (Table 3.4b), and in the maximum quantum yield of photosynthesis ϕ_m (Table 3.4c), in each province and season.

In the case of α^B , the dominant independent variables were silicate concentration and the blue-to-red-absorption ratios R_a and R_c (Table 3.4a and Appendix I). A significant relationship could be established between P_m^B and temperature, depth or the distance between the sampling depth and the top of the nitracline, which explained up to 76% of the variance in P_m^B . It should be noted that the distance between the sampling depth and the top of the nitracline is an index of the potential supply of nitrogen; the actual supply would depend on the rate of vertical mixing,

induced by turbulent fluid motion (Lewis et al. 1984). As for α^B , silicate concentration in combination with other variables played an important role (Table 3.4b & Appendix I). The implication of the correlation between silicate concentration and the photosynthesis parameters will be discussed later.

When the data were grouped into the two domains, the relationship between α^B and independent variables changed significantly. Here, temperature and nitrate plus nitrite (N) became important (Table 3.5). In the case of P_m^B , temperature and sampling depth (Z) remained significant, whereas the importance of nitrate plus nitrite (concentration and potential supply) was diminished. These results from the domains suggest that pooling data into larger regions does not necessarily produce the same relationships as for smaller regions, i.e., provinces, which implies that the relationship between parameters and environmental co-variables could be scale-dependent.

3.4.2 Factors Affecting α^B

The initial slope of the photosynthesis-irradiance curve α^B is a function of photochemical processes in photosynthesis. It depends on the maximum quantum yield of photosynthesis ϕ_m and on the amount of light absorbed (Platt and Jassby 1976). Therefore, it was not surprising to find that the blue-to-red ratio of phytoplankton absorption, $a_p(435):a_p(676)$ [R_a], and that of chl-*a* absorption, $p(435):p(676)$ [R_c], taken separately, could each account for a significant fraction of total variance in α^B (Table 3.4a). Indeed, as early as 1963, Margalef suggested a relationship between primary production and the index $[D_{430}/D_{665}]$, which is the ratio of optical densities at 430 and 665 nm for phytoplankton pigments extracted in acetone. Since variations in R_a and R_c could imply changes in the phytoplankton community structure or in the physiological state of the cells (Margalef 1963, Cleveland *et al.* 1989, Sathyendranath *et al.* 1996), the correlation between α^B and R_a or R_c suggests

that the magnitude of α^B could be controlled by changes in species composition or physiological conditions of phytoplankton.

It is known that absorption by pigments packed into chloroplasts, which are enclosed in phytoplankton cells, is lower than that of the same materials distributed in a solution: pigment absorption is lowered through self shading of pigments inside the cell, a phenomenon known as the package or flattening effect (Duysens 1956, Morel and Bricaud 1981, Sathyendranath *et al.* 1987). If the phytoplankton populations were dominated by large cells, or by cells with high intracellular pigment concentration, the package effect would be amplified and the *in vivo* absorption spectra would be 'flattened', relative to that of the solution, mostly at the wavelength of maximum absorption (the blue peak around 435 nm). This would result in low values of R_a and R_c . The decrease in absorption due to self shading could in turn affect the magnitude of α^B because of its dependency on the absorbed light.

Taguchi (1976, 1981) found that α^B for a diatom culture of *Coscinodiscus centralis* and for a natural population of the dinoflagellate *Ceratium longipes* (Bailey) decreased with increasing self shading, showing the effect of cell size. Similarly, Côté and Platt (1983) found that α^B was negatively correlated with mean cell volume, which also suggests the effect of self shading on light absorption, and in turn on the initial slope α^B . Other variables that have been shown to affect the magnitude of α^B include nutrient availability through grazing (the ratio of phaeopigments to chl-*a*, Côté and Platt 1983), solar radiation and photoperiod (Smith *et al.* 1983), and nitrate concentration (Platt *et al.* 1992). On the other hand, for a study covering a wide latitudinal range from high- to mid-latitudes of the Eastern Canadian Arctic (Baffin Bay, Labrador Sea and Ungava Bay), Harrison and Platt (1986) showed that the tested environmental variables (temperature, depth, inorganic nitrogen concentration and chlorophyll-*a* concentration) could not explain more than 10% of the variance in α^B . In the present study, temperature accounted for only 31% of the variance in α^B in the STGE province during the spring cruise; nitrogen concentration explained about 67% of the total variance in α^B , in the NWCS province

during spring; but depth was significant only when used in combination with other variables (in both fall and spring cruises, Table 3.4a).

3.4.3 Factors Affecting P_m^B

The parameter P_m^B , being the rate of photosynthesis at saturating irradiance, is expected to increase with increasing light levels. The negative correlation between P_m^B and depth observed in some of our data (see examples in Tables 3.4b and 3.5) supports this idea, because light decreases with depth. In most phytoplankton species, P_m^B has been found to be higher for cells acclimated to high light than for those acclimated to low light levels (reviewed by Richardson *et al.* 1983). This could be partly attributed to the activity of enzymes involved in the dark reaction of photosynthesis. Beardall and Morris (1976) and Glover and Morris (1979) have showed a relation between P_m^B and the activity of the enzyme ribulose-1,5,bisphosphate carboxylase (RuBPCase). Several studies, both on laboratory cultures and on natural phytoplankton populations, have shown a correlation between P_m^B and light levels, P_m^B being higher under high irradiance than in low light levels (e.g., Falkowski 1980, Platt *et al.* 1982, 1992, Harrison and Platt 1986, Cullen and Lewis 1988, Ulloa *et al.* 1997). In the present study, P_m^B was sometimes found to be negatively correlated with depth (a proxy for light level), in agreement with these findings in the literature.

The magnitude of P_m^B is also known to be controlled by temperature (Eppley 1972). The correlation between P_m^B and temperature could be linked to the fact that P_m^B is a function of chemical (enzymatic) processes, which are accelerated by increasing temperature (up to an optimum level; Li 1980). Smith *et al.* (1983) showed a strong positive correlation between P_m^B and the activity of a carboxylating enzyme, RuBPCase. For natural phytoplankton assemblages, Harrison and Platt (1986) found that temperature was the most important variable in explaining the variance in P_m^B , both in high latitudes and in temperate environments. Similarly, we

found a positive correlation between P_m^B and temperature in some of the provinces and domains sampled here (Tables 3.4b and 3.5).

It is unequivocally evident, from several studies (as mentioned above), that both temperature and light levels control the magnitude of P_m^B . However, in natural environments, other variables such as species composition (e.g., Côté and Platt 1983), nutrients (e.g., Glover 1980), and time of day (e.g., MacCaull and Platt 1977, Hecky and Fee 1981, Harding *et al.* 1981) have been shown to affect the magnitude of P_m^B . Because of this, there is the possibility that the relationship between P_m^B and temperature or irradiance could be masked on occasion. For example, in our study, although P_m^B was positively correlated with temperature in some provinces, the slope of the regression lines changed from one region or season to another, while in other regions no significant relation between P_m^B and temperature could be found (especially during the fall 1992 cruise; Table 3.4b). Furthermore, pooling the data into larger regions (domains) resulted in a decrease in the fraction of the explained variance or, sometimes, the correlation became insignificant.

These results are in agreement with other findings in which no significant positive correlation could be found between P_m^B and temperature. For example, Banse and Yong (1990) showed that a multiple regression between P_{opt}^B (the maximum carbon fixation rate in the water column, noted as $(P/Chl)_{opt}$ in their paper, a proxy for P_m^B) and environmental variables (temperature, irradiance and nitrate concentration) for their data set, explained only a small fraction of the total variance in P_{opt}^B . On the other hand, Behrenfeld and Falkowski (1997) found a non-linear relationship between P_{opt}^B and sea-surface temperature, while Balch *et al.* (1992) found that P^B at the surface, which was taken as an approximation for P_m^B , assuming no photoinhibition, was negatively correlated with sea-surface temperature (SST). The authors attributed the negative correlation to the combined effect of relationships between the variables that control the magnitude of P^B , that is, a positive

relation between temperature and dark reaction of photosynthesis; a positive relation between nitrate and growth; and a negative relation between temperature and nitrate.

The control of P_m^B by several factors might also explain, in the present study, why a significant variance in P_m^B especially for the JGOFS 93 data set, was better explained by combinations of variables rather than individual ones (Table 3.4b). Overall, the results obtained here support the idea that relationships between P_m^B and environmental variables are best established at scales which could be considered to be under a common physical forcing, such as a biogeochemical province, in a given season.

3.4.4 Factors Affecting ϕ_m

The correlation between the realized maximum quantum yield of photosynthesis, ϕ_m , and different independent variables was examined. In some studies of natural phytoplankton populations, ϕ_m , or the ratio of quantum yield of photosynthesis to that of fluorescence, has been related to variables such as nutrient availability or concentration (Cleveland *et al.* 1989, Lizotte and Priscu 1994, Sathyendranath *et al.* 1996, Sosik 1996, Babin *et al.* 1996); temperature (e.g., Tilzer 1985, Chamberlin and Marra 1992); depth and light (e.g., Dubinsky *et al.* 1984, Kishino *et al.* 1986, Chamberlin *et al.* 1990, Lizotte and Priscu 1994, Babin *et al.* 1995, Sathyendranath *et al.* 1996); and changes in the blue-to-red ratio of phytoplankton absorption $a_p(435):a_p(676)$ (Cleveland *et al.* 1989, Sathyendranath *et al.* 1996) or the ratio of peak heights of chl-*a* absorption $p(435):p(676)$ (Sathyendranath *et al.* 1996). Yet other studies have shown no significant correlation between ϕ_m and the tested independent variable, which might be temperature, nitrate, light and accessory pigments (e.g., Schofield *et al.* 1993) or nitrate concentration and distance between sampling depth and the nitracline (e.g., Olaizola *et al.* 1996).

In the present study, nine independent variables were tested for their correlation with the maximum quantum yield of photosynthesis (Table 3.4c). As in the case of α^B and P_m^B , silicate concentration (S_i) was a significant predictor of ϕ_m ; phosphate concentration (P) was equally important, but nitrate (N) was not significant (Table 3.4c; Figure 3.7). When the data were grouped into domains, neither S_i nor P could explain a significant (at $p \leq 5\%$) proportion of the variance in ϕ_m (Table 3.5). Instead, chl-*a* concentration and the absorption ratios [$a_p(435):a_p(676)$ and $p(435):p(676)$] became significant predictors of ϕ_m . The maximum quantum yield of photosynthesis is the ratio of α^B to the spectral mean absorption coefficients of phytoplankton. Therefore, the magnitude of ϕ_m could be influenced by factors affecting phytoplankton absorption or those regulating α^B , as discussed earlier.

3.4.5 Effect of Silicate Concentration on Photosynthesis Parameters

Silicon is an essential element for growth and cell division of diatoms and silicoflagellates. In several coastal areas (e.g., Wetsteyn *et al.* 1990, Levasseur *et al.* 1990, Conley and Malone 1992, Dortch and Whitedge 1992), in open-ocean waters (e.g., Dugdale *et al.* 1995, Brzezinski and Nelson 1995) and in mesocosm experiments (e.g., Egge and Aksnes 1992, Egge and Jacobsen 1997), a significant increase in silicate concentration, or the depletion of it, has been linked to the initiation or termination, respectively, of diatom blooms. However, given that the most abundant phytoplankton groups during both the JGOFS 92 and JGOFS 93 cruises were prochlorophytes, cyanophytes and picoeukaryotes in most areas (Li 1994, 1995), it was surprising to find significant correlations between silicate concentration (S_i) and the photosynthesis parameters α^B , P_m^B and ϕ_m (Tables 3.4a, 3.4b and 3.4c).

It is possible that the observed relation between the parameters and S_i arose from an association between silicate concentration and other environmental or biological variables controlling the magnitudes of α^B , P_m^B or ϕ_m . However, such an association was found only in two provinces during the spring (JGOFS 93) cruise:

silicate concentration was correlated with the absorption ratios R_a and R_c in the CNRY province, and with temperature and with the potential supply of nitrate in the GFST province (data not shown). The correlation between silicate and nitrate or phosphate was not significant at the 5% level.

Another possible explanation for the correlation between S_i and the photosynthesis parameters could be the effect of silicate concentration on the taxonomic composition of phytoplankton assemblages. Some investigations (e.g., Egge and Aksnes 1992, Conley and Malone 1992, Taylor *et al.* 1993, Sommer 1994, Egge and Jacobsen 1997) have revealed that the depletion of silicate results in a shift of phytoplankton community structure from diatom domination to a dominance by non-diatom groups. In the present study, S_i was generally low at the depths from which samples for measuring the photosynthesis parameters were collected. The mean silicate concentration in the five biogeochemical provinces sampled here ranged from 0.57 to 0.88 μM in the JGOFS 92 and from 0.56 to 1.64 μM in the JGOFS 93 cruise. These values are below the concentration of 2 μM considered by Wetsteyn *et al.* (1990) and Egge and Aksnes (1992) to be the minimum requirement for diatoms to dominate the phytoplankton assemblages, given that nitrate and phosphate are not limiting. However, the 2 μM threshold cannot be taken as universal in all conditions. For example, in the Sargasso Sea (at the Bermuda-Atlantic time series study site), where silicate concentration ranged from 0.5 to 1.8 μM in the upper 160 m throughout the study period of about four years, Brzezinski and Nelson (1995) observed an increase in biogenic silica due to diatom blooms every winter/spring time, even though silicate concentration did not reach 2 μM .

The relatively low concentration of silicate (and other nutrients) during the present study (fall 1992 and spring 1993) could be one of the reasons why picophytoplankton dominated. However, at some stations in coastal regions where silicate concentration was elevated (up to 4.1 μM in the CNRY province and 3.5 μM in the NWCS province during the JGOFS 93 cruise), diatoms were also present in high abundance, in addition to coccolithophorids and dinoflagellates (H. Benavides,

unpublished data). Throughout the transect during the JGOFS 93 cruise, diatoms and dinoflagellates were observed, even though they were not the dominant groups. The commonly-observed diatom genera were *Rhizosolenia* and *Chaetoceros*; *Ceratium* was the dominant genus for dinoflagellates, and the common prymnesiophyte was *Emiliania huxleyi* (H. Benavides, unpublished data). If we assume that high concentrations of silicate would favour the growth of large diatoms, then the presence of diatoms (and other large cells) at some of the stations could explain the observed negative correlation between the photosynthesis parameters and silicate concentration in some provinces (regression equations not shown), consistent with the observation that photosynthesis parameters decreased with increasing mean cell volume (Taguchi 1976, 1981, Côté and Platt 1983; see also Glover 1980).

Positive correlations between S_i and the photosynthesis parameters in other provinces could be explained by the presence of smaller cells that also require silicate for their growth such as silicoflagellates or small diatoms. In a mesocosm experiment, Egge and Jacobsen (1997) found that, apart from stimulating rapid growth of diatoms, the addition of silicate (in the presence of nitrate and phosphate) increased the abundance of other phytoplankton cells (*Phaeocystis pouchetii*, dinoflagellates and small flagellates) relative to a treatment in which only nitrate and phosphate were added.

The results presented here (Figure 3.7, Tables 3.4a, 3.4b, 3.4c & 3.5 and Appendices I & II) indicate that the correlation of physiological parameters of phytoplankton with environmental or biological variables in different biogeochemical provinces or domains varies significantly. That is to say, the correlation between a parameter and a certain variable found in one province was not always applicable to the neighbouring provinces, in a given season. Even within the same province, a relationship observed in a given season was not necessarily the same in the other season. For example if we look at the neighbouring subtropical gyre provinces (STGE and STGW), a significant fraction of the variance in P_m^B for the STGE province

during the fall cruise (Table 3.4b) could be explained by the distance between the sampling depth and the top of the nitracline (Z_n), whereas in the STGW, it was silicate concentration. Within the STGE province alone, while Z_n was significant during the fall cruise, in spring temperature and sampling depth were the important variables (Table 3.4b).

Of the three parameters studied, only P_m^B showed some consistency in the way it correlated with other variables. Values of P_m^B were always positively correlated with temperature and potential nitrogen supply (Z_n , that is, the distance between the sampling depth and the top of the nitricline), but always negatively correlated with depth. However, the regression coefficients differed between provinces and domains (Appendixes I & II), which could be an indication of 'interference' by other variables that control the magnitude of P_m^B . The values of α^B and ϕ_m were sometimes positively or negatively correlated with a given variable, depending on the province, domain or season, implying differences in the forcing variables between both provinces and seasons.

Differences in the photosynthesis parameters, environmental factors, phytoplankton biomass or primary production have been linked to changes in the physical, chemical or biological variables (e.g., Côté and Platt 1983, Frazel and Berberian 1990, Sosik and Mitchell 1995, Olaizola et al. 1996). These variations, either initiated by a slow progression of seasonal changes in environmental conditions or by transient physical phenomena, could affect light levels, nutrient availability and phytoplankton species composition within the area. Therefore, the physical characteristics of the regions studied here (such as upwelling, circulation patterns and mixed-layer depth) could have contributed to the observed differences in the photosynthesis parameters and corresponding independent variables.

3.5 Concluding Remarks

The results presented here showed that the average physiological parameters were more variable between seasons (in a given province) than between provinces (within a given season). The seasonal variation in the parameters (α^B , P_m^B and ϕ_m) and the differences between provinces in the shapes of the action and absorption spectra was evident in all the five biogeochemical provinces of the North Atlantic sampled during the two cruises (Tables 3.1, 3.2 and 3.3; Figures 3.3 and 3.6). The differences in the parameters between spring and fall data collected on the same track suggest that different environmental conditions prevailed in the two seasons, resulting in changes in their magnitudes (see also Platt et al. 1992). For example the average nutrient concentrations (nitrate, silicate and phosphate) in the euphotic zone were higher during the spring cruise than in the fall cruise; the daily-averaged PAR (Photosynthetically Available Radiation) values measured just above the sea surface was overall higher during the spring cruise than during the fall cruise; and the average chlorophyll-*a* concentration from the sampled depths was higher during the fall than in the spring cruise.

These results emphasize the significance of considering seasonal changes in the parameters, within a given biogeochemical province, as has been pointed out earlier (Platt and Sathyendranath 1988, Platt et al. 1991, Longhurst 1995). The variations in the parameters between provinces was not as significant as between seasons. However, when data collected from one season were grouped into large regions (domains), the results did not provide a single, simple solution: the predicting (independent) variables changed and, in some cases, the previous relation found in individual provinces disappeared. Only ϕ_m remained relatively constant between the Coastal and Westerlies domains for both cruises. An attempt to find a relationship between the pooled ϕ_m (supposedly not significantly different between domains) and nitrogen concentration (Babin et al. 1996) was unsuccessful for the present data set (Figure 3.7a).

Thus, in the context of estimating large-scale primary production (say yearly), seasonal variation in the parameters should be taken into consideration. It is also suggested that variation between provinces should not be ignored; if information on the photosynthesis parameters in a given province is lacking, application of parameters from neighbouring provinces should be made with caution. The five provinces studied here differ in their physical characteristics (Longhurst 1995). Therefore, the observation that mean values of the parameters were not significantly different between provinces in most cases could have been coincidental or could be an indication of the stability in the representative values of the photosynthesis parameters.

Several independent variables, individually or in combinations, were able to explain a high and significant proportion of the total variance (as high as 95% in some cases) in the photosynthesis parameters of phytoplankton (α^B , P_m^B and ϕ_m). The correlation between the physiological parameters and the selected independent variables between the provinces and seasons was variable, although some general trends were observed. These results imply that the magnitudes of the parameters depend on the combined effect of several factors. Therefore, assuming that phytoplankton within a given province are under similar physical forcing, prediction at large scales would have to be made at the level of the province and season.

Overall, seasonal differences in the magnitude of the mean values of the photosynthesis parameters in each province were strong and consistent. What was also striking were the differences in the independent variables that could explain their variance between seasons. Why is there such a difference? It could be hypothesized that one of the major causes of the significant and consistent change in the magnitude of the three parameters and the shapes of action and absorption spectra was changes in species composition between the two distinct seasons studied. This possibility is explored in the next chapter (Chapter 4), in which the effects of changing species composition on the variation in the photosynthesis properties are examined.

CHAPTER 4

Changes in Phytoplankton Population Structure: Effects on the Action and Absorption Spectra

4.1 Introduction

Knowledge of the variation in the action and absorption spectra of phytoplankton is important in the estimation of primary production using spectrally-resolved photosynthesis-light models. If ignored, variation in the action spectrum $\alpha^B(\lambda)$ (where λ is the wavelength, and the superscript indicates normalization to phytoplankton biomass B) may cause errors in the computed water-column primary production: a 20% systematic error in $\alpha^B(\lambda)$ could result in an error of up to 10% in the calculated water-column primary production (Chapter 2). The action spectrum $\alpha^B(\lambda)$ is proportional to the biomass-specific absorption coefficient of phytoplankton $a_p^B(\lambda)$, with the proportionality constant being the maximum quantum yield of photosynthesis ϕ_m (Platt and Jassby 1976), i.e., $\alpha^B(\lambda) = \phi_m \times a_p^B(\lambda)$. Therefore, variation in $\alpha^B(\lambda)$ may be caused by changes in ϕ_m or in $a_p^B(\lambda)$ or in both.

The shapes of action and absorption spectra have been shown to vary both spatially and temporally, and even between two species of the same group. One of the major causes of variation in the action and absorption spectra is changes in pigment composition (e.g., Lewis et al. 1986, Hoepffner and Sathyendranath 1992, Schofield et al. 1996, Lutz et al. 1996).

Other factors known to cause variation in the spectra are acclimation to light quality or levels (e.g., Sakshaug et al. 1991, Johnsen and Sakshaug 1993, Johnsen et al. 1994a, Schofield et al. 1996); intracellular pigment concentration or cell size (e.g., Sathyendranath et al. 1987, Sosik and Mitchell 1994, Stuart et al. submitted); and the presence of photosynthetically-inactive pigments (e.g., Sosik and Mitchell 1995,

Lazzara et al. 1996). The results presented in Chapters 2 and 3 showed that the shape of the absorption spectrum is a good proxy for that of the action spectrum in certain oceanic regimes. The question then would be: How do the action and absorption spectra change in response to changes in the physical, chemical and biological conditions of the water in natural environments?

In the present study, carried out at a single location during late summer to fall 1994, week-to-week variations in the action spectra, absorption spectra, quantum yield of carbon fixation, pigment (species) composition and hydrographic conditions, are explored. The main objective is to examine the extent to which changes in water conditions and species composition between two seasons (summer and fall) affect the shapes and amplitudes of the action spectra, the absorption spectra and the magnitude of maximum quantum yield of photosynthesis. This study is undertaken to test the hypothesis that the seasonal variation in the photosynthesis parameters and in the shapes of the spectra, observed in the previous chapter (Chapter 3), was caused by changes in phytoplankton species composition.

4.2 Materials and Methods

Sampling was done in the Bedford Basin, Nova Scotia, Canada. Bedford Basin is a small marine inlet, with a maximum depth of 70 m and a surface area of about 17 km². The basin is separated from the ocean by a 20 m deep sill; the water inside the basin and open-ocean waters move across the sill in response to physical forcing by winds, tides and freshwater runoffs (Platt and Conover 1971, Platt et al. 1972).

Samples were collected weekly from four depths (1, 5, 10 and 60 m) at a single station in the middle of the Basin from 10 August to 21 December 1994, a total of 20 weeks. Sampling took place every Wednesday at approximately 9:00 a.m. Samples for the determination of absorption spectra, chlorophyll-*a* (chl-*a*) concentration

(by Turner fluorometry), oxygen concentration, pigment composition (by High Performance Liquid Chromatography, HPLC), and concentrations of nutrients (nitrate plus nitrite, silicate and phosphate) were collected at each of the four depths using a Niskin bottle. For the action spectrum and phytoplankton identification, samples were collected only at 5 m. Profiles of temperature, *in situ* fluorescence (as a proxy of chl-*a*), salinity and photosynthetically available radiation (PAR) were determined using a CTD probe. Meteorological observations of wind speed and direction, air temperature, rainfall and hours of bright sunshine were available from Shearwater Airport as daily averages and were obtained from Atmospheric Environment Service, Bedford, Nova Scotia.

The photosynthetic action spectra were determined using a spectral incubator, as explained in Chapter 2. Absorption by total particulate materials was determined as in Chapter 3, by the filter technique (Kishino et al. 1985); correction for the pathlength amplification (β factor) was made using the method of Hoepffner and Sathyendranath (1992), and detrital absorption was estimated using the approach of Hoepffner and Sathyendranath (1993), which assumes an exponential function for the shape of the detrital absorption spectrum. Fourth-derivatives of the absorption spectra (Butler and Hopkins 1970, Owens et al. 1987, Bidigare et al. 1989, Millie et al. 1995) were calculated to resolve absorption maxima of major pigments present in each sample. Concentrations of nutrients were determined by a standard automated method using an Alpkem autoanalyser, as in Irwin et al. (1989).

Pigment composition was determined by HPLC following the method of Head and Horne (1993). The samples were kept in a deep freezer (-70°C) and the analysis was made two years later. Fluorometric determination of chl-*a* was made the day following sampling, using the method of Holm-Hansen et al. (1965). Both the action and absorption spectra were normalized to chl-*a* determined fluorometrically because, in this case, it was more reliable than that determined by the HPLC. The comparison between chl-*a* determined by the Turner fluorometer with that determined by the HPLC revealed that the HPLC-determined chl-*a* was lower than

that determined fluorometrically by about a factor of two. This suggests that chl-*a* might have been gradually lost during the two-year storage in the freezer (Erica Head, pers. comm.). Therefore, for samples determined by the HPLC, only qualitative analysis to determine the type of pigments present was made.

Oxygen concentration was measured using an automated dissolved oxygen titration system (Jones et al. 1992). Samples for identification of dominant phytoplankton groups were collected in the last half of the sampling period (from 19 October to 21 December 1994), fixed in Lugol's solution and identified the following day; no cell counting was undertaken. It should also be noted that samples collected at 60 m were excluded from all analyses, because no live phytoplankton were present at that depth.

The broad-band parameters of the photosynthesis–irradiance (P^B vs. I) curve were not determined in the present study. Therefore, the maximum quantum yield of photosynthesis ϕ_m was estimated as the ratio of the mean value of the spectrally-resolved initial slopes of the P^B vs. I curve, $\bar{\alpha}^B$, to the mean value of the biomass-specific absorption coefficient of phytoplankton, \bar{a}_p^B :

$$\phi_m = 0.023 \times \frac{\bar{\alpha}^B}{\bar{a}_p^B} \quad (4.1)$$

where the constant 0.023 converts mg C to moles, hours to seconds and μmol to moles of photons; the mean values, $\bar{\alpha}^B$ and \bar{a}_p^B , were calculated over the wavelength range from 400 to 700 nm.

4.3 Results

4.3.1 Hydrography and Shapes of the Spectra

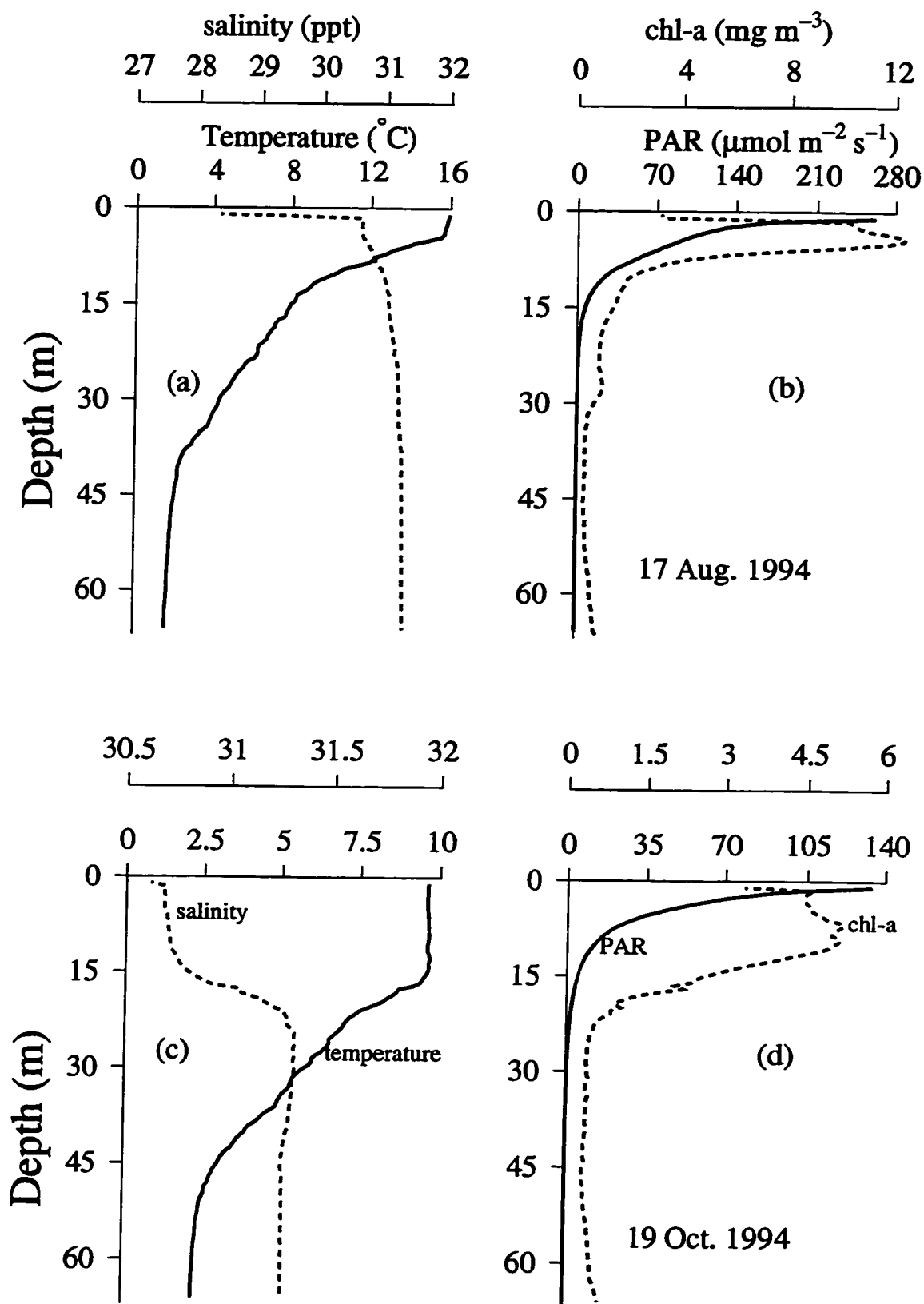
The water-column conditions were different from one sampling week to another. Nevertheless, they could be classified into two major groups with reference to stratification, or lack of it, in the first three depths sampled: 1, 5 and 10 m. The first

group could be referred to as 'stratified', and it included the late-summer months of August and September. During this period, the water-column was stratified with a shallow mixed layer of about 3-5 m. The depth of the chlorophyll maximum (DCM) ranged from 5 to 9 m, but was frequently at 5 m, and the peak was relatively narrow. Salinity was low at 1 m, but increased slightly with depth below the mixed layer. An example from this group is given in Figures (4.1a) & (4.1b) for profiles determined on 17 August 1994.

The second group could be categorized as 'mixed', and it occurred in the months of October through December, during fall. In this period, the stratification at the surface was eroded, and the mixed layer extended to between 10 and 20 m. Most likely the mixing was associated with an influx of freshwater, because a layer of low salinity formed on the top 15 m or so, and a strong halocline developed between 15 and 25 m. The chlorophyll maximum peak was broader than in the first group, and extended from the surface to 10 m or more. Figures (4.1c & d) show the hydrographic conditions for 19 October 1994, as an example from this period. In both periods, the photic zone was shallow and did not exceed 20 m.

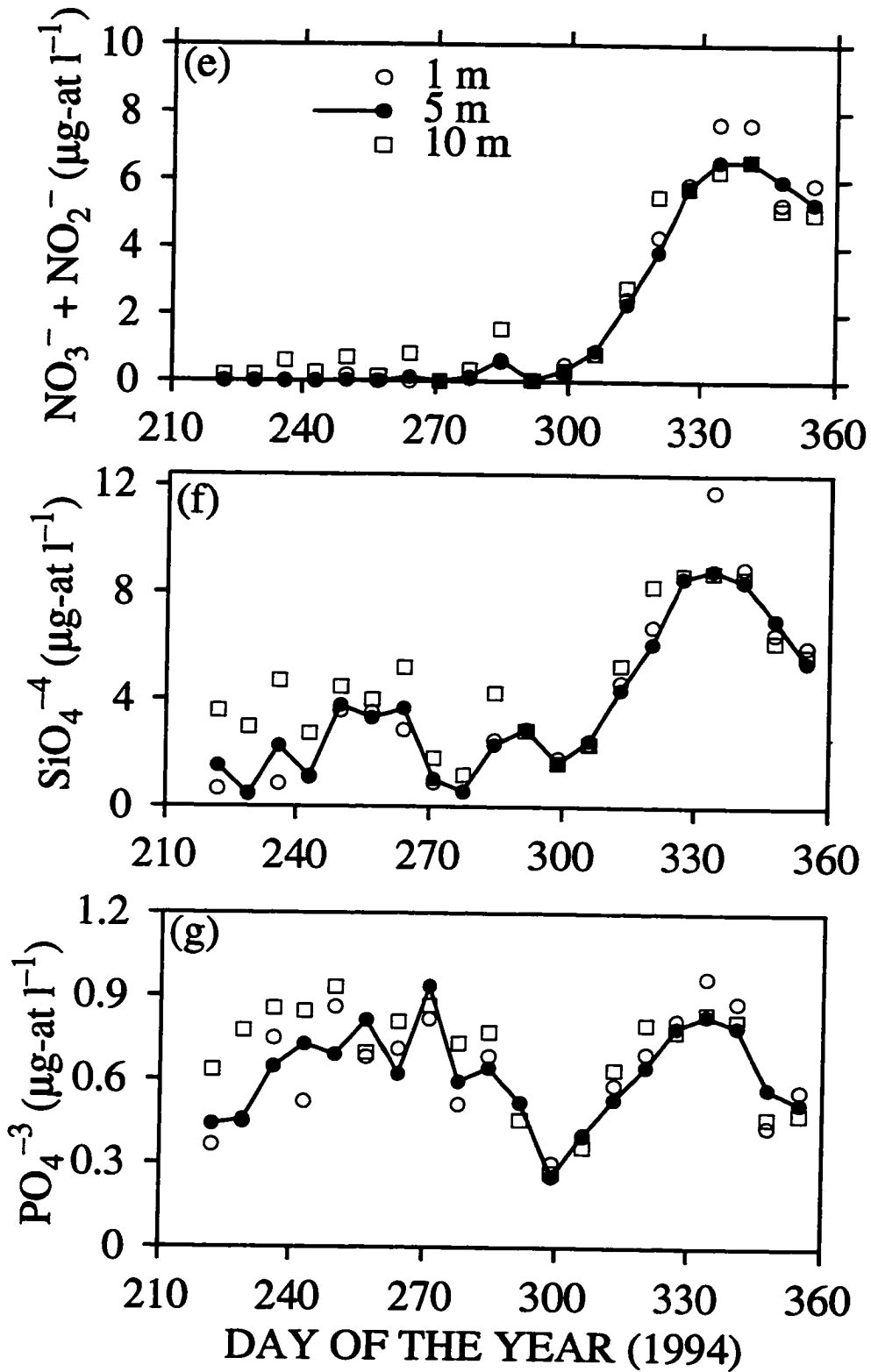
Nutrient concentrations ($\mu\text{g-at l}^{-1}$) for the entire sampling period are shown in Figures (4.1e to g). Nitrate (plus nitrite; referred to henceforth as nitrate) was very low at 1 and 5 m during the stratified period, and then increased sharply during the mixed period (Figure 4.1e). A similar trend was observed for silicate, although the concentration was relatively high in the stratified period (Figure 4.1f). Phosphate concentration, on the other hand, was of similar magnitude in both periods (Figure 4.1g), with a notable decrease around day 300 (in October). All nutrients reached maximum concentration between late November and early December (day 327 to 341) then started to decrease by the second week of December, day 348. The figures also show that nitrate was apparently a limiting nutrient during the stratified period, with its concentration at 5 m being below the detection limit.

Figure 4.1 Profiles of temperature, salinity, photosynthetically available radiation (PAR) and chl-*a* concentration for two sampling dates in the Bedford Basin: (a & b) 17 August 1994 and (c & d) 19 October 1994. Nutrient concentrations for the whole sampling period are presented as a function of day of the year (1994): (e) nitrate plus nitrite, (f) silicate and (g) phosphate; in all cases, open circles indicate data collected at 1 m, filled circles joined by lines show data taken from 5 m and open squares indicate data sampled at 10 m. The meteorological data as a function of day of the year are given as daily averages (thin lines) and weekly averages, filled circles joined by thick lines: (h) air temperature, (i) rainfall, (j) hours of bright sunshine, (k) wind speed and (l) wind direction.



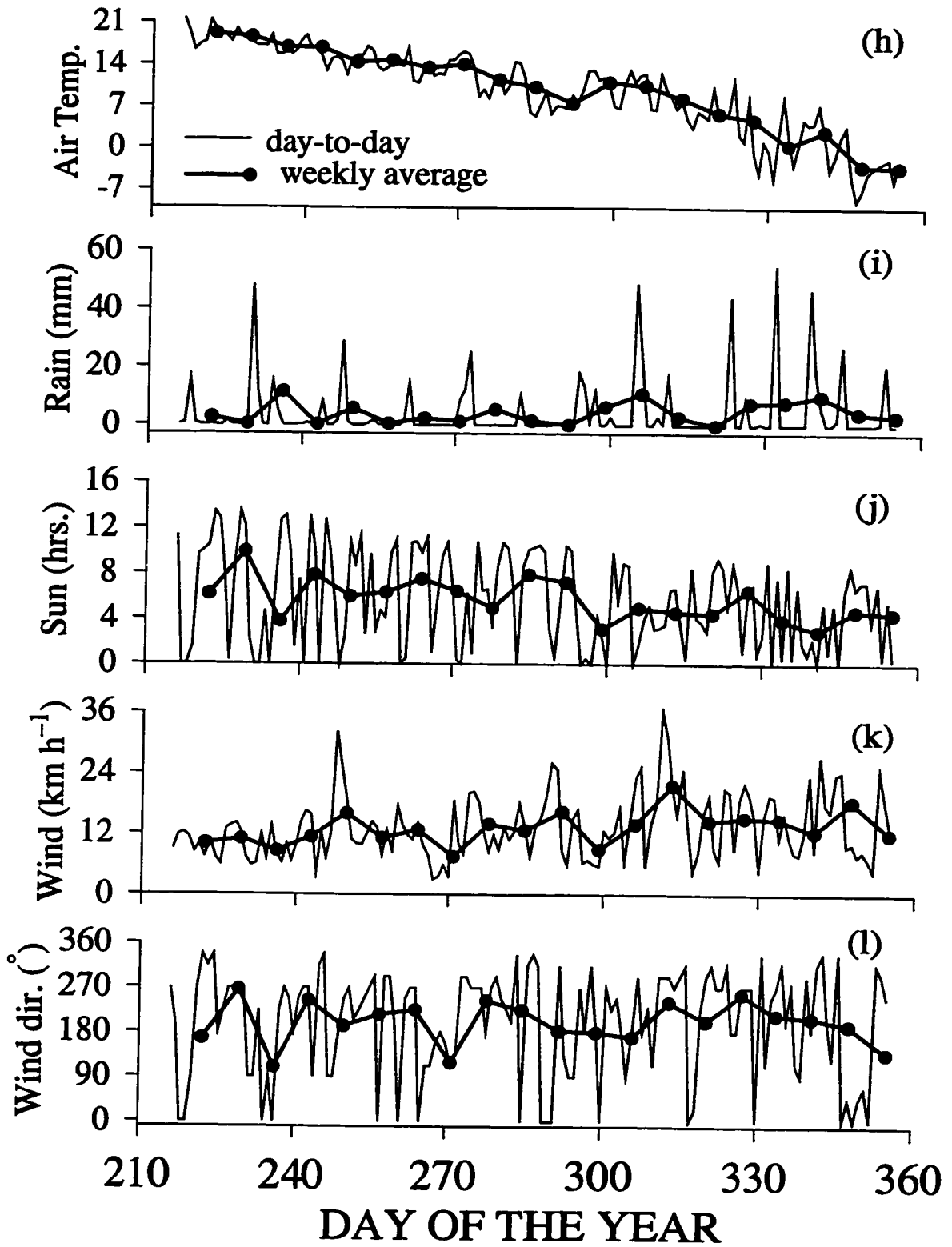
Figures 4.1a to d

Nutrient Concentrations: August to December 1994



Figures 4.1e to g

Meteorological data: 10 Aug. - 21 Dec. 1994



Figures 4.1h to l

The meteorological conditions for the sampling period are given in Figures (4.1h to l). The day-to-day variation (thin lines) and the weekly averages (filled circles joined by thick lines) show high fluctuations with time; the distinction between the two periods, stratified and mixed, that were identifiable in the oceanic data, were not as clearly discernible in the meteorologic data. However, some patterns could be identified: for example, air temperature (Figure 4.1h) and hours of bright sunshine (Figure 4.1j) decreased with time, as expected. Figure (4.1l) shows that, on average, the prevailing wind was south-westerly (between 180 and 270°); the weekly-averages in wind speed were between 10 and 20 km h⁻¹, although the daily-average speed could be as high as 35 km h⁻¹ (Figure 4.1k). The weekly averages in rainfall were low, around 12 mm, but on individual days, rain could be heavy and could sometimes reach 50 mm (Figure 4.1i). Although the meteorological data fluctuated, some of the day-to-day variation could be linked to the variation in the biology of the water, as will be discussed later.

The variations in the shapes of action spectra in each month are shown in Figure (4.2), and those of the corresponding absorption spectra in Figure (4.3). The spectra were normalized to their mean values to compare the *shapes*. The spectra for August and September have the distinct peaks and shoulders in the blue and the peaks in the red parts of the spectra, but are featureless in the blue-green to yellow region, reflecting the presence of diverse pigments with overlapping absorption bands. Derivative analysis has been shown to be useful in separating secondary absorption peaks and shoulders caused by such overlapping as the maxima of absorption peaks for major pigments present in each sample are revealed (see e.g, Owens et al. 1987, Bidigare et al. 1989, Millie et al. 1995) as peaks in the fourth-derivative spectra.

Figure 4.2 Shapes of action spectra for five months: (a) August, (b) September, (c) October, (d) November and (e) December, sampled in 1994, in the Bedford Basin. Each spectrum is normalized to its mean value, averaged over the spectral range from 400 to 700 nm.

Photosynthetic Action Spectra: Bedford Basin 1994

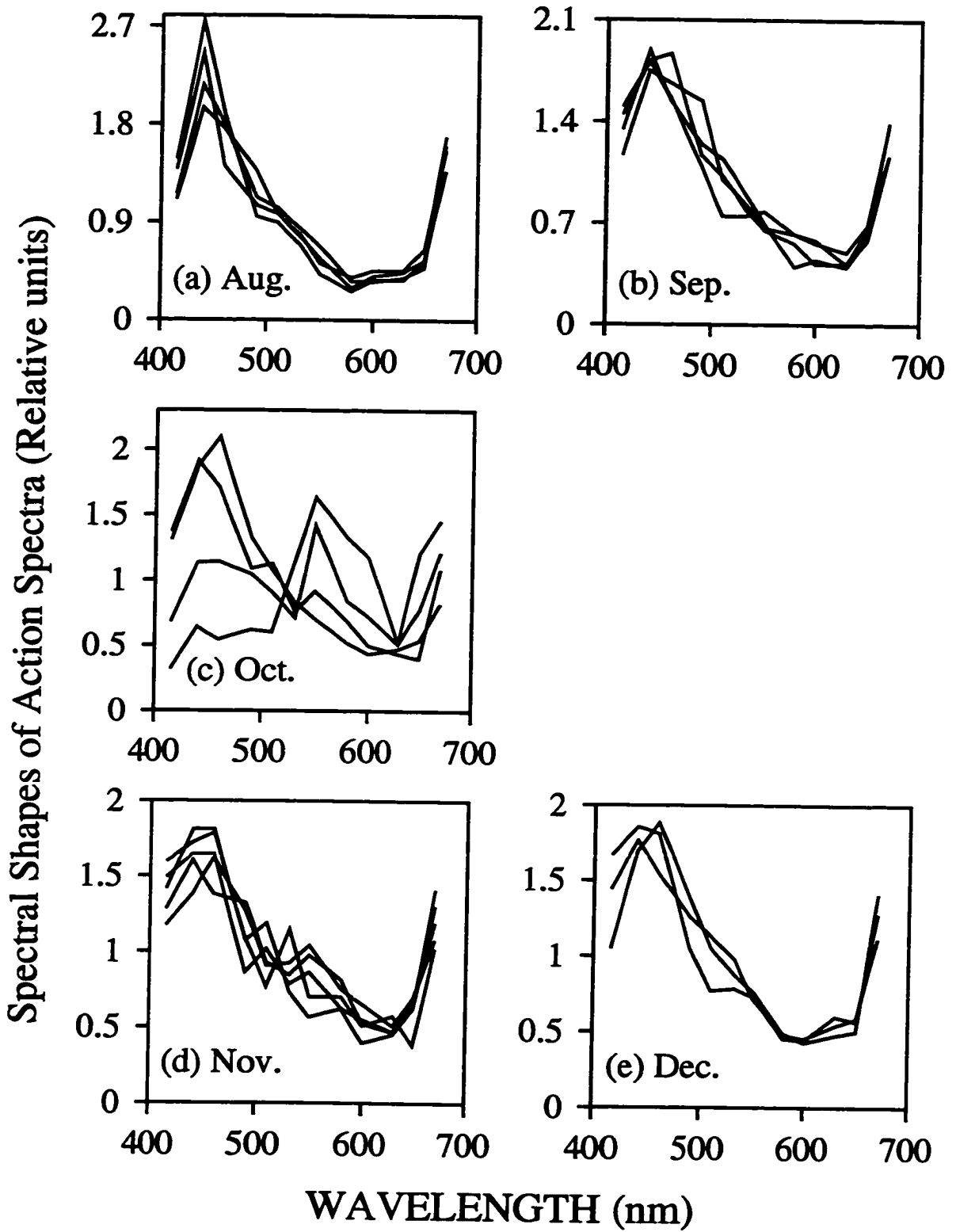


Figure 4.2

Figure 4.3 As in Figure (4.2), but for the corresponding absorption spectra.

Absorption Spectra of Phytoplankton: Bedford Basin 1994

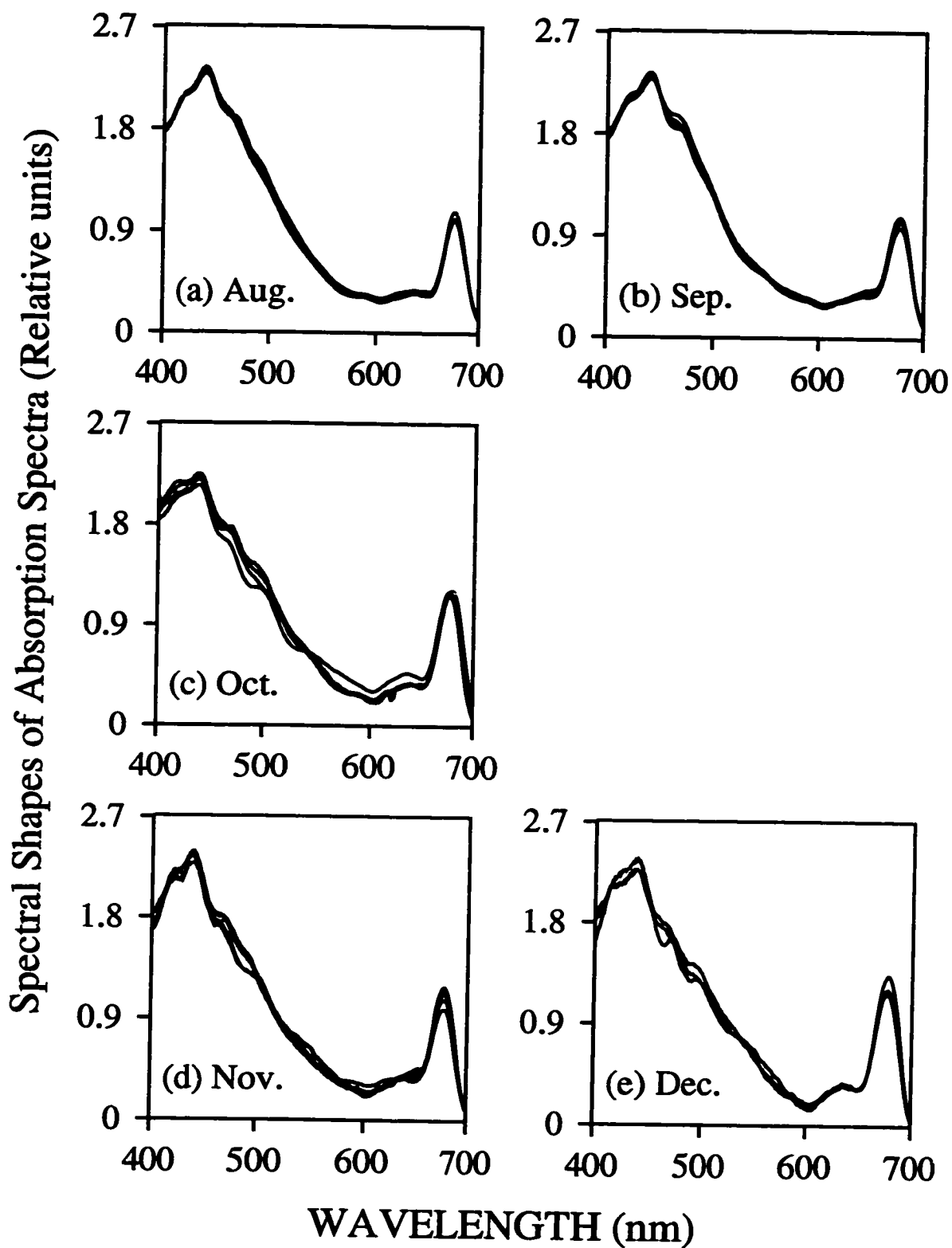


Figure 4.3

Table 4.1. Centres (nm) of wave crests of the fourth-derivative spectra calculated for each absorption spectrum for samples collected from 5 m.

| Date (1994) | Blue (nm) | | | Blue-green (nm) | | | Red (nm) | | |
|-------------|-----------|-----|-----|-----------------|-----|-----|----------|-----|-----|
| Aug. 10 | 416 | 440 | 466 | 495 | – | 591 | 618 | 641 | 676 |
| Aug. 17 | 418 | 441 | 465 | 495 | – | 590 | 615 | 641 | 677 |
| Aug. 24 | 415 | 440 | 467 | 494 | – | 593 | 618 | 641 | 677 |
| Aug. 31 | 416 | 440 | 471 | 496 | – | 593 | 617 | 645 | 678 |
| Sep. 7 | 416 | 441 | 467 | 498 | 548 | 594 | 618 | 646 | 679 |
| Sep. 14 | 416 | 441 | 469 | 494 | 547 | 593 | 618 | 644 | 679 |
| Sep. 21 | 416 | 440 | 467 | 494 | 545 | 592 | 618 | 644 | 680 |
| Sep. 28 | 415 | 441 | 469 | 497 | 545 | 591 | 618 | 643 | 678 |
| Oct. 5 | 414 | 441 | 469 | 497 | 545 | 589 | 617 | 640 | 676 |
| Oct. 12 | 417 | 441 | 472 | 495 | 547 | 587 | 617 | 643 | 676 |
| Oct. 19 | 415 | 441 | 468 | 499 | 545 | 591 | 616 | 640 | 684 |
| Oct. 26 | 417 | 441 | 471 | 496 | 542 | 591 | 616 | 645 | 681 |
| Nov. 2 | 416 | 441 | 472 | 493 | – | – | 617 | 647 | 680 |
| Nov. 9 | 419 | 440 | 469 | 495 | 545 | 591 | 616 | 640 | 684 |
| Nov. 16 | 416 | 439 | 471 | 495 | – | – | 620 | 647 | 679 |
| Nov. 23 | 417 | 441 | 470 | 500 | 546 | 589 | – | 642 | 680 |
| Nov. 30 | 417 | 440 | 471 | 499 | – | – | 621 | 640 | 681 |
| Dec. 7 | 413 | 441 | 472 | 497 | 548 | 591 | – | 642 | 678 |
| Dec. 14 | 414 | 441 | 469 | 499 | – | – | 616 | 637 | 682 |
| Dec. 21 | 414 | 441 | 469 | 499 | 567 | 588 | 618 | 642 | 680 |

The fourth-derivative spectra were therefore calculated, and the results are summarized in Table (4.1). The peaks due to chl-*a* absorption at around 416, 440, 618 and 676 nm were detectable in all the spectra, although the centre wavelengths changed slightly between stations. Another common feature of all derivative spectra was the maximum in the blue region around 465-472 nm, which could be attributed to absorption by chl-*c*, chl-*b* or carotenoids (Bidigare et al. 1989, 1990, Johnsen et al. 1992, 1994a, Johnsen and Sakshaug 1993, Hoepffner and Sathyendranath 1993). The carotenoid peak around 497 nm and the peak of chl-*c* or chl-*b* absorption in the red at about 646 nm (Owens et al. 1987, Bidigare et al. 1990, Johnsen et al. 1994) were present in all samples. However, the centres of these peaks varied between stations (up to 6 nm difference). Most of the differences in the fourth-derivative spectra were found in the blue-green region (Table 4.1).

The month-to-month variation in the spectral shapes was more pronounced in the action spectra (Figure 4.2) than in the absorption spectra, with the most significant changes being observed in the months of October and November. In August and September, the shapes of the absorption spectra did not change significantly. On the other hand, the shapes of the corresponding action spectra showed some differences. Regarding the weather, rainfall was higher in August (day 213 to 243) than in September (day 244 to 273), but wind speed was lower (Figures 4.1i and k). Silicate and phosphate concentrations were low in August, and then increased in September (Figures 4.1f & g), although nitrate stayed low. Presumably, the change in the water conditions caused a slight change in species composition and therefore cell size and intracellular pigment concentration (see for example Côté and Platt 1983), which in turn had an effect on the spectral shapes. In August, the action spectra were narrower in the region between 400 and 500 nm, with sharp blue peaks at 440 nm whereas the blue peaks in September were broader and some spectra had shoulders at 460 or 490 nm (compare Figures 4.2a & b). Identification of phytoplankton using a microscope was not made for samples collected in August

and September. Although pigment composition was determined by HPLC, it is still difficult to infer the dominant species from pigment data alone.

Microscopic identification was prompted by the appearance of a brick-red colour on the filters, during the second week of October. The colour was caused by a bloom of autotrophic ciliates identified as *Mesodinium rubrum* (formerly known as *Cyclotrichium meunieri* Powers), containing phycoerythrin (Barber et al. 1969, Taylor et al. 1971, White et al. 1977). The geographic distribution of *Mesodinium rubrum* is very wide, with most occurrences reported for extreme neritic locations such as inlets, fjords and bays, and also for upwelling systems (reviewed by Taylor et al. 1971). An examination of the meteorological data revealed changes in some of the conditions between the last week of September and the first week of October (day 271 to 278). Prior to the sampling day in October, there was an increase in wind speed (Figure 4.1k), which could have been responsible for mixing the water column, and extending the mixed layer from 3 m to about 15 m (Figures 4.1a & c). As a result, the species composition was affected, and probably the conditions became favourable for the initiation of the *Mesodinium rubrum* bloom. The *M. rubrum* bloom continued throughout October, peaking in the last two weeks; the ciliates could still be observed in the samples in November and December, although their concentration decreased with time.

These phycoerythrin-containing cells were responsible for the occurrence of the peaks in the green part of the action spectra in October and November (Figures 4.2c & d). The presence of *Mesodinium* cells also affected the shapes of the absorption spectra, although to a lesser extent than those of the action spectra. In the absorption spectra, absorption by phycoerythrin appeared as shoulders in the green part of the spectra around 543 nm, and shoulders at ≈ 497 nm became prominent (Figures 4.3c, d & e). Absorption spectra determined for samples collected at 1 and 10 m also showed features similar to their 5 m counterparts (data not shown).

4.3.2 Phytoplankton Pigments

The phytoplankton pigments will be discussed without reference to species or groups they represent, because most pigments are present in two or more phytoplankton groups. Since chlorophyll-*a* is present in all phytoplankton, all pigments were normalized to chl-*a* for a better comparison of the proportions of pigments present. The chlorophylls determined were chl-*a*, chl-*b*, chl-*c*₃ and chl-*c*₁ + *c*₂. The carotenoids which were present in significant amounts included: fucoxanthin, alloxanthin, peridinin, diadinoxanthin, 19'-hexanoyloxy-fucoxanthin and zeaxanthin + lutein. The last two pigments co-elute and could not be separated. The ratios of the chlorophylls *b*, *c*₁ + *c*₂ and *c*₃ to chl-*a* are plotted as a function of sampling day of the year in Figures (4.4d to f). The ratios of carotenoids to chl-*a* are also plotted as a function of day of the year, in Figures (4.5a to f). Because the action spectra were measured only at 5 m, more emphasis will be given to samples collected at that depth than to those from 1 and 10 m. Therefore, data representing samples collected at 5 m are shown as filled circles and joined by lines to distinguish them from those taken at the other depths.

There was a considerable weekly variation, and depth variation in some cases, in the pigment ratios throughout the sampling period. Significant depth variation was found in the proportions (relative to chl-*a*) of alloxanthin, diadinoxanthin and 19'-hexanoyloxy-fucoxanthin, and were notable in the stratified period (Figures 4.5b, d & e, respectively). The relative concentration of fucoxanthin was inversely related to that of chl-*b* (Figures 4.4d *vs.* 4.5a), while the proportions of chl-*c*₃ and 19'-hexanoyloxy-fucoxanthin showed similarity in their distribution patterns and were present in significant amount only in August and September, the stratified period (Figures 4.4f & 4.5e).

Figure 4.4 Time-series variation for data collected from the Bedford Basin between 10 August and 21 December 1994. (a) chlorophyll-*a* (chl-*a*) concentration, (b) concentration of dissolved oxygen, (c) water temperature, (d) the ratio of chlorophyll-*b* (chl-*b*) to chl-*a*, (e) ratio of chl-*c*₁ + *c*₂ to chl-*a* and (f) the ratio of chl-*c*₃ to chl-*a*. The symbols are as defined in Figure (4.1).

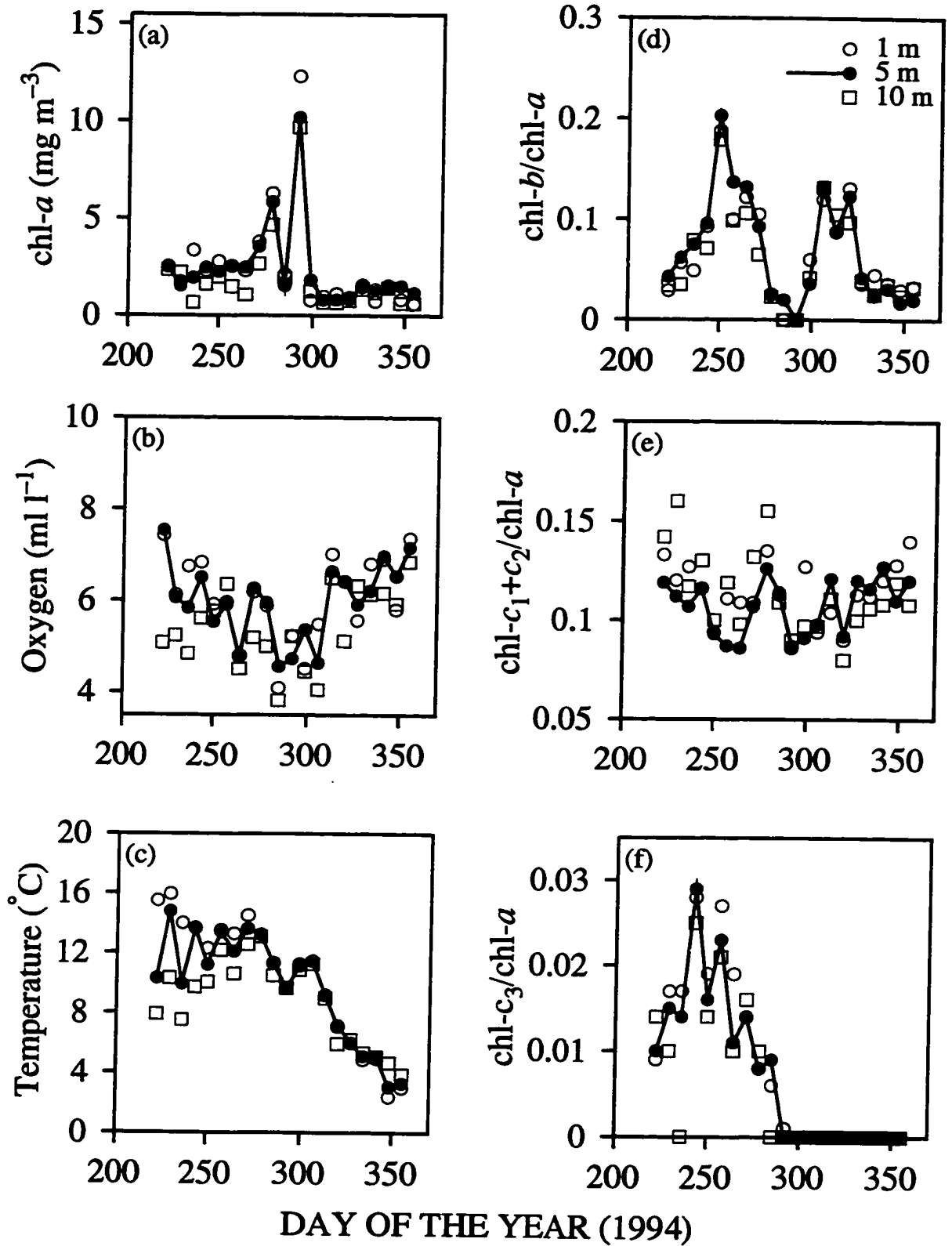


Figure 4.4

Figure 4.5 Time-series variation in the ratios of carotenoids to chl-a for samples collected from 10 August to 21 December 1994 in the Bedford Basin. (a) fucoxanthin (fuco), (b) alloxanthin (allo), (c) peridinin (perid), (d) diadinoxanthin (diadi), (e) 19'-hexanoyloxy-fucoxanthin (19'hexa) and (f) zeaxanthin + lutein (ze+lut). The symbols are as defined in Figure (4.1).

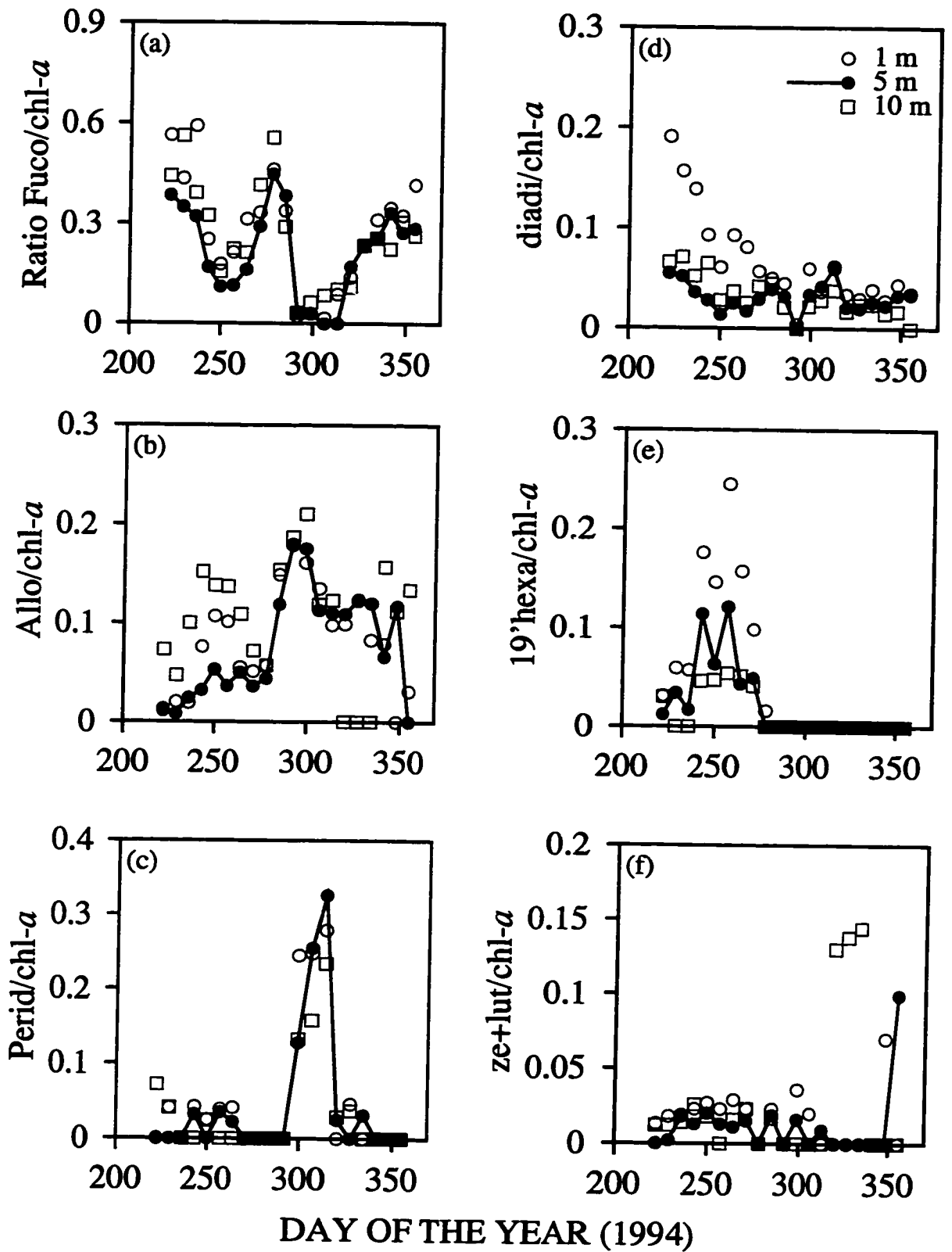


Figure 4.5

The highest concentrations in fucoxanthin, alloxanthin and peridinin occurred out of phase, two weeks apart: fucoxanthin peaked first (at day 278), followed by alloxanthin (at day 292), and lastly peridinin (at day 306; Figures 4.5a, b & c, respectively), which could imply species succession (see also Smith et al. 1983). The relative concentration of chl- c_1+c_2 fluctuated more or less like that of fucoxanthin and, interestingly, showed a pattern similar to that of dissolved oxygen concentration (Figures 4.4b & e). The concentration of zeaxanthin + lutein relative to chl- a remained low (ratio below 0.04; Figure 4.5f), with an exception of the last three weeks in November at 10 m, and at 1 and 5 m in the first two weeks of December.

4.3.3 Physiological Parameters

The maximum quantum yield of photosynthesis, ϕ_m , ranged from 0.014 to 0.052, with a mean of 0.024 ± 0.008 mol C (mol photons) $^{-1}$ for the entire 20 weeks of sampling. The average ϕ_m in the present study is lower than that found by Taguchi (1981; a mean of 0.054 ± 0.025 mol C (mol photons) $^{-1}$) during a bloom of a dinoflagellate *Ceratium longipes* Bailey in the Bedford Basin, which occurred between 30 October to 20 November 1974. The ϕ_m values observed here were low during the stratified period, in August and September, then increased and reached their highest values in October during the *Mesodinium rubrum* bloom. In November, ϕ_m decreased again, then increased slightly in December (Figure 4.6a). The mean values of $\alpha^B(\lambda)$ and $a_p^B(\lambda)$ (Figures 4.6b & 4.6c) showed a pattern opposite to that of ϕ_m ; they were relatively high in August and September, decreased to a minimum in October, increased again in November, then decreased in December. Given that ϕ_m is directly proportional to α^B but inversely proportional to a_p^B (Equation 4.1), the patterns observed in Figures 4.6a to c suggest that, changes in \bar{a}_p^B had a greater influence on the magnitude of ϕ_m than changes in $\bar{\alpha}^B$.

Figure 4.6 Time-series variation in data collected at 5 m from the Bedford Basin between 10 August and 21 December 1994. (a) The quantum yield of carbon fixation, (b) the average value of the action spectrum, $\alpha^B(\lambda)$ [$\text{mg C (mg chl-}a)^{-1} \text{ h}^{-1} (\mu\text{mol m}^{-2} \text{ s}^{-1})^{-1}$] and (c) the mean value of the biomass-specific absorption coefficients, $a_p^B(\lambda)$ [$\text{m}^2 (\text{mg chl-}a)^{-1}$].

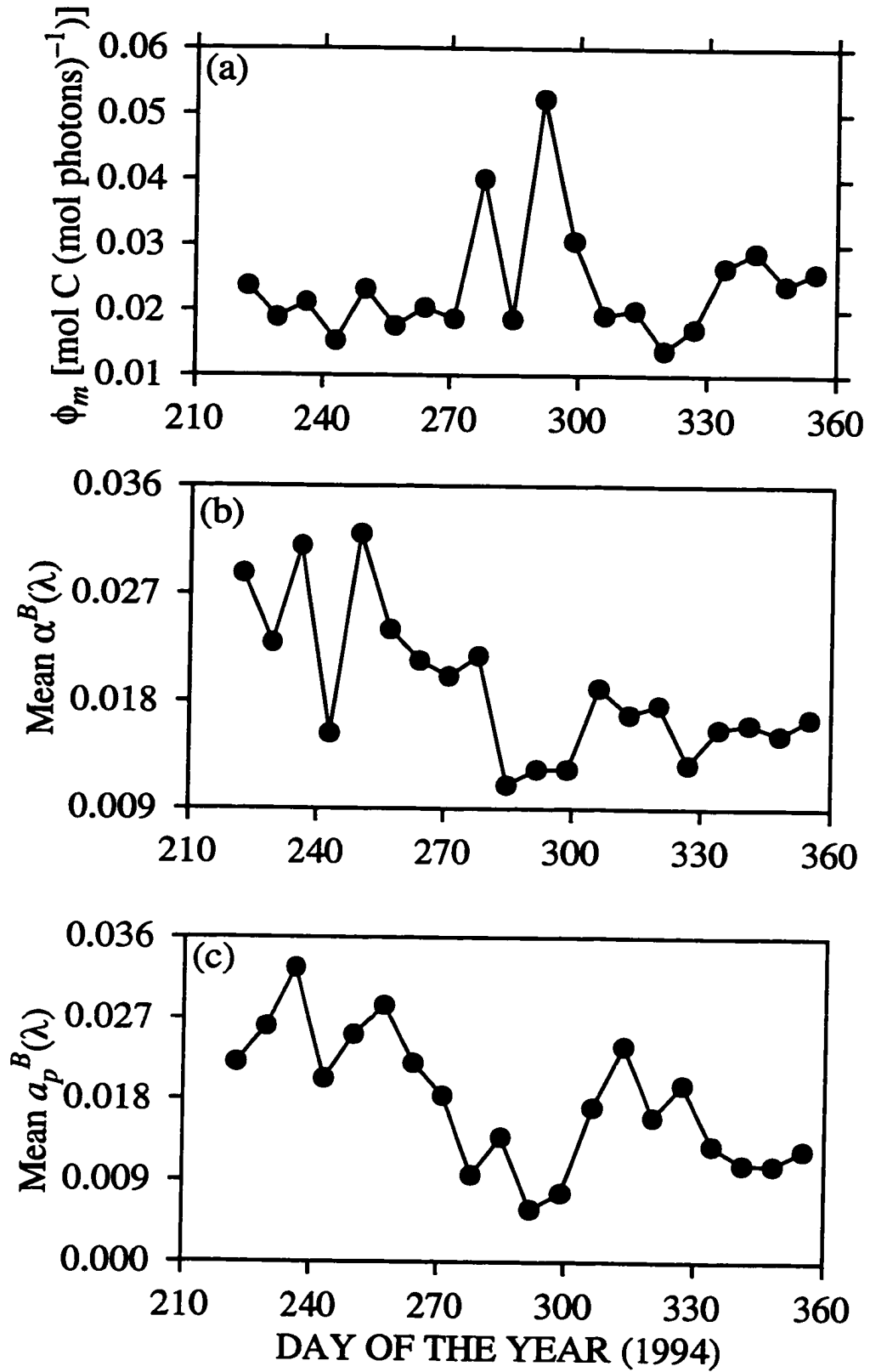


Figure 4.6

Figure 4.7 Time-series variation in the amplitudes of the (a) action (b) absorption spectra for values at the blue peaks (filled circles) and at the red peaks (open circles), for data collected at 5 m in the Bedford Basin. (c) Ratios of blue-to-red values for the action spectra ($\alpha^B(440):\alpha^B(670)$; filled circles) and absorption spectra ($a_p(440):a_p(676)$; open circles).

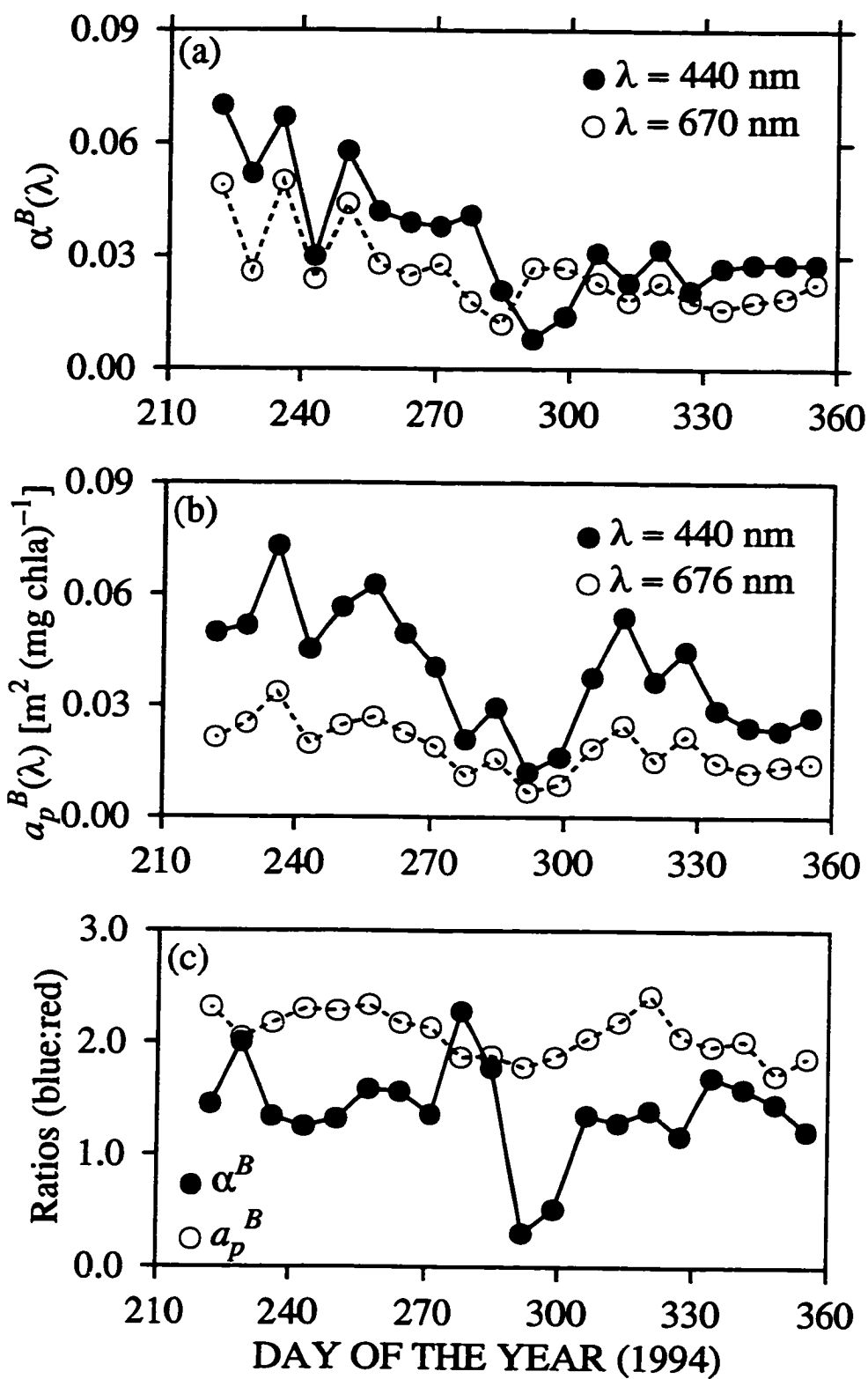


Figure 4.7

To assess the variation in the amplitudes of both the action and absorption spectra, values at the peaks in the blue part of the spectrum at $\lambda = 440$ nm and those in the red part at $\lambda = 670$ nm for the action spectra or $\lambda = 676$ nm for the absorption spectra were examined (Figures 4.7a & b). At 440 nm, the α^B values ranged from 0.008 to 0.07, a factor of about 9, with a mean of 0.035 ± 0.016 mg C (mg chl-*a*)⁻¹ h⁻¹ (μ mol m⁻² s⁻¹)⁻¹. The values at 670 nm ranged from 0.012 to 0.05, with a mean of 0.026 ± 0.01 mg C (mg chl-*a*)⁻¹ h⁻¹ (μ mol m⁻² s⁻¹)⁻¹. The biomass-specific absorption coefficients at the blue wavelength, $a_p^B(440)$, ranged from 0.012 to 0.07, a factor of about six, with a mean value of 0.039 ± 0.016 m² (mg chl-*a*)⁻¹; the corresponding $a_p^B(676)$ ranged from 0.007 to 0.034, averaging 0.019 ± 0.007 m² (mg chl-*a*)⁻¹.

In general, the amplitudes of the spectra were higher during the stratified period than in the mixed one. The pattern in the peak values at the blue and red wavelengths, for both α^B and a_p^B , resembled that of the corresponding mean values of the spectra (compare Figures 4.6b & c with 4.7a & b). The blue-to-red absorption ratio, $a_p(440):a_p(676)$, did not change significantly over the sampling time, although it was slightly lower in October than in September and November (Figure 4.7c). It ranged from 1.7 to 2.3, which is within the range reported for healthy phytoplankton (1.1 to 2.5; reviewed by Cleveland et al. 1989). The ratio of $\alpha^B(440):\alpha^B(670)$, on the other hand, showed variation with time, with the greatest change being observed in October; both the maximum (2.2) and minimum (0.3) values occurred in this month (Figure 4.7c). Overall, the ratios were above 1.0 except for the two weeks in October during the bloom of *Mesodinium rubrum*.

4.4 Discussion

The changes in the *shapes* and *amplitudes* of the action and absorption spectra from month to month could be related to the changes in the water conditions and

phytoplankton species composition. In the months of August and September, the water-column was stratified and nitrate was low: in general the spectra showed a maximum in the blue part of the spectrum, a minimum in the green part, and another peak in the red region around 676 nm (Figures 4.2a, 4.2b, 4.3a & 4.3b). During this period, the water temperature was high (Figure 4.4c), nitrate concentration was low and chl-*a* concentration was moderate (Figure 4.4a). The samples in this stratified group were characterised by high values of $\alpha^B(440)$ and $a_p^B(440)$ (Figures 4.7a & b), which could imply the presence of populations with low package effect, that is, a community of small cell size or low intracellular pigment composition (Duysens 1956, Morel and Bricaud 1981, Sathyendranath et al. 1987).

The phytoplankton assemblages were dominated by cells with high proportions of chl-*c*₃ and 19'-hexanoyloxy-fucoxanthin (Figures 4.4f & 4.5c), but low alloxanthin and peridinin (Figures 4.5b & c). Fucoxanthin and chl-*c*₁+*c*₂ were relatively high in August when the wind was low and rainfall was high, but decreased in September with increasing winds (Figures 4.4e & 4.5a). The reverse situation was seen for the proportion of chl-*b* in the two months (Figure 4.4d).

The most distinct features in the absorption spectra for August and September were the blue and red peaks due primarily to chl-*a* absorption, and the shoulders in the blue region due to absorption by other chlorophylls and carotenoids. The peaks of the fourth-derivative spectra (Table 4.1) for samples collected in August and September were similar, except that the August samples lacked an absorption peak at about 545-548 nm in the blue-green region. This peak, presumably due to phycoerythrin absorption (Barber et al. 1969, White et al. 1977, Bidigare et al. 1989, 1990), was present in the September samples although the amplitude was low. The difference between the peaks in the blue-green region for August and September samples could be attributed to changes in species composition, given also that fucoxanthin and chl-*b* were inversely correlated.

For the months of October, November and December, that is, the mixed period, microscopic analysis showed that the samples were dominated by big cells

(photosynthetic ciliates, diatoms and dinoflagellates), although small cells were also present. Nitrate and silicate started to increase in October but phosphate was relatively low during this month. The most significant change in the shapes of the spectra, especially the action spectra, was found in October and was associated with the bloom of *Mesodinium rubrum*, a phycoerythrin-rich photosynthetic ciliate. The magnitudes of the blue peaks (at 440 nm) for both the action and absorption spectra were lower during this time than in any other month (Figures 4.7a & b); this could be attributed to the package effect since *Mesodinium rubrum* cells are relatively large with numerous chloroplasts (Taylor et al. 1971).

Although the absorption peak due to phycoerythrin started to appear in September (Table 4.1, column six), it became more prominent in October during the bloom. Mixing brought deep nutrient-rich waters to the surface (Figure 4.1e), replenishing the surface waters depleted of nutrients due to summer stratification. The wind speed stayed high in the first three weeks of October (days 278 – 292) then decreased on the last week, around day 299 (Figure 4.1k). In November, the wind was at its highest speed, and stayed relatively high to the end of the sampling period. During this period also (days 306 – 355) there was heavy rainfall at least twice every week (Figure 4.1i).

A typical action spectrum has a maximum (peak) in the blue part of the spectrum at around 440 nm, a minimum (valley) in the green to yellow region, and a minor peak in the red at about 675 nm. Contrary to this, at the time of the *M. rubrum* bloom in the last two weeks of October, the spectra had peaks in the green region, which were higher than the blue and red peaks (Figure 4.2c). The low values of $\alpha^B(440)$ and $\alpha^B(670)$ could be attributed to an imbalance in the distribution of chl-*a* between photosystem I (PS I) and photosystem II (PS II), which can be acute in biliprotein-containing algae such as red algae and cyanobacteria (e.g., Lüning & Dring 1985, Neori et al. 1986, 1988, Lewis et al. 1986, 1988; Prézelin & Boczar 1986). The effect of such an imbalance would be pronounced in the un-enhanced action spectra measured here (Emerson 1957, Schofield et al. 1990, 1996).

In phycobilin-rich algae like *Mesodinium rubrum*, almost all the accessory pigments are associated with PS II whereas most of the chl-*a* is associated with PS I (Kirk 1983, Neori et al. 1986, Prézelin & Boczar 1986). Since PS I is unable to transfer its excess excitation energy to PS II, a decrease in the photosynthetic efficiency at the wavelengths at which chl-*a* absorb could have occurred, resulting in a deviation in the shape of the spectrum from that of a typical action spectrum, as observed here.

In the absorption spectra, shoulders were present only in the blue-green and green region, a consequence of absorption by phycoerythrin (Barber et al. 1969, Shimura and Fujita 1975, Lewis et al. 1988): furthermore, they were not as prominent as might have been expected from the action spectra. A possible explanation of the small peaks due to phycoerythrin absorption during the bloom period in October (Figure 4.8) is the possibility that the water-soluble pigment (phycoerythrin) was lost during the filtration process. *Mesodinium rubrum* is extremely fragile and ruptures easily when subjected to pressure or exposure to preservatives like formalin (Barber et al. 1969, White et al. 1977, Smith and Barber 1979). When the cells burst during filtration, the red pigment has been shown to move away from the centre to the edge of the filter (Smith and Barber 1979). This phenomenon was observed during filtration in the present study, implying that there was some loss of phycoerythrin. Barber et al. (1969) compared absorption spectra of *M. rubrum* before and after washing in distilled water (their Figure 1); they showed that a phycoerythrin peak present in the spectrum of the unwashed sample was reduced to a shoulder in the spectrum of the washed one. The authors thus demonstrated how easily phycoerythrin may be lost during filtration. Indeed, the shapes of the absorption spectra for October (Figure 4.3c) resemble their spectrum for the washed cells.

Figure 4.8 Fourth-derivative spectrum (top panel) showing peaks of absorption maxima for different pigments present in the sample collected from 5 m on 19 October 1994 (bottom panel). The approximate positions of the peaks and shoulders corresponding to the peaks in the fourth-derivative spectrum are indicated by arrows. The contributing pigments are discussed in the text, but note the peak for phycoerythrin absorption at about 545 nm.

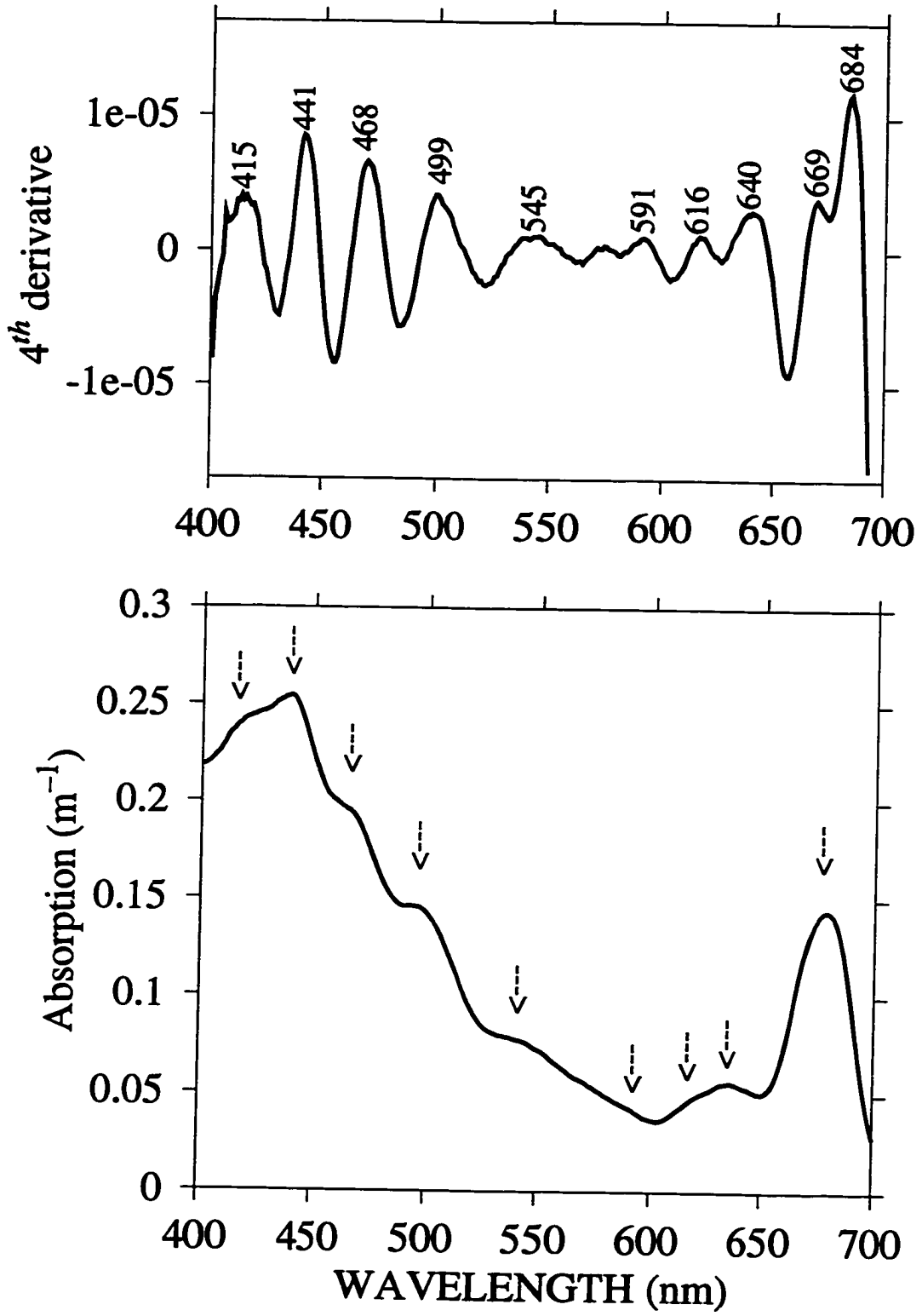


Figure 4.8

Another noticeable feature of the shapes of absorption spectra was a shoulder between about 600 and 650 nm (Figures 4.3c, d & e), which was not prominent in the first two months. The shoulders were well resolved in the fourth-derivative spectra, and were present in all samples (Table 4.1). They became prominent only early in October, perhaps due to the presence of *M. rubrum*, which is rich in chl-*c* (Barber et al. 1969, White et al. 1977). However, contribution to the shoulders by absorption from other pigments, such as chl-*b*, is also possible. Figure (4.8) shows, as an example, the fourth derivative of the absorption spectrum for the sample collected on 19 October 1994. The maxima in the spectra are associated with (top panel) the peaks and shoulders (corresponding to the arrows in the bottom panel) due to absorption by major pigments.

Species composition in the mixed period was as follows: in October, the dominant phytoplankters were *Mesodinium rubrum*, microflagellates, diatoms, and silicoflagellates. In November, a month with the highest wind speed and nutrient concentrations, dinoflagellates (mostly *Ceratium*, *Gonyaulax* and *Dinophysis*) were the most abundant, followed by diatoms and the photosynthetic ciliates. Taguchi (1981) also found dinoflagellates, *Ceratium longipes* (Bailey) Gran, to bloom from late October to November in the Bedford Basin. However, diatoms become dominant in spring. In a study carried out during a spring bloom, in the Bedford Basin, Smith et al. (1983) found that the bloom was dominated by diatoms. This bloom was preceded by that of dinoflagellates and other flagellates. In December, there was a mixture of different phytoplankton: the dominant ones included *Chaetoceros*, *Nitzschia*, *Ceratium*, *Gonyaulax*, silicoflagellates and other small cells. *Mesodinium rubrum* was present but in less abundance than in October and November.

The associated pigment composition and hydrographic conditions showed that chl-*a* concentration was high during the *Mesodinium* bloom, then it decreased and stayed low, whereas dissolved oxygen concentration showed the opposite pattern (Figures 4.4a & b), and the water temperature progressively decreased with time, but stayed uniform with depth (Figure 4.4c). The proportion of fucoxanthin was

low during the bloom, then increased as *Mesodinium* decreased (Figure 4.5a). Alloxanthin increased during the bloom, then decreased slightly after it, but stayed high for the remaining time of the sampling period (except on the last week; Figure 4.5b). Peridinin was relatively low, but increased strongly in November when dinoflagellates were dominant (Figure 4.5c). Unlike in the stratified period, the proportions of chl- c_3 and 19'-hexanoyloxy-fucoxanthin were undetectable during this period (Figures 4.4f & 4.5e).

4.5 Concluding Remarks

Between late summer and fall 1994, in the Bedford Basin, the hydrographic conditions controlled species composition and, in turn, changes in pigment composition affected the shapes and amplitudes of both the action and absorption spectra. For the first two months (August and September), the water column was stratified, temperature and salinity were high but nitrate concentration was low (at 5 m). This period was associated with cells rich in chl- c_3 and 19'-hexanoyloxy-fucoxanthin but generally poor in chl- c_1+c_2 , alloxanthin and peridinin. The spectral shapes had no particular features in the blue-green, green or yellow regions of the spectrum. The samples had relatively high values $\alpha^B(\lambda)$ and specific absorption coefficients, which could imply that the phytoplankton community was dominated by small cells.

In the following three months (October, November and December), the water column in the top 15 m was well mixed. This period was associated with relatively low salinity and temperature but high nutrient concentrations. The samples were dominated by large phytoplankton cells; thus, the $\alpha^B(\lambda)$ and specific absorption coefficients were lower than in the stratified period, probably due to the package effect. Likewise, pigment composition and the shapes of the action and absorption spectra were different from those of the stratified case. In general, the spectra became relatively broad in the blue part of the spectrum, and peaks or shoulders were observed in the green and yellow region, reflecting changes in pigment composition.

The samples from the mixed period were rich in phycoerythrin, alloxanthin and peridinin, but poor in chl- c_3 and 19'-hexanoyloxy-fucoxanthin.

Overall, the results obtained here showed strong seasonal differences in the shapes and magnitudes of the photosynthesis properties: there was a clear distinction in the properties between the two seasons, summer and fall, which was attributable to changes in pigment (species) composition. The most significant change in the ϕ_m values, and in the *shapes* and *amplitudes* of both the action and absorption spectra was observed in October when the bloom of the phycoerythrin-rich *Mesodinium rubrum* occurred. Therefore, the outcome from this study supports the hypothesis put forth in Chapter 3, which stated that the significant seasonal variation in the photosynthesis parameters was caused mainly by changes in species composition.

CHAPTER 5

Summary and Conclusions

5.1 Summary

From measurements made at 20 stations sampled across the North Atlantic in the fall of 1992 (Chapter 2), I have shown that the shape of the absorption spectrum is a good proxy for that of the corresponding action spectrum, and, because there was a good agreement in amplitudes between the measured and the constructed $\alpha^B(\lambda)$ in the majority of the samples, that the broad-band α^B provides an appropriate scaling factor. When the estimated action spectra were used to compute water-column primary production, the resulting values were not significantly different from those computed using the measured spectra.

I made a sensitivity analysis to assess the error in the computed water-column primary production caused by random and systematic errors in the action spectrum. A maximum of 20% error was chosen as appropriate, based on the analysis of Platt et al. (1977). It was concluded that, although random errors of up to 20% caused little effect on the estimation of water-column primary production, systematic errors of the same magnitude could not be ignored.

Furthermore, I assessed the variation in the shapes of action and absorption spectra, and in the non-spectral photosynthesis parameters of phytoplankton at large spatial and temporal scales (Chapter 3). Working with data collected from five biogeochemical provinces during fall 1992 and spring 1993, I have shown that in large oceanic regions, the representative photosynthesis properties in each province were significantly different between *seasons*, but that there were no significant differences between *provinces* in most cases. The five sampled provinces covered a wide range of hydrography: from nutrient-rich coastal waters to oligotrophic subtropical gyre waters. This gave a good representation of a variety of natural environments.

The nature of variability in the photosynthesis parameters was also examined, in Chapter 3, through linear regression analyses of the parameters on various environmental and biological variables. In most cases, the variables, individually or in combinations of two or three, explained a significant fraction of the variance in the parameters between the provinces and seasons.

In Chapter 4, I examined one of the major factors that could influence the shapes of action and absorption spectra: changes in species (pigment) composition (e.g., Lewis et al. 1986, Hoepffner and Sathyendranath 1992, Schofield et al. 1996, Lutz et al. 1996). Here, I have explored the effect of seasonal changes in pigment composition on the corresponding changes in the photosynthesis properties of phytoplankton. The study was carried out at one station in the Bedford Basin for twenty consecutive weeks from 10 August to 21 December 1994. The results showed that variation in the water conditions induced changes in species composition, which in turn affected the action and absorption spectra, and the quantum yield of photosynthesis. It was also found that the effect of changes in pigment composition was more pronounced in the shapes of the action spectra than in those of the corresponding absorption spectra.

During this five-month period, the water conditions could be partitioned into two phases: the stratified period, from August to September, characterized by a shallow thermocline and low nutrient concentrations; and the mixed period, observed during the months of October, November and December, in which the water conditions were the opposite of those in the stratified period. The photosynthesis properties were different between the two periods.

5.2 Conclusions and Recommendations for Future Work

Spectrally-resolved primary production models provide more accurate estimates of primary production than non-spectral ones, and it has been shown that the application of spectrally-resolved models provides results not significantly different

from *in situ* measurements of primary production (e.g., Platt and Sathyendranath 1988, results from Chapter 2). Ignoring spectral dependencies of the wavelength-dependent inputs in production models could lead to significant errors in estimated production relative to *in situ* production (e.g., Kyewalyanga et al. 1992).

However, some of the inputs required to implement spectral models are difficult to measure: direct determinations of the photosynthetic action spectrum (Lewis et al. 1985a, Warnock 1990, Schofield et al. 1990, 1991, Chapter 2) are complicated, expensive and labour intensive, thus limiting the use of these models. As a contribution to relieving this limitation, I have developed a simple method for estimating the action spectrum. The method uses the absorption spectrum of phytoplankton and the broad-band α^B , both of which are easier to measure than the photosynthetic action spectrum. Furthermore, the bias in the action spectrum determined in monochromatic light (e.g., Lewis et al. 1985a) towards the activity of PS II reaction centres (Kirk 1983, Prézelin and Boczar 1986), introduced by lack of enhancing background light (Emerson 1957, Schofield et al. 1990), is eliminated. This is achieved by the combined use of α^B measured in polychromatic light, and the absorption spectrum $a_p(\lambda)$, which contains information on absorption of pigments associated with both PS I and PS II. Elimination of bias due to lack of enhancing background light is considered to be a significant advantage of the proposed method over methods that exploit the fluorescence excitation spectrum.

Therefore, the method developed here offers an advantage over direct measurements of the photosynthetic action spectrum: because of its simplicity and effectiveness, it could be applied anywhere in the aquatic environment, at any time of the year, in a variety of studies. That is to say, since only broad-band α^B and $a_p(\lambda)$ need to be measured, detailed studies of the action spectrum, such as depth-dependent changes (Lewis et al. 1985b, Ulloa et al. 1997) and diurnal or day-to-day variation, could be undertaken, as could be those dealing with variation in the action spectra with change in species, or in response to changing environmental conditions (e.g., Lewis et al. 1988, Schofield et al. 1990, 1996, Chapter 4).

Similarly, more general studies could be carried out, such as determination of the action spectrum for use in models to estimate primary production at a particular station (Lewis et al. 1985a, Warnock 1990, Schofield et al. 1991, Chapter 2), or for establishment of representative action spectra in different biogeochemical provinces (Chapter 3), for further application in large-scale estimation of primary production. In addition, if primary production has to be estimated for previous years, in regions where data on the action spectra are lacking, but those on the broad-band α^B and phytoplankton absorption spectra exist, spectrally-resolved computations could still be made since $\alpha^B(\lambda)$ can be estimated from the existing information.

A limitation of the method could be the effect of non-photosynthetic pigments, such as photoprotective carotenoids (Krinsky 1979, Siefermann-Harms 1987, Johnsen & Sakshaug 1993, Sosik & Mitchell 1995), which absorb light energy but do not transfer it to the reaction centers for use in photosynthesis. To get a good representation of the shape of the action spectrum, the effect of light absorption by non-photosynthetic pigments has to be negligible, or corrected for, if information on the types, concentration, and absorption properties of those pigments is available (Bidigare et al. 1987, 1989, Sosik and Mitchell 1995). However, in the present study, the error in the computed water-column primary production, resulting from the contribution to light absorption by non-photosynthetic pigments, was shown to be negligible. This suggests that the variation in the *shape* of the action spectrum causes little errors in the computed production. For example, when an invariant shape of the action spectrum was applied to all stations (Chapter 2), the estimated production was not significantly different from that in which the shape was allowed to vary from station to station.

Another aspect to consider when applying the newly-developed method is that systematic measurement errors in the scaling factor, i.e. the broad-band α^B , should be minimised. For example, we have seen that the shape of the irradiance spectrum from the tungsten-halogen lamp, used in the broad-band incubator, introduced a significant bias in the measured α^B , which had to be corrected (see also Dubinsky

et al. 1986, Cleveland et al. 1989, Schofield et al. 1991, Babin et al. 1995). This conclusion is further supported by the results of a sensitivity analysis to assess errors on the action spectrum: it was found that, in the computation of water-column primary production, although the effects of plausible random errors in $\alpha^B(\lambda)$ were negligible, systematic errors of similar magnitudes led to significant errors in estimated production.

It is the systematic changes in the photosynthesis properties that we seek to explain. Variation in the photosynthesis properties with time and location, its causes and consequences, is a subject that has occupied several researchers. Often, the aim is to find a correlation between the photosynthesis parameters and environmental variables (Jassby and Platt 1976, Williams 1978, Harrison and Platt 1980, Smith et al. 1983, Côté and Platt 1983, Cleveland et al. 1989, Platt et al. 1992, Sosik and Mitchell 1995, Babin et al. 1996), or to determine the major factors responsible for changes in the action or absorption spectra of phytoplankton (Lewis et al. 1986, Sakshaug et al. 1991, Hoepffner and Sathyendranath 1992, Johnsen et al. 1994a, Lutz et al. 1996, Lazzara et al. 1996, Schofield et al. 1996). The results from such studies contribute to a better understanding of the variation in, and predictability of, the photosynthesis properties, with the ultimate goal of application to primary production modelling both at small and large scales.

The results from Chapters 3 and 4 showed clearly that seasonal variations in the photosynthesis properties within a large oceanic region, and at a single station, were significant. Seasonal change in the phytoplankton biomass, production, growth, physiological parameters or species composition is a phenomenon known both in freshwater (e.g., Hecky and Fee 1981, Hama et al. 1990) and marine (e.g., Ryther and Menzel 1960, Taguchi 1981, Platt et al. 1992, Veldhuis et al. 1997) environments. It was hypothesized in Chapter 3 that the major cause of significant seasonal changes in the photosynthesis properties is species succession, in response to changing environmental conditions. This view was supported by the results obtained from a time-series of samples collected at a fixed site (Chapter 4).

Although variability in the photosynthesis parameters between seasons was significant, the variation between provinces within seasons was not. This conclusion, however, does not undermine the need to partition the ocean into biogeochemical provinces, because different physical forces operate within the individual regions (Longhurst 1995, Sathyendranath et al. 1995), which in turn may affect the dependence of photosynthesis properties on environmental variables, as was shown by pooling data into domains. Therefore, in the estimation of primary production at large scales, both regional and seasonal variation in the photosynthesis parameters should be taken into consideration.

For the predictability of the photosynthesis parameters from environmental and biological variables a variety of correlations was found, although no generalized parameter-variable relationship throughout all the provinces could be established. What makes it difficult to get a consistent relationship between a parameter and a certain variable is that, for natural environments, in addition to changes in species composition, several variables act together (sometimes in opposite directions) to control the magnitude of the parameters (Eppley 1972, Harding et al. 1981, Côté and Platt 1983, Banse and Yong 1990, Falkowski and LaRoche 1991). However, it was interesting to see that, the correlation between P_m^B and some variables was consistent regardless of the province, domain or season: P_m^B was positively correlated with temperature and potential supply of nitrogen, but negatively correlated with depth (a proxy for light level). This is a promising result, suggesting that it could be possible to predict P_m^B from easily-measured environmental variables. One such demonstration was shown by Behrenfeld and Falkowski (1997) who predicted P_{opt}^B , a proxy for P_m^B , from sea-surface temperature (SST). They showed that when their model, in which P_{opt}^B is estimated from SST was used to compute daily water-column primary production for a large data set, the estimated values could account for 58% of the variance in the measured values.

Also, it should be noted that the results obtained here for the five provinces of the North Atlantic were based on data collected only in spring and fall. Such

a sampling frequency is not intensive enough to establish stability in, or general relationships between, variables and the photosynthesis properties. For example, to establish that α^B and P_m^B were remarkably constant for a given season in the Northern Sargasso Sea, Platt et al. (1992) analysed data collected from different cruises over a span of several years. Similarly, to show that nutrients regulate growth rates and primary production in the Equatorial Pacific Ocean, and to test the hypothesis that iron limits primary production in high-nutrient regions, Barber and Chavez (1991) analysed data collected from more than 300 stations occupied during 16 cruises undertaken across the basin (between 5°N and 5°S) in a period of seven years.

Therefore, the results obtained here should be taken as a first step or contribution towards building an archive of the representative parameters and spectra and defining their seasonal variation, in the provinces studied. Such an archive would be an important tool in assimilating ocean colour data for remote sensing of large-scale primary production (Platt and Sathyendranath 1988). The photosynthesis parameters determined here could be used in the estimation of primary production, in the regions and seasons studied. Nevertheless, additional work in the four seasons of the year, for a number of years, is needed for further understanding of the variation or stability in these parameters, and to establish correlations between environmental variables and the photosynthesis properties in these provinces.

APPENDIX I

Regression equations showing the relation between the physiological parameters of phytoplankton: α^B (Table 3.4a), P_m^B (Table 3.4b) and ϕ_m (Table 3.4c) on the environmental and biological variables. The symbols of the variables are defined in Table (3.4a).

| Province | Cruise | Regression Equation |
|----------|----------|--|
| CNRY | JGOFS 92 | $\alpha^B = 0.01 \times R_a$ |
| CNRY | JGOFS 93 | $\alpha^B = 0.09 - 0.01 \times S_i$ |
| CNRY | JGOFS 93 | $\alpha^B = 0.23 - 0.03 \times S_i - 0.06 \times R_a$ |
| CNRY | JGOFS 93 | $\alpha^B = 0.19 - 0.03 \times S_i - 0.05 \times R_c$ |
| STGE | JGOFS 93 | $\alpha^B = -0.17 + 0.012 \times T$ |
| STGE | JGOFS 93 | $\alpha^B = 0.12 - 0.06 \times S_i$ |
| STGE | JGOFS 93 | $\alpha^B = -0.24 + 0.0004 \times Z + 0.015 \times T$ |
| STGE | JGOFS 93 | $\alpha^B = 0.13 - 0.06 \times S_i - 0.22 \times P$ |
| STGE | JGOFS 93 | $\alpha^B = 0.16 - 0.06 \times S_i - 0.02 \times R_a$ |
| STGE | JGOFS 93 | $\alpha^B = 0.04 + 0.0007 \times Z - 0.04 \times S_i + 0.004 \times Z_n$ |
| STGW | JGOFS 92 | $\alpha^B = 0.0002 \times Z + 0.006 \times R_a$ |
| STGW | JGOFS 93 | $\alpha^B = 0.002 + 0.13 \times S_i$ |
| STGW | JGOFS 93 | $\alpha^B = 0.01 + 0.94 \times P$ |
| GFST | JGOFS 92 | $\alpha^B = 0.04 + 0.0002 \times Z - 0.02 \times S_i$ |
| GFST | JGOFS 93 | $\alpha^B = 0.03 + 0.09 \times S_i$ |
| GFST | JGOFS 93 | $\alpha^B = 0.03 + 0.54 \times P$ |
| GFST | JGOFS 93 | $\alpha^B = 0.35 - 0.15 \times R_c$ |
| NWCS | JGOFS 93 | $\alpha^B = 0.04 + 0.013 \times N$ |

Appendix I *cont.*

| | | |
|------|----------|---|
| CNRY | JGOFS 92 | $P_m^B = -12 + 0.99 \times T - 0.05 \times Z$ |
| CNRY | JGOFS 93 | $P_m^B = 8 - 0.07 \times Z$ |
| CNRY | JGOFS 93 | $P_m^B = -49 + 2.98 \times T$ |
| CNRY | JGOFS 93 | $P_m^B = 20 - 0.02 \times Z - 0.3 \times S_i$ |
| STGE | JGOFS 92 | $P_m^B = 1.1 + 0.06 \times Z_n$ |
| STGE | JGOFS 93 | $P_m^B = 10 - 0.06 \times Z$ |
| STGE | JGOFS 93 | $P_m^B = -18 + 1.26 \times T$ |
| STGE | JGOFS 93 | $P_m^B = -11 - 0.04 \times Z + 0.98 \times T$ |
| STGW | JGOFS 92 | $P_m^B = 10 - 6.3 \times S_i$ |
| STGW | JGOFS 93 | $P_m^B = 0.36 + 11.6 \times S_i$ |
| STGW | JGOFS 93 | $P_m^B = -49 + 2.8 \times T + 5.5 \times S_i$ |
| STGW | JGOFS 93 | $P_m^B = 35 \times N + 15 \times S_i$ |
| STGW | JGOFS 93 | $P_m^B = 55 \times N + 140 \times P$ |
| STGW | JGOFS 93 | $P_m^B = 13 \times S_i + 0.03 \times Z_n$ |
| GFST | JGOFS 92 | $P_m^B = 2.2 + 0.07 \times Z_n$ |
| GFST | JGOFS 93 | $P_m^B = 6.4 - 0.08 \times Z + 1 \times N$ |
| GFST | JGOFS 93 | $P_m^B = 5.7 - 0.08 \times Z + 2.6 \times S_i$ |
| GFST | JGOFS 93 | $P_m^B = -58 + 3.4 \times T + 1.9 \times N$ |
| GFST | JGOFS 93 | $P_m^B = -53 + 3.1 \times T + 4.9 \times S_i$ |
| GFST | JGOFS 93 | $P_m^B = 2.3 + 1.9 \times N + 0.12 \times Z_n$ |
| GFST | JGOFS 93 | $P_m^B = 5.6 \times S_i + 0.13 \times Z_n$ |
| NWCS | JGOFS 92 | $P_m^B = -2.7 + 7.9 \times S_i$ |
| NWCS | JGOFS 93 | $P_m^B = -4.9 + 0.67 \times T$ |
| CNRY | JGOFS 93 | $\phi_m = 0.03 - 0.003 \times C - 0.008 \times R_a$ |
| STGE | JGOFS 92 | $\phi_m = -0.018 + 0.09 \times S_i$ |
| STGW | JGOFS 93 | $\phi_m = 0.031 \times S_i$ |
| STGW | JGOFS 93 | $\phi_m = 0.2 \times P$ |

Appendix I cont.

| | | |
|------|----------|---|
| STGW | JGOFS 93 | $\phi_m = 0.19 \times P + 0.008 \times R_a$ |
| STGW | JGOFS 93 | $\phi_m = 0.19 \times P + 0.011 \times R_c$ |
| GFST | JGOFS 92 | $\phi_m = 0.023 + 0.0002 \times Z$ |
| NWCS | JGOFS 92 | $\phi_m = 0.057 - 0.04 \times S_i$ |
| NWCS | JGOFS 93 | $\phi_m = 0.008 + 0.007 \times S_i$ |
| NWCS | JGOFS 93 | $\phi_m = 0.004 + 0.037 \times P$ |

APPENDIX II

Regression equations showing the relation between the physiological parameters of phytoplankton: α^B , P_m^B and ϕ_m (Table 3.5), for two different domains, and the environmental and biological variables. The symbols of the variables are defined in Table (3.4a).

| Province | Cruise | Regression Equation |
|----------|----------|--|
| COAST | JGOFS 92 | $\alpha^B = -0.02 + 0.001 \times T + 0.01 \times R_a$ |
| COAST | JGOFS 92 | $\alpha^B = -0.03 + 0.001 \times T + 0.02 \times R_c$ |
| WESTL | JGOFS 93 | $\alpha^B = 0.07 + 0.024 \times N$ |
| WESTL | JGOFS 93 | $\alpha^B = -0.11 + 0.009 \times T + 0.03 \times N$ |
| COAST | JGOFS 92 | $P_m^B = 0.34 \times T - 0.05 \times Z$ |
| COAST | JGOFS 92 | $P_m^B = -6.19 + 0.7 \times T$ |
| WESTL | JGOFS 92 | $P_m^B = -8.5 + 0.59 \times T$ |
| WESTL | JGOFS 92 | $P_m^B = 2.12 + 0.05 \times Z_n$ |
| WESTL | JGOFS 92 | $P_m^B = 7.8 - 0.06 \times Z - 1.33 \times S_i$ |
| WESTL | JGOFS 93 | $P_m^B = 9.08 - 0.06 \times Z$ |
| WESTL | JGOFS 93 | $P_m^B = -14 + 1.09 \times T$ |
| WESTL | JGOFS 93 | $P_m^B = -10 - 0.05 \times Z + 0.94 \times T$ |
| WESTL | JGOFS 93 | $P_m^B = -15 - 0.047 \times Z + 1.08 \times T + 2.55 \times S_i$ |
| WESTL | JGOFS 93 | $P_m^B = -19 + 1.3 \times T + 0.99 \times N$ |
| COAST | JGOFS 92 | $\phi_m = 0.019 \times R_a$ |
| COAST | JGOFS 92 | $\phi_m = 0.019 \times R_c$ |
| COAST | JGOFS 92 | $\phi_m = -0.06 + 0.002 \times T + 0.009 \times C + 0.02 \times R_a$ |
| COAST | JGOFS 92 | $\phi_m = -0.09 + 0.003 \times T + 0.01 \times C + 0.03 \times R_c$ |

Appendix II cont.

| | | |
|-------|----------|--|
| COAST | JGOFS 93 | $\phi_m = 0.016 - 0.004 \times C + 0.002 \times N$ |
| COAST | JGOFS 93 | $\phi_m = 0.039 - 0.004 \times C - 0.009 \times R_c$ |
| COAST | JGOFS 93 | $\phi_m = 0.02 - 0.003 \times C - 0.0001 \times Z_n$ |
| WESTL | JGOFS 92 | $\phi_m = 0.025 + 0.002 \times R_a$ |
| WESTL | JGOFS 92 | $\phi_m = 0.027 + 0.002 \times R_c$ |

REFERENCES

- Babin, M. & Morel, A. 1994. An incubator designed for extensive and sensitive measurements of phytoplankton photosynthesis parameters. *Limnol. Oceanogr.* **39**: 694-702.
- Babin, M., Morel, A., Claustre, H., Bricaud, A., Kolber, Z. & Falkowski, P. G. 1996. Nitrogen- and irradiance-dependent variations of the maximum quantum yield of carbon fixation in eutrophic, mesotrophic and oligotrophic marine systems. *Deep Sea Res.* **43**: 1241-1272.
- Babin, M., Therriault, J.-C., Legendre, L., Nieke, B., Reuter, R. & Condal, A. 1995. Relationship between the maximum quantum yield of carbon fixation and the minimum quantum yield of chlorophyll a in vivo fluorescence in the Gulf of St. Lawrence. *Limnol. Oceanogr.* **40**: 956-968.
- Balch, W., Evans, R., Brown, J., Feldman, G., McClain, C. & Esaias, W. 1992. The remote sensing of ocean primary productivity: Use of a new data compilation to test satellite algorithms. *J. Geophys. Res.* **97**: 2279-2293.
- Banse, K. & Yong, M. 1990. Sources of variability in satellite-derived estimates of phytoplankton production in the eastern Tropical Pacific. *J. Geophys. Res.* **95**: 7201-7215.
- Barber, R. T. & Chavez, F. P. 1991. Regulation of primary productivity rate in the equatorial Pacific. *Limnol. Oceanogr.* **36**: 1803-1815.
- Barber, R. T., White, A. W. & Siegelman, H. W. 1969. Evidence for a cryptomonad symbiont in the ciliate, *Cyclotrichium meunieri*. *J. Phycol.* **5**: 86-88.
- Beardall, J. & Morris, I. 1976. The concept of light intensity adaptation in marine phytoplankton: Some experiments with *Phaeodactylum tricoratum*. *Mar. Biol.* **37**: 377-387.
- Behrenfeld, M. J. & Falkowski, P. G. 1997. Photosynthetic rates derived from

- satellite-based chlorophyll concentration. *Limnol. Oceanogr.* **42**(1): 1-20.
- Bidigare, R. R., Morrow, J. H. & Kiefer, D. A. 1989. Derivative analysis of spectral absorption by photosynthetic pigments in the western Sargasso Sea. *J. Mar. Res.* **47**: 323-341.
- Bidigare, R. R., Ondrusek, M. E., Morrow, J. H. & Kiefer, D. A. 1990. *In vivo* absorption properties of algal pigments. *Ocean Optics* **13**(2): 290-302.
- Bidigare, R. R., Prézelin, B. B. & Smith, R. C. 1992. Bio-optical models and the problems of scaling. *In: Falkowski, P. G. & Woodhead, A. D. (eds.). Primary productivity and biogeochemical cycles in the ocean.* Plenum Press, New York. pp. 175-212.
- Bidigare, R. R., Schofield, O. & Prézelin, B. B. 1989. Influence of zeaxanthin on quantum yield of photosynthesis of *Synechococcus* clone WH7803 (DC2). *Mar. Ecol. Prog. Ser.* **56**: 177-188.
- Bidigare, R. R., Smith, R. C., Baker, K. S. & Marra, J. 1987. Oceanic primary production estimates from measurements of spectral irradiance and pigment concentrations. *Global Biogeochem. Cycles* **1**: 171-186.
- Britton, J. R. 1956. *Calculus.* Rinehart and Winston, New York. 584 pp.
- Brzezinski, M. A. & Nelson, D. M. 1995. The annual silica cycle in the Sargasso Sea near Bermuda. *Deep Sea Res.* **42**: 1215-1237.
- Butler, W. L. & Hopkins, D. W. 1970. An analysis of fourth derivative spectra. *Photochem. Photobiol.* **12**: 451-456.
- Chamberlin, S. & Marra, J. 1992. Estimation of photosynthetic rate from measurements of natural fluorescence: Analysis of the effects of light and temperature. *Deep-Sea Res.* **39**: 1695-1706.
- Chamberlin, W. S., Booth, C. R., Kiefer, D. A., Morrow, J. H. & Murphy, R. C. 1990. Evidence for a simple relationship between natural fluorescence, photosynthesis and chlorophyll in the sea. *Deep Sea Res.* **37**: 951-973.
- Cleveland, J. S., Perry, M. J., Kiefer, D. A. & Talbot, M. C. 1989. Maximal quantum yield of photosynthesis in the northwestern Sargasso Sea. *J. Mar. Res.* **47**: 869-886.

- Cleveland, J. S. & Weidemann, A. D. 1993. Quantifying absorption by aquatic particles: A multiple scattering correction for glass-fiber filters. *Limnol. Oceanogr.* **38**: 1321-1327.
- Conley, D. J. & Malone, T. C. 1992. Annual cycle of dissolved silicate in Chesapeake Bay: Implications for the production and fate of phytoplankton biomass. *Mar. Ecol. Prog. Ser.* **81**: 121-128.
- Côté, B. & Platt, T. 1983. Day-to-day variations in the spring-summer photosynthetic parameters of coastal marine phytoplankton. *Limnol. Oceanogr.* **28**: 320-344.
- Côté, B. & Platt, T. 1984. Utility of the light-saturation curve as an operational model for quantifying the effects of environmental conditions on phytoplankton photosynthesis. *Mar. Ecol. Prog. Ser.* **18**: 57-66.
- Cullen, J. J. 1982. The deep chlorophyll maximum: Comparing vertical profiles of chlorophyll *a*. *Can. J. Fish. Aquat. Sci.* **39**: 791-803.
- Cullen, J. J. & Lewis, M. R. 1988. The kinetics of algal photoadaptation in the context of vertical mixing. *J. Plank. Res.* **10**(5): 1039-1063.
- Demers, S., Roy, S., Gagnon, R. & Vignault, C. 1991. Rapid light-induced changes in cell fluorescence and in xanthophyll-cycle pigments of *Alexandrium excavatum* (Dinophyceae) and *Thalassiosira pseudonana* (Bacillariophyceae): A photoprotective mechanism. *Mar. Ecol. Prog. Ser.* **76**: 185-193.
- Demmig-Adams, B. & Adams, W. W. 1992. Photoprotection and other responses of plants to high light stress. *Annu. Rev. Plant Physiol.* **43**: 599-626.
- Dortch, Q. & Whitedge, R. E. 1992. Does nitrogen or silicon limit phytoplankton production in the Mississippi River plume and nearby regions? *Contin. Shelf Res.* **12**: 1293-1309.
- Dubinsky, Z., Berman, T. & Schanz, F. 1984. Field experiments for *in situ* measurements of photosynthetic efficiency and quantum yield. *J. Plankton Res.* **6**: 339-349.

- Dubinsky, Z., Falkowski, P. G. & Wyman, K. 1986. Light harvesting and utilization by phytoplankton. *Plant Cell Physiol.* **27**: 1335-1349.
- Dugdale, R. C., Wilkerson, F. P. & Minas, H. J. 1995. The role of a silicate pump in driving new production. *Deep Sea Res.* **42**: 697-719.
- Duysens, L. N. M. 1956. The flattening of the absorption spectrum of suspensions, as compared to that of solutions. *Biochim. Biophys. Acta* **19**: 1-12.
- Egge, J. K. & Aksnes, D. L. 1992. Silicate as regulating nutrient in phytoplankton competition. *Mar. Ecol. Prog. Ser.* **83**: 281-289.
- Egge, J. K. & Jacobsen, A. 1997. Influence of silicate on particulate carbon production in phytoplankton. *Mar. Ecol. Prog. Ser.* **147**: 219-230.
- Emerson, R. 1957. Dependence of yield of photosynthesis in long-wave red and on wavelength and intensity of supplementary light. *Science* **123**: 746.
- Eppley, R. W. 1972. Temperature and phytoplankton growth in the sea. *Fish. Bull.* **70**: 1063-1085.
- Falkowski, P. G. 1980. Light-shade adaptation in marine phytoplankton. In: Falkowski, P. G. (ed.). Primary production in the sea. Plenum Press, New York. pp. 99-119.
- Falkowski, P. G. & LaRoche, J. 1991. Acclimation to spectral irradiance in algae. *J. Phycol.* **27**: 8-14.
- Frazel, D. W. & Berberian, G. 1990. Distribution of chlorophyll and primary productivity in relation to water column structure in the eastern North Atlantic. *Global Biogeochem. Cycles* **4**(3): 241-251.
- Geider, R. J. & Osborne, B. A. 1992. *Algal photosynthesis: the measurement of algal gas exchange*. Chapman & Hall, Inc. New York. 256 pp.
- Glover, H. E. & Morris, I. 1979. Photosynthetic carboxylating enzymes in marine phytoplankton. *Limnol. Oceanogr.* **24**(3): 510-519.
- Glover, H. E. 1980. Assimilation numbers in cultures of marine phytoplankton. *J. Plankton Res.* **2**: 69-79.

- Gordon, H. R. & Clark, D. K. 1980. Atmospheric effects in the remote sensing of phytoplankton pigments. *Boundary-Layer Meteorol.* **18**: 299-313.
- Gordon, H. R. & McCluney, W. R. 1975. Estimation of the depth of sunlight penetration in the sea for remote sensing. *Appl. Optics* **14**: 413-416.
- Gordon, H. R. & Morel, A. 1983. *Remote Assessment of Ocean Color for Interpretation of Satellite Visible Imagery. A Review.* Springer-Verlag, New York. 114 pp.
- Gordon, H. R. & Wang, M. 1994. Retrieval of water-leaving radiance and aerosol optical thickness over the oceans with SeaWiFS: A preliminary algorithm. *Appl. Optics* **33**: 443-452.
- Hama, T., Matsunaga, K., Handa, N. & Takahashi, M. 1990. Nitrogen budget in the euphotic zone of Lake Biwa from spring to summer, 1986. *J. Plankton Res.* **12**: 125-131.
- Harding, L. W., Meeson, B. W., Prézelin, B. B. & Sweeney, B. M. 1981. Diel periodicity of photosynthesis in marine phytoplankton. *Mar. Biol.* **61**: 95-105.
- Harrison, W. G. & Platt, T. 1980. Variations in assimilation number of coastal marine phytoplankton: Effects of environmental co-variates. *J. Plankton Res.* **2**: 249-260.
- Harrison, W. G., Platt, T. & Lewis, M. R. 1985. The utility of light-saturation models for estimating marine primary productivity in the field: A comparison with conventional "simulated" in situ methods. *Can. J. Fish. Aquat. Sci.* **42**: 864-872.
- Harrison, W. G. & Platt, T. 1986. Photosynthesis-irradiance relationship in Polar and Temperate phytoplankton populations. *Polar Biol.* **5**: 153-164.
- Head, E. J. H. & Horne, E. P. W. 1993. Pigment transformation and vertical flux in an area of convergence in the North Atlantic. *Deep-Sea Res.* **40**: 329-346.
- Hecky, R. E. & Fee, E. J. 1981. Primary production and rates of algal growth in Lake Tanganyika. *Limnol. Oceanogr.* **26**: 532-547.

- Herman, A. W., Mitchell, M. R. & Young, S. W. 1984. A continuous pump sampler for profiling copepods and chlorophyll in the upper oceanic layers. *Deep Sea Res.* **31**: 439-450.
- Hoepffner, N. & Sathyendranath, S. 1991. Effect of pigment composition on absorption properties of phytoplankton. *Mar. Ecol. Prog. Ser.* **73**: 11-23.
- Hoepffner, N. & Sathyendranath, S. 1992. Bio-optical characteristics of coastal waters: Absorption spectra of phytoplankton and pigment distribution in the western North Atlantic. *Limnol. Oceanogr.* **37**: 1660-1679.
- Hoepffner, N. & Sathyendranath, S. 1993. Determination of the major groups of phytoplankton pigments from the absorption spectra of total particulate matter. *J. Geophys. Res.* **98**: 22789-22803.
- Holm-Hansen, O., Lorenzen, C. J., Holmes, R. W. & Strickland, J. D. H. 1965. Fluorometric determination of chlorophyll. *J. cons. int. Explor. Mer* **30**: 3-15.
- Hooker, S. B., Esaias, W. E., Feldman, G. C., Gregg, W. W. & McClain, C. R. 1992. *An overview of SeaWiFS and ocean color*. SeaWiFS Technical Report Series. NASA; Greenbelt, Maryland. **1**: 24 pp.
- Irwin, B., Anning, J., Caverhill, C. & Platt, T. 1990. Primary production on the Labrador Shelf and in the Strait of Belle Isle in May 1988. *Can. Data Rep. Fish. Aquat. Sci.* **784**: iv+96pp.
- Irwin, B., Caverhill, C., Anning, J., Macdonald, A., Hodgson, M., Horne, E. P. W. & Platt, T. 1989. Productivity localized around seamounts in the Atlantic (PLASMA) during June and July 1987. *Can. Data Rep. Fish. Aquat. Sci.* **732**: iv+227pp.
- Ishizaka, J., Fukushima, H. & Kishino, M. 1997. Ocean Colour and Temperature Scanner (OCTS) update. *backscatter* **8**: 13-15.
- Jassby, A. D. & Platt, T. 1976. Mathematical formulation of the relationship between photosynthesis and light for phytoplankton. *Limnol. Oceanogr.* **21**: 540-547.

- Jeffrey, S. W. 1981. An improved thin-layer chromatographic technique for marine phytoplankton pigments. *Limnol. Oceanogr.* **26**: 191-197.
- Johnsen, G., Nelson, N. B., Jovine, R. V. & Prezelin, B. B. 1994a. Chromoprotein- and pigment-dependent modeling of spectral light absorption in two dinoflagellates, *Prorocentrum minimum* and *Heterocapsa pygmaea*. *Mar. Ecol. Prog. Ser.* **114**: 245-258.
- Johnsen, G. & Sakshaug, E. 1993. Bio-optical characteristics and photoadaptive responses in the toxic and bloom-forming dinoflagellates *Gyrodinium aureolum*, *Gymnodinium galatheanum*, and two strains of *Prorocentrum minimum*. *J. Phycol.* **29**: 627-642.
- Johnsen, G., Sakshaug, E. & Vernet, M. 1992. Pigment composition, spectral characterization and photosynthetic parameters in *Chrysochromulina polylepsis*. *Mar. Ecol. Prog. Ser.* **83**: 241-249.
- Johnsen, G., Samset, O., Granskog, L. & Sakshaug, E. 1994b. *In vivo* absorption characteristics in 10 classes of bloom-forming phytoplankton: Taxonomic characteristics and responses to photoadaptation by means of discriminant and HPLC analysis. *Mar. Ecol. Prog. Ser.* **105**: 149-157.
- Kiefer, D. A. & Mitchell, B. G. 1983. A simple, steady state description of phytoplankton growth based on absorption cross section and quantum efficiency. *Limnol. Oceanogr.* **28**: 770-776.
- Kiefer, D. & Strickland, J. D. H. 1970. A comparative study of photosynthesis in seawater samples incubated under two types of light attenuator. *Limnol. Oceanogr.* **15**: 408-412.
- Kingslake, R. 1965. *Applied optics and optical engineering. I. Light: Its generation and modification*. Academic Press Inc., New York. 423 pp.
- Kirk, J. T. O. 1983. *Light and photosynthesis in aquatic ecosystems*. Cambridge University Press, Cambridge. 401 pp.
- Kishino, M., Okami, N., Takahashi, M. & Ichimura, S. 1986. Light utilisation efficiency and quantum yield of phytoplankton in a thermally-stratified sea. *Limnol. Oceanogr.* **31**: 557-566.

- Kishino, M., Takahashi, M., Okami, N. & Ichimura, S. 1985. Estimation of the spectral absorption coefficients of phytoplankton in the sea. *Bull. Mar. Sci.* **37**: 634-642.
- Kolber, Z., Wyman, K. D. & Falkowski, P. G. 1990. Natural variability in photosynthetic energy conversion efficiency: A field study in the Gulf of Maine. *Limnol. Oceanogr.* **35**: 72-79.
- Kywalyanga, M., Platt, T. & Sathyendranath, S. 1992. Ocean primary production calculated by spectral and broad-band models. *Mar. Ecol. Prog. Ser.* **85**: 171-185.
- Lastein, E. & Gargas, E. 1978. Relationship between phytoplankton photosynthesis and light, temperature and nutrients in shallow lakes. *Verh. Internat. Verin. Limnol.* **20**: 678-689.
- Lazzara, L., Bricaud, A. & Claustre, H. 1996. Spectral absorption and fluorescence excitation properties of phytoplanktonic populations at a mesotrophic and an oligotrophic site in the tropical North Atlantic (EUMELI program). *Deep Sea Res.* **43**: 1215-1240.
- Levasseur, M. E., Harrison, P. J., Heimdahl, B. R. & Therriault, J.-C. 1990. Simultaneous nitrogen and silicate deficiency of a phytoplankton community in a coastal jet-front. *Mar. Biol.* **104**: 329-338.
- Lewis, M. R., Cullen, J. J. & Platt, T. 1984. Relationship between vertical mixing and photoadaptation of phytoplankton: Similarity criteria. *Mar. Ecol. Prog. Ser.* **15**: 141-149.
- Lewis, M. R., Ulloa, O. & Platt, T. 1988. Photosynthetic action, absorption, and quantum yield spectra for a natural population of *Oscillatoria* in the North Atlantic. *Limnol. Oceanogr.* **33**: 92-98.
- Lewis, M. R., Warnock, R. E., Irwin, B. & Platt, T. 1985a. Measuring photosynthetic action spectra of natural phytoplankton populations. *J. Phycol.* **21**: 310-315.

- Lewis, M. R., Warnock, R. E. & Platt, T. 1985b. Absorption and photosynthetic action spectra for natural phytoplankton populations: Implications for production in the open ocean. *Limnol. Oceanogr.* **30**: 794-806.
- Lewis, M. R., Warnock, R. E. & Platt, T. 1986. Photosynthetic response of marine picoplankton at low photon flux. *In*: Platt, T. & Li, W. K. W. (eds.). Photosynthetic Picoplankton. *Can. Bull. Fish. Aquat. Sci.*, Ottawa. pp. 235-250.
- Li, W. K. W. 1980. Temperature adaptation in phytoplankton: Cellular and photosynthetic characteristics. *In*: Falkowski, P. G. (ed.). Primary production in the sea. Plenum Press, New York. pp. 259-279.
- Li, W. K. W. 1994. Phytoplankton biomass and chlorophyll concentration across the North Atlantic. *Scient. Mar.* **58**: 67-79.
- Li, W. K. W. 1995. Composition of ultraphytoplankton in the central North Atlantic. *Mar. Ecol. Prog. Ser.* **122**: 1-8.
- Lizotte, M. P. & Priscu, J. C. 1994. Natural fluorescence and quantum yields in vertically stationary phytoplankton from perennially ice-covered lakes. *Limnol. Oceanogr.* **39**: 1399-1410.
- Longhurst, A. 1995. Seasonal cycles of pelagic production and consumption. *Prog. Oceanogr.* **36**: 77-167.
- Longhurst, A., Sathyendranath, S., Platt, T. & Caverhill, C. 1995. An estimate of global primary production in the ocean from satellite radiometer data. *J. Plankton Res.* **17**: 1245-1271.
- Lunning, K. & Dring, M. J. 1985. Action spectra and spectral quantum yield of photosynthesis in marine macroalgae with thin and thick thalli. *Mar. Biol.* **87**: 119-129.
- Lutz, V. A., Sathyendranath, S. & Head, E. J. H. 1996. Absorption coefficient of phytoplankton: regional variations in the North Atlantic. *Mar. Ecol. Prog. Ser.* **135**: 197-213.
- MacCaull, W. A. & Platt, T. 1977. Diel variations in the photosynthetic parameters of coastal marine phytoplankton. *Limnol. Oceanogr.* **22**: 723-731.

- Margalef, R. 1963. Modelos simplificados del ambiente marino para el estudio de la sucesión y distribución del fitoplancton y del valor indicador de sus pigmentos. *Investigación pesq.* **23**: 11-52.
- Mantoura, R. F. C. & Llewellyn, C. A. 1983. The rapid determination of algal chlorophyll and carotenoid pigments and their breakdown products in natural waters by reverse-phase high-performance liquid chromatography. *Anal. Chim. Acta* **151**: 297-314.
- Millie, D. F., Kirkpatrick, G. J. & Vinyard, B. T. 1995. Relating photosynthetic pigments and *in vivo* optical density spectra to irradiance for the Florida red-tide dinoflagellate *Gymnodinium breve*. *Mar. Ecol. Prog. Ser.* **120**: 65-75.
- Mitchell, B. G. & Kiefer, D. A. 1984. Determination of absorption and fluorescence excitation spectra for phytoplankton. *In*: Holm-Hansen, O., Bolis, L. & Gilles, R. (eds.). Marine phytoplankton and productivity. Springer-Verlag, Berlin. pp. 157-169.
- Moore, L. R., Goericke, R. & Chisholm, S. W. 1995. Comparative physiology of *Synechococcus* and *Prochlorococcus*: Influence of light and temperature on growth, pigments, fluorescence and absorptive properties. *Mar. Ecol. Prog. Ser.* **116**: 259-275.
- Morel, A., Antoine, D., Babin, M. & Dandonneau, Y. 1996. Measured and modeled production in the northeast Atlantic (EUMELI JGOFS program): The impact of natural variation in photosynthetic parameters on model predictive skill. *Deep Sea Res.* **43**: 1273-1304.
- Morel, A. & Berthon, J.-F. 1989. Surface pigments, algal biomass profiles, and potential production of the euphotic layer: Relationships reinvestigated in view of remote-sensing applications. *Limnol. Oceanogr.* **34**: 1545-1562.
- Morel, A. & Bricaud, A. 1981. Theoretical results concerning light absorption in a discrete medium, and application to specific absorption of phytoplankton. *Deep Sea Res.* **28**: 1375-1393.

- Mueller, J. L. & Lange, R. E. 1989. Bio-optical provinces of the northeast Pacific Ocean: A provisional analysis. *Limnol. Oceanogr.* **34**: 1572-1586.
- Neori, A., Vernet, M., Holm-Hansen, O. & Haxo, F. T. 1986. Relationship between action spectra for chlorophyll *a* fluorescence and photosynthetic O₂ evolution in algae. *J. Plankton Res.* **8**: 537-548.
- Neori, A., Vernet, M., Holm-Hansen, O. & Haxo, F. T. 1988. Comparison of chlorophyll far-red and red fluorescence excitation spectra with photosynthetic oxygen action spectra for photosystem II in algae. *Mar. Ecol. Prog. Ser.* **44**: 297-302.
- Olaizola, M., Geider, R. J., Harrison, W. G., Graziano, L. M., Ferrari, G. M. & Schlittenhardt, P. M. 1996. Synoptic study of variations in the fluorescence-based maximum quantum efficiency of photosynthesis across the North Atlantic Ocean. *Limnol. Oceanogr.* **41**: 755-765.
- Owens, T. G., Gallagher, J. C. & Alberte, R. S. 1987. Photosynthetic light-harvesting function of violaxanthin in *Nannochloropsis* spp. (Eustigmatophyceae). *J. Phycol.* **23**: 79-85.
- Pickett, J. M. & Myers, J. 1966. Monochromatic light saturation curves for photosynthesis in *Chlorella*. *J. Plant Physiol.* **41**: 90-98.
- Platt, T., Caverhill, C. & Sathyendranath, S. 1991. Basin-scale estimates of oceanic primary production by remote sensing: The North Atlantic. *J. Geophys. Res.* **96**: 15147-15159.
- Platt, T. & Conover, R. J. 1971. Variability and its effect on the 24h chlorophyll budget of a small marine basin. *Mar. Biol.* **10**: 52-65.
- Platt, T., Denman, K. L. & Jassby, A. D. 1977. Modeling the productivity of phytoplankton. *In*: Goldberg, E. D. (ed.). *The sea: Ideas and observations on progress in the study of the seas*. John Wiley, New York. pp. 807-856.
- Platt, T., Gallegos, C. L. & Harrison, W. G. 1980. Photoinhibition of photosynthesis in natural assemblages of marine phytoplankton. *J. Mar. Res.* **38**: 687-701.

- Platt, T. & Jassby, A. D. 1976. The relationship between photosynthesis and light for natural assemblages of coastal marine phytoplankton. *J. Phycol.* **12**: 421-430.
- Platt, T., Prakash, A. & Irwin, B. 1972. Phytoplankton nutrients and flushing of inlets on the coast of Nova Scotia. *Naturaliste Can.* **99**: 253-261.
- Platt, T., Harrison, W. G., Irwin, B., Horne, E. P. & Gallegos, C. L. 1982. Photosynthesis and photoadaptation of marine phytoplankton in Arctic. *Deep Sea Res.* **29**: 1159-1170.
- Platt, T. & Sathyendranath, S. 1988. Oceanic primary production: Estimation by remote sensing at local and regional scales. *Science* **241**: 1613-1620.
- Platt, T. & Sathyendranath, S. 1991. Biological production models as elements of coupled, atmosphere-ocean models for climate research. *J. Geophys. Res.* **96**: 2585-2592.
- Platt, T., Sathyendranath, S., Caverhill, C. M. & Lewis, M. R. 1988. Ocean primary production and available light: Further algorithms for remote sensing. *Deep Sea Res.* **35**: 855-879.
- Platt, T., Sathyendranath, S. & Ravindran, P. 1990. Primary production by phytoplankton: Analytic solutions for daily rates per unit area of water surface. *Proc. R. Soc. Lond. Ser. B.* **241**: 101-111.
- Platt, T., Sathyendranath, S., Ulloa, O., Harrison, W. G., Hoepffner, N. & Goes, J. 1992. Nutrient control of phytoplankton photosynthesis in the western North Atlantic. *Nature* **356**: 229-231.
- Prézelin, B. B. & Boczar, B. A. 1986. Molecular bases of cell absorption and fluorescence in phytoplankton: potential application to studies in optical oceanography. *Prog. Phycol. Res.* **4**: 350-464.
- Prézelin, B. B., Tilzer, M. M., Schofield, O. & Haese, C. 1991. The control of the production process of phytoplankton by the physical structure of the aquatic environment with special reference to its optical properties. *Aquat. Sci.* **53**: 136-186.

- Richardson, K. Beardall, J. & Raven, J. A. 1983. Adaptation of unicellular algae to irradiance: An analysis of strategies. *New Phytol.* **93**: 157-191.
- Ryther, J. H. & Menzel, D. W. 1960. The seasonal and geographical range of primary production in the western Sargasso Sea. *Deep Sea Res.* **6**: 235-238.
- Sakshaug, E., Johnsen, G., Andresen, K. & Vernet, M. 1991. Modeling of light-dependent algal photosynthesis and growth: Experiments with the Barents Sea diatoms *Thalassiosira nordenskiöldii* and *Chaetoceros furcellatus*. *Deep Sea Res.* **38**: 415-430.
- Sathyendranath, S. 1986. Remote sensing of phytoplankton: A review, with specific reference to picoplankton. *Can. Bull. Fish. Aquat. Sci.* **214**: 561-583.
- Sathyendranath, S., Lazzara, L. & Prieur, L. 1987. Variations in the spectral values of specific absorption of phytoplankton. *Limnol. Oceanogr.* **32**: 403-415.
- Sathyendranath, S., Longhurst, A., Caverhill, C. M. & Platt, T. 1995. Regionally and seasonally differentiated primary production in the North Atlantic. *Deep-Sea Res.* **42**: 1773-1802.
- Sathyendranath, S. & Platt, T. 1988. The spectral irradiance field at the surface and in the interior of the ocean: A model for applications in oceanography and remote sensing. *J. Geophys. Res.* **93**: 9270- 9280.
- Sathyendranath, S. & Platt, T. 1989a. Computation of aquatic primary production: Extended formalism to include effect of angular and spectral distribution of light. *Limnol. Oceanogr.* **34**: 188-198.
- Sathyendranath, S. & Platt, T. 1989b. Remote sensing of ocean chlorophyll: Consequence of non-uniform pigment profile. *Appl. Optics* **28**: 490-495.
- Sathyendranath, S. & Platt, T. 1993a. Remote sensing of water-column primary production. *In*: Li, W. K. W. & Maestrini, S. Y. (eds.). Measurement of Primary Production from the Molecular to the Global Scale. ICES Marine Science Symposia, Vol. 197, Copenhagen. pp. 236-243.

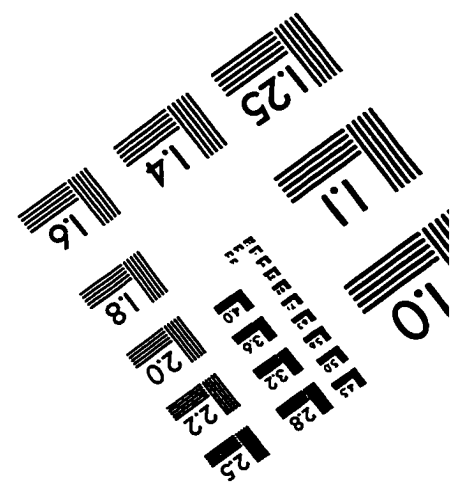
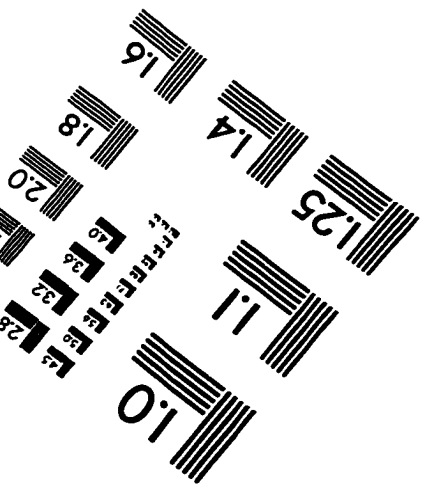
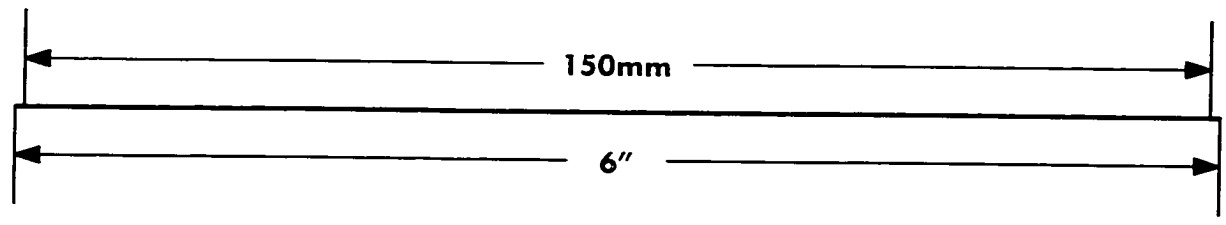
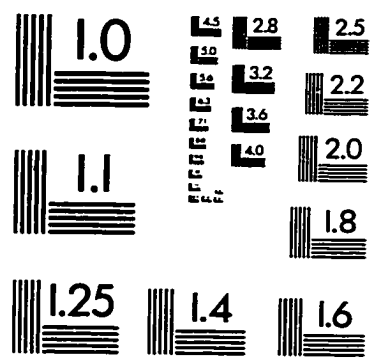
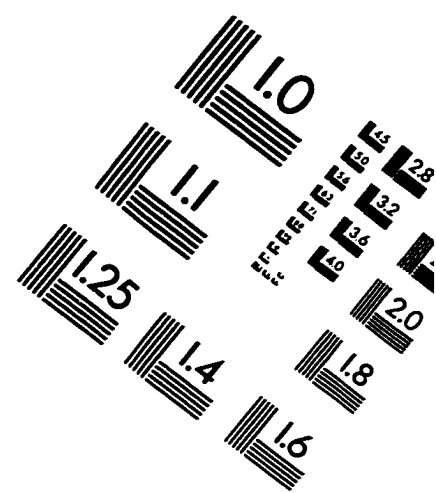
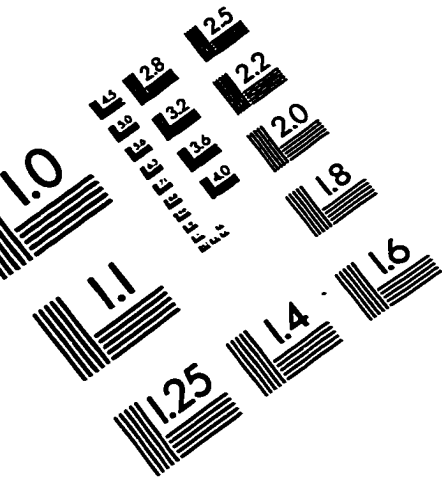
- Sathyendranath, S. & Platt, T. 1993b. Underwater light field and primary production: Application to remote sensing. *In*: Barale, V. & Schlittenhardt, P. M. (eds.). *Ocean Colour: Theory and Applications in a Decade of CZCS Experience*. Kluwer Academic Publishers, Brussels. pp. 79-93.
- Sathyendranath, S., Platt, T., Caverhill, C. M., Warnock, R. E. & Lewis, M. R. 1989. Remote sensing of oceanic primary production: Computations using a spectral model. *Deep Sea Res.* **36**: 431-453.
- Sathyendranath, S., Platt, T., Horne, E. P. W., Harrison, W. G., Ulloa, O., Outerbridge, R. & Hoepffner, N. 1991. Estimation of new production in the ocean by compound remote sensing. *Nature* **353**: 129-133.
- Sathyendranath, S., Platt, T., Stuart, V., Irwin, B. D., Veldhuis, M. J. W., Kraay, G. W. & Harrison, W. G. 1996. Some bio-optical characteristics of phytoplankton in the NW Indian Ocean. *Mar. Ecol. Prog. Ser.* **132**: 299-311.
- Schofield, O., Bidigare, R. R. & Prézelin, B. B. 1990. Spectral photosynthesis, quantum yield and blue-green light enhancement of productivity rates in the diatom *Chaetoceros gracile* and the prymnesiophyte *Emiliana huxleyi*. *Mar. Ecol. Prog. Ser.* **64**: 175-186.
- Schofield, O., Prézelin, B. B., Bidigare, R. R. & Smith, R. C. 1993. *In situ* photosynthetic quantum yield: Correspondence to hydrographic and optical variability within the Southern California Bight. *Mar. Ecol. Prog. Ser.* **93**: 25-37.
- Schofield, O., Prézelin, B. & Johnsen, G. 1996. Wavelength dependency of the maximum quantum yield of carbon fixation for two red tide dinoflagellates, *Heterocapsa pygmaea* and *Prorocentrum minimum* (Pyrrophyta): Implications for measuring photosynthetic rates. *J. Phycol.* **32**: 574-583.
- Schofield, O., Prézelin, B. B., Smith, R. C., Stegmann, P. M., Nelson, N. B., Lewis, M. R. & Baker, K. S. 1991. Variability in spectral and nonspectral measurements of photosynthetic light utilization efficiencies. *Mar. Ecol. Prog. Ser.* **78**: 253-271.

- Shimura, S. & Fujita, Y. 1975. Changes in the activity of fucoxanthin-excited photosynthesis in the marine diatom *Phaeodactylum tricornerutum* grown under different culture conditions. *Mar. Biol.* **33**: 185-194.
- Siefermann-Harms, D. 1987. The light-harvesting and protective functions of carotenoids in photosynthetic membranes. *Physiol. Plant.* **69**: 561-568.
- Smith, J. C., Platt, T. & Harrison, W. G. 1983. Photoadaptation of carboxylating enzymes and photosynthesis during a spring bloom. *Prog. Oceanogr.* **12**: 425-459.
- Smith Jr., W. O. & Barber, R. T. 1979. A carbon budget for the autotrophic ciliate *Mesodinium rubrum*. *J. Phycol.* **15**: 27-33.
- Snedecor, G. W. & Cochran, W. G. 1989. *Statistical methods. 8th ed.* Iowa State University Press, Ames. 503 pp.
- Sommer, U. 1994. The impact of light intensity and daylength on silicate and nitrate competition among marine phytoplankton. *Limnol. Oceanogr.* **39**: 1680-1688.
- Sosik, H. M. 1996. Bio-optical modelling of primary production: Consequences of variability in quantum yield and specific absorption. *Mar. Ecol. Prog. Ser.* **143**: 225-238.
- Sosik, H. & Mitchell, B. G. 1994. Effect of temperature on growth, light absorption, and quantum yield in *Dunaliella tertiolecta* (Chlorophyceae). *J. Phycol.* **30**: 833-840.
- Sosik, H. M. & Mitchell, B. G. 1995. Light absorption by phytoplankton, photosynthetic pigments and detritus in the California Current System. *Deep-Sea Res.* **42**: 1717-1748.
- Strickland, J. D. H. & Parsons, T. J. 1972. A practical handbook of seawater analysis. *Bull. Fish. Res. Board Can.* **167**: 311 pp.
- Stuart, V., Sathyendranath, S., Platt, T., Maass, H. & Irwin, B. submitted. Pigments and species composition of natural phytoplankton populations: Effect on the absorption spectra. *J. Plankton Res.*

- Taguchi, S. 1976. Relationship between photosynthesis and cell size of marine diatoms. *J. Phycol.* **12**: 185-189.
- Taguchi, S. 1981. Seasonal studies of the dinoflagellate *Ceratium longipes* (Bailey) Gran in the Bedford Basin, Canada. *J. Exp. Mar. Biol. Ecol.* **55**: 115-131.
- Taylor, A. H., Harbour, D. S., Harris, R. P., Burkill, P. H. & Edwards, E. S. 1993. Seasonal succession in the pelagic ecosystem of the North Atlantic and the utilization of nitrogen. *J. Plankton Res.* **15**: 875-891.
- Taylor, F. J. R., Blackbourn, D. J. & Blackbourn, J. 1971. The red-water ciliate *Mesodinium rubrum* and its "incomplete symbionts": A review including new ultrastructural observations. *J. Fish. Res. Board Can.* **28**: 391-407.
- Therriault, J.-C. & Platt, T. 1978. Spatial heterogeneity of phytoplankton biomass and related factors in the near-surface waters of an exposed coastal embayment. *Limnol. Oceanogr.* **23**: 888-899.
- Therriault, J.-C. & Platt, T. 1981. Environmental control of phytoplankton patchiness. *Can. J. Fish. Aquat. Sci.* **38**: 638-641.
- Tilzer, M. M., von Bodungen, B. & Smetacek, V. 1985. Light-dependence of phytoplankton photosynthesis in the Antarctic Ocean: Implications for regulating productivity. *In*: Siegfried, W. R., Condy, P. R. & Laws, R. M. (eds.). Antarctic Nutrient Cycles and Food Webs. Springer-Verlag Berlin Heidelberg, pp. 60-69.
- Ulloa, O., Hoepffner, N. & Larkin, D. (1997): Depth and wavelength dependence of phytoplankton photosynthesis: Implications for the remote sensing of marine primary production. *In*: Ocean Optics XIII, Steven G. Ackleson, Robert Frouin, Editors, Proc. SPIE **2963**: 284-289.
- Van Camp, L., Nykjær, L., Mittelstaedt, E. & Schlittenhardt, P. 1991. Upwelling and boundary circulation off Northwest Africa as depicted by infrared and visible satellite observations. *Prog. Oceanogr.* **26**: 357-402.
- Vernon, L. P. 1960. Spectrophotometric determination of chlorophylls and phaeophytins in plant extracts. *Anal. Chem.* **32**: 1144-1150.

- Warnock, R. E. (1990): Photosynthetic characteristics of picoplankton and natural phytoplankton assemblages. Ph.D. Dissertation, Dalhousie University, Halifax, Nova Scotia. 616 pp. (Volumes 1 and 2).
- Waser, N. A. D., Harrison, W. G., Head, E. J. H., Lutz, V. A., Calvert, S. E. & Nielsen, B. Submitted. Geographic variation in ^{15}N natural abundance of surface particulate nitrogen and new production across the North Atlantic ocean. *Deep Sea Res.*
- Wetsteyn, L. P. M. J., Peeters, J. C. H., Duin, R. N. M., Vegter, F. & de Visscher, P. R. M. 1990. Phytoplankton primary production and nutrients in the Oosterschelde (The Netherlands) during the pre-barrier period 1980-1984. *Hydrobiol.* **195**: 163-177.
- White, A. W., Sheath, R. G. & Hellebust, J. A. 1977. A red tide caused by the marine ciliate *Mesodinium rubrum* in Passamaquoddy Bay, including pigment and ultrastructure studies of the endosymbiont. *J. Fish. Res. Board Can.* **34**: 413-416.
- Williams, N. J. 1978. Annual variation of photosynthetic parameters in Lake Tahoe. *Verh. Internat. Verein. Limnol.* **20**: 419-425.
- Yentsch, C. S. 1962. Measurement of visible light absorption by particulate matter in the ocean. *Limnol. Oceanogr.* **7**: 207-217.
- Yentsch, C. S. & Menzel, D. W. 1963. A method for the determination of phytoplankton chlorophyll and phaeophytin by fluorescence. *Deep Sea Res.* **10**: 221-231.
- Zscheile, F. P. & Comar, C. L. 1941. Influence of preparative procedure on the purity of chlorophyll components as shown by absorption spectra. *Bot. Gaz.* **102**: 463-481.

IMAGE EVALUATION TEST TARGET (QA-3)



APPLIED IMAGE, Inc
1653 East Main Street
Rochester, NY 14609 USA
Phone: 716/482-0300
Fax: 716/288-5989

© 1993, Applied Image, Inc., All Rights Reserved